PLANAR RRRP LINKAGE SYNTHESIS AND ANALYSIS TUTORIAL

M. John D. Hayes, Alia Nichol, Mirja Rotzoll
Department of Mechanical and Aerospace Engineering, Carleton University, Ottawa, ON K1S 5B6, Canada
Email: john.hayes@carleton.ca; alia.nichol@carleton.ca; mirja.rotzoll@carleton.ca

ABSTRACT

A complete classification scheme of the mobility characteristics of the input link for every planar RRRP[1] linkage reported in this paper is obtained in a novel and efficient way. To lay the foundation of this work, recent results are first briefly summarised. The algebraic input-output (IO) equation for any planar RRRP linkage is obtained by simply re-collecting the coefficients in the algebraic IO equation for a general planar 4R linkage in terms of the input link angle and the output slider linear displacement. The coefficients factor into two pairs of bilinear terms in the design parameters, the lengths of the input and coupler links and the offset distance of the slider longitudinal centreline from the ground-fixed R-pair centre. These four bilinear factors can be viewed as the four plane faces of a regular square pyramid in the three-dimensional space implied by the three design parameter directed lengths. Intersections of the pyramid with any plane represented by any value (positive, negative, or zero) of the offset distance produce line bound regions each containing points that represent all possible planar RRRP linkages. The numerical values of the four bilinear factors of the algebraic IO equation imply a complete classification scheme for the mobility characteristics of the input links of these planar four-bar mechanisms.

This version of the paper is more comprehensive than the conference version, and intended for use as a reference for the Project in MAAE 3004, Dynamics of Machinery. This version of the paper also includes detailed notes on: exact kinematic synthesis of planar RRRP function generators using the algebraic IO equation; the three species of double points of algebraic curves and their implications for the mobility of the RRRP input link; the projective extension of the Euclidean plane of the mechanism motion; interpretation of the IO curves of RRRP mechanisms and finally; determining 4R and RRRP mechanism coupler point curves. All other information required to successfully complete the tasks demanded by the project will be presented in the online course lectures and may also be found in the MAAE 3004 required textbook: *Theory of Machines and Mechanisms, 5th edition* by Uicker, Pennock, and Shigley.

Keywords: planar RRRP linkages; kinematic synthesis; double points of planar algebraic equations; design parameter space; input link mobility classification; coupler point curves.

[1] This terminology refers to a mechanical system comprising four rigid links connected to each other with three sequential revolute joints (R-pairs) and one prismatic (slider) joint (P-pair) forming a closed RRRP kinematic chain.

1. INTRODUCTION

As James T. Kirk, Captain of the Starship Enterprise, may one day say many thousands of years from now in a galaxy far, far away: "In the firmament of mechanical design the four-bar linkage burns as it's brightest star [1]." Indeed, four-bar linkages are ubiquitous. They can be identified in mechanical systems we encounter every day: mechanical pencils; fold-out table-tops in class room chairs; bicycle lock mechanisms; etc.. Ever since humans had the ability to formulate abstract thoughts, for countless thousands of years, four-bar linkages, in their many forms, have been used to perform a large variety of tasks everywhere there have been human beings [2]. However, only in the last 3000 years have the engineering sciences been applied, in ever increasingly more sophisticated ways, to the synthesis and analysis of linkages for achieving desired outputs for given inputs [3]. The science of mechanisms has evolved such that now nearly every article of clothing you wear, the vehicles you are transported by, the household devices you use, even the streets you walk on have all been touched by at least one, or two, if not many thousands, of four-bar linkages. These mechanical systems can be designed to generate general displacements and motions in 3D space, on the surface of a sphere, and in 2D space which we will call the Euclidean plane.

The term *kinematic pair* indicates a joint between *two* links, hence the use of the word *pair*. Joints are mechanical constraints imposed on the links. Those involving surface contact are called *lower pairs*. Those normally involving point, line, or curve contact are *higher pairs*. Lower pairs enjoy innate practical advantages over higher pairs: applied loads are spread continuously over the contacting surfaces; they can, in general, be more easily and accurately manufactured. There are six types of lower pair (see Figure 1) classified in the following way [4, 5].

1. **R-Pair.** The revolute R-pair is made up of two congruent mating surfaces of revolution. It has one rotational degree-of-freedom (DOF) about its axis.

2. **P-Pair.** The prismatic P-pair comprises two congruent non-circular cylinders, or prisms. It has one translational DOF. It's axis is a line at infinity orthogonal to the direction of translation.

3. **H-Pair.** The helical H-pair, or screw, consists of two congruent helicoidal surfaces whose elements are a convex screw and a concave nut. For an angle θ of relative rotation about the screw axis there is a coupled translation of distance S in a direction parallel to the screw axis. The sense of translation depends on the *hand* of the screw threads and on the sense of rotation. The distance S is the thread *pitch* for a rotation of $\theta = 360^\circ$. When $S = 0$ it becomes an R-pair; when $S = \infty$ it becomes a P-pair. The H-pair has one DOF specified as a translation or a rotation, coupled by the pitch S.

4. **C-Pair.** The cylindrical C-pair consists of mating convex and concave circular cylinders. They can rotate relative to each other about their common axis, and translate relative to each other in a direction parallel to the axis. Hence the C-pair has two DOF: one rotational, the other translational.

5. **S-Pair.** The spherical S-pair, also called *ball-joints*, consists of a solid sphere which exactly conforms with a spherical shell. S-pairs permit three rotational DOF about intersecting orthogonal axes.

6. **E-Pair.** The planar E-pair (for the German word "ebene", meaning "plane") is a special S-pair comprising two concentric spheres of infinite radius. They permit two orthogonal translations and one rotational DOF about an axis orthogonal to the plane of translation. They provide three DOF in total.

In many classes of applications, the four-bar mechanism is driven by a human actuator. Examples of this class are numerous, and sometimes taken for granted, e.g., when cutting a paper sheet with scissors, when pedalling a bicycle, etc.. In the case of scissors, the two blades of this tool form a two-link open chain coupled by an R-pair. When held by a user, this chain is coupled to a second, similar chain formed by the

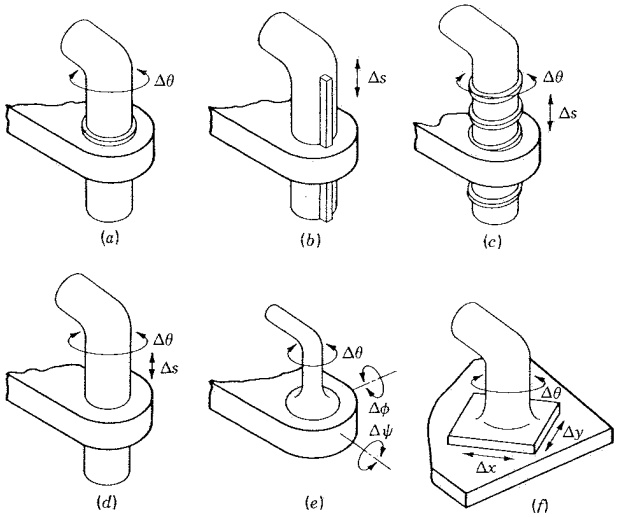

Fig. 1. The six lower pairs: (a) revolute or pin; (b) prismatic; (c) helical; (d) cylindrical; (e) spherical; (f) planar.

Table 1. Summary of the lower pairs and their respective DOF.

Pair type	Symbol	DOF
Revolute	R	1
Prismatic	P	1
Helical	H	1
Cylindrical	C	2
Spherical	S	3
Planar	E	3

proximal phalanx of the thumb and the intermediate phalanx of the index finger, thereby forming a four-bar linkage. Likewise, in the case of a bicycle, the frame and one of the two pedals form an open chain, which couples with a second, similar chain, formed by the calf and the thigh of a human user, coupled by the R-pair of the knee, thereby forming, again, a four-bar linkage.

In the context of planar mechanism kinematics, a *dyad* is a single rigid body link coupled to two other rigid bodies with two kinematic pairs. The two other rigid bodies are a relatively non-moving ground link, while the other is the coupler, which is connected to another dyad thereby forming a four-bar mechanism. The coupler is the link that joins, or couples, the two dyads. For planar displacements there are only two types of lower pair that can be used to generate a motion in the plane: R- and P-pairs. This means there are only four practical planar dyads

RR, PR, RP, and PP.

These 3-link serially connected open kinematic chains of rigid bodies are the building blocks of every planar mechanism. They are designated according to the type of joints connecting the rigid links, and listed in series starting with the joint connected to ground, each illustrated in Figure 2.

When a pair of dyads are coupled to each other, a four-bar linkage is obtained. However, the designation

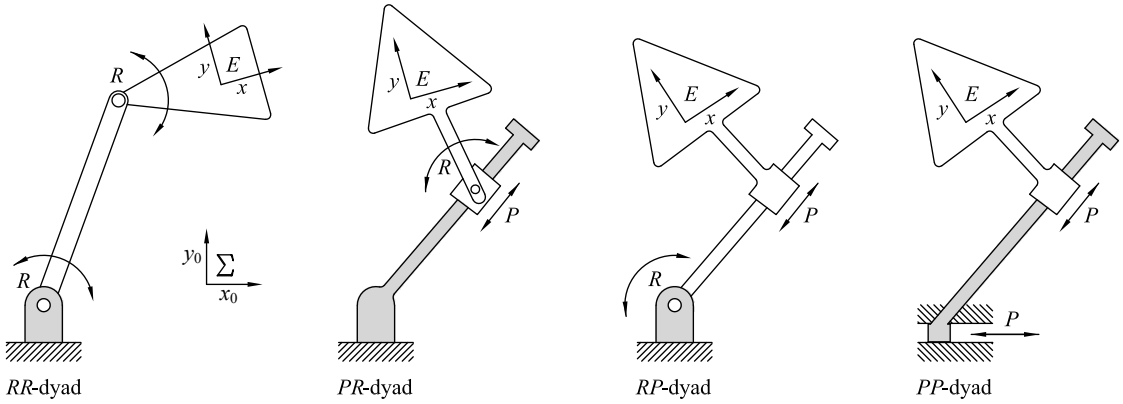

Fig. 2. Types of dyads.

of the *output* dyad may change. For example, consider a planar four-bar linkage composed of an *RR*-dyad on the *left-hand side* of the mechanism, and a PR-dyad on the *right-hand side*, where the *input* link is the *grounded* link in the RR-dyad and the *output* link is the slider of the PR-dyad, see Figure 3.

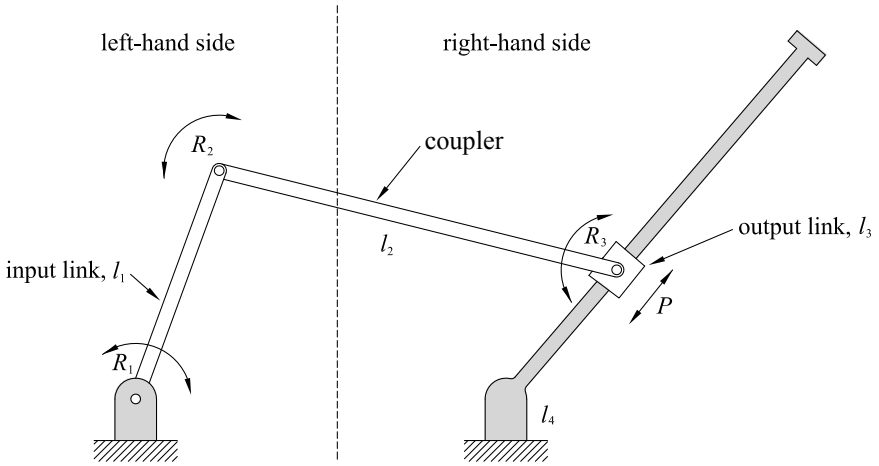

Fig. 3. A four-bar linkage with RR-dyad on the left-hand side and PR-dyad on the right-hand side coupled via link l_2 creates an RRRP mechanism.

Suppose revolute joint R_1 is actuated by some form of torque supplied by an electric rotary motor transferred by a transmission, in turn driving the input link, l_1. The linkage is designated by listing the joints in sequence from the ground fixed actuated joint, starting with the input link listing the joints in order. Thus, the mechanism composed of a driving RR-dyad, and an output PR-dyad is called an RRRP linkage, where the order of PR is switched to RP. If the output were an RP-dyad, the mechanism would be an RRPR linkage. If the input were an RP-dyad while the output was an RR-dyad, the resulting mechanism would be an RPRR linkage, with no noticeable alteration in the designation.

Because a four-bar mechanism possesses only a single DOF then only a single actuated input joint will cause the three movable links to move. Two of the links are connected to the fixed base link of the mechanism by either R- or P-pairs. Let us suppose that one of the joints connected to the fixed non-moving link is the actuated joint. Now the other ground fixed link can be caused to move by a change in input of the actuated joint, and the middle link couples the motion of the actuated input link to the non-actuated base fixed

moving link. Hence, the three relatively moving links in a four-bar mechanism are called the input, coupler, and output links respectively. If the mechanism links are joined by two R-pairs and two P-pairs then the coupler can move with general plane motion. That is, a coordinate system painted onto the coupler can both translate and rotate. If the linkage contains more than two P-pairs then the coupler coordinate system can only have curvilinear or linear displacements. For this reason, we will only discuss mechanisms containing no more than two P-pairs.

2. INPUTS REQUIRED TO GENERATE DESIRED OUTPUTS

We will presently briefly discuss the standard output motion generation problems associated with planar, spherical, and spatial four-bar mechanisms. While the input-output (IO) design problems listed next can be applied to mechanical systems of any kind, our focus will be mostly on planar RRRP mechanisms. The three most common design problems are termed *function generation*, *motion generation*, and *path generation*, which will now be discussed in that order.

2.1. Function Generation

A function generating four-bar mechanism converts a change in input to a change in output correlated by a mathematical function. That is, the output is a desired function of the input. The classical problem of function generation was first formulated trigonometrically by Ferdinand Freudenstein in a seminal paper that has been recognized as the origin of modern kinematics [6]. For a four-bar 4R mechanism the design task becomes identifying the link lengths, which we abstractly define as the *design parameters*, in terms of the constant distances between sequential R-pair centres required to correlate the output link angle, over a prescribed range, as a desired mathematical function of the input angle. In an RRRP linkage the input is still an angle, but the output is a displacement along a line. Function generating mechanisms are found in most sewing machines, washing machines, windshield wiper mechanisms, automotive suspensions, aircraft aileron mechanical systems, etc..

2.2. Motion Generation

The design task for motion generation, or rigid body guidance, involves identifying the design parameters of a four-bar mechanism that will guide the coupler through a desired motion. The coupler motion can be defined as the motion of any line on the coupler. Without loss in generality we may consider this as the motion of any coordinate system rigidly attached to the coupler. The motion of the coupler coordinate system consists of the translation of the origin of the coordinate system combined with the change in orientation of the coordinate system. Rigid body guidance is also known as the *Burmester problem*, since Ludwig Burmester published the very first recorded work in 1888 outlining a general solution to the rigid body guidance problem [7]. Motion generating four-bar mechanisms are typically found in aircraft landing gear mechanisms, pick-and-place mechanical systems on automated assembly and packaging conveyors, camera pointing devices, etc..

2.3. Path Generation

Guiding a point along a desired path (curve) is, perhaps, the oldest four-bar linkage problem and was investigated by Archimedes more than two thousand years ago [3] and very likely by many others far earlier. In those times the mechanical devices that generated the desired curve were powered by humans, working animals, or water wheels. This design problem involves identifying the design parameters that will enable a point on the coupler to be guided along a desired curve over a desired range of motion. This point, known as the *coupler point*, is guided along the *coupler point curve* by the motion of the input link and the constraints imposed by the mechanism link lengths. The coupler point can be anywhere on the coupler, and is rarely

on the line connecting the centres of the two R-pairs connecting the coupler to the input and output links. Coupler curves are quite complicated and subtle so we won't dwell on them here. However, it is simple to remember that coupler curves are of degree 6 (sextic) for 4R mechanisms, degree 4 (quartic) for RRRP linkages, and degree 2 (quadratic) for PRRP linkages.

The steam age spawned the *Industrial Revolution* in the 1700s. Coal was needed to boil water to generate the steam that powered the revolution. The need to pump water out of coal mines in England led James Watt to devise a *straight line* linkage that could transfer the oscillating input of a steam power driven piston to a rotating link connected to the piston by a coupler. The concept of the mechanism was patented in 1784 [8]. The coupler was also connected, via an R-pair, to a pumping piston. Thus the power generated by the steam driven piston was transferred to the pumping mechanism which, by design, only needed to do work along the straight line portion of the coupler curve. The Watt linkage, illustrated in Figure 4a, is designed to move point C, located at the midpoint of the coupler, approximately along a straight line over a portion of the curve on which it is constrained to move. This linkage it is still widely used in a large variety of automotive and locomotive suspension systems.

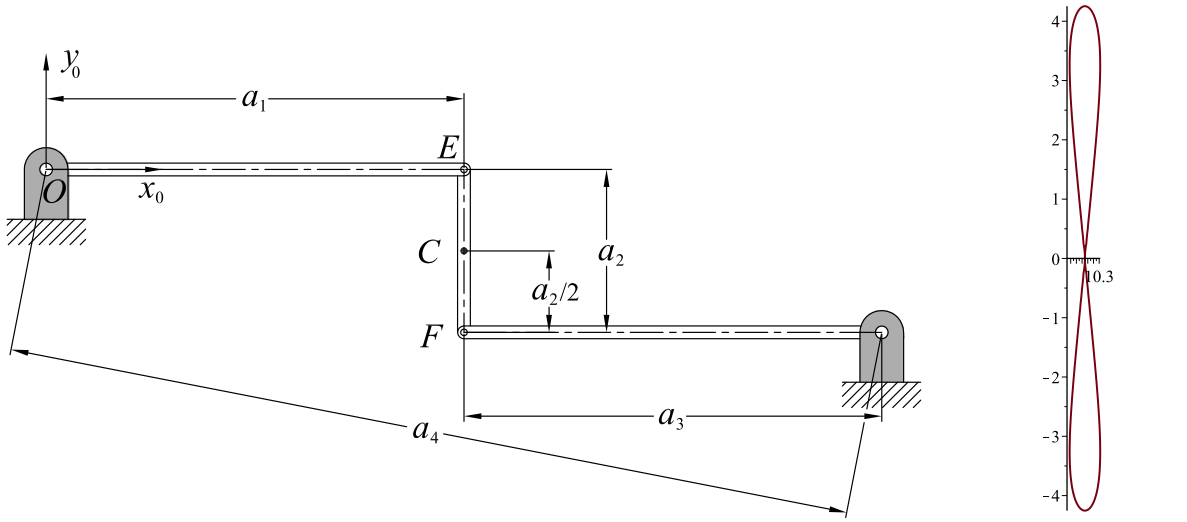

(a) Watt straight line linkage.

(b) Watt coupler curve.

Fig. 4. Watt straight-line linkage and coupler point curve where $a_1 = a_3 = 10$ and $a_2 = 2$.

The link length conditions for an arbitrary Watt mechanism are as follows. The input and output links have the same length, $a_1 = a_3$. The coupler point C is located at $a_2/2$ along the longitudinal centre line of the coupler. The distance between the centres of the two ground-fixed R-pairs can be expressed by the coordinates in the $x_0 - y_0$ coordinate system as $(2a_1,\ a_2)$, and the distance between the two centres is $a_4 = \sqrt{(2a_1)^2 + a_2^2}$. The longest link is always a_4. The coupler point curve for the Watt linkage illustrated in Figure 4a is plotted in Figure 4b.

The mobility constraints on the input and output links are determined by the numerical values of the linear coefficient factors A_1, C_1, and D_1 of Equation (1) are [1]:

$$\begin{aligned} A_1 &= a_1 - a_2 - a_3 + a_4, \\ C_1 &= a_1 - a_2 + a_3 - a_4, \\ D_1 &= a_1 + a_2 - a_3 - a_4. \end{aligned}$$

Because $a_1 = a_3$ and a_4 always represents the longest link length in a Watt mechanism then A_1 is always

a positive non-zero number while D_1 is always a negative non-zero number. Moreover, C_1 is always a negative non-zero number as well since $2a_1 < a_2 + a_4$. Therefore, a Watt straight line mechanism is always a non-Grashof 0-rocker-π-rocker, according to the planar 4R input-output link mobility classification found in [1].

Path generating linkages are now very common in automated manufacturing and assembly operations. Consider an automobile assembly station where windshields are attached to the vehicle body. A uniform bead of adhesive must be applied to the windshield just before a robotic arm picks it up and places it in the precise location on the gasket in the windshield opening on the body. This adhesive is typically applied by a four-bar linkage where the point on the coupler that follows the required adhesive bead path is generated by the input link rotating with constant angular velocity. However, in this case the adhesive bead must be uniform. This means that the coupler point, the nozzle of the adhesive applicator, must also have a constant velocity as it moves along the coupler point curve. Therefore the designer must simultaneously address the position level and velocity level kinematics.

3. RRRP LINKAGES

The planar RRRP four-bar linkage, colloquially known as a *crank-slider*, has been a workhorse in the realm of mechanical and aerospace engineering for centuries, if not millennia [3]. While trigonometric analytical methods to study the relationship between the motions of the input and output links, based on the distances between the R-pair centres as well as the offset and inclination angle of the P-pair, have existed for at least 150 years [9], purely algebraic methods have not. This means that the theory of algebraic differential geometry [10, 11] cannot be used to identify the structure of the relationship between the input and output parameters. Still, trigonometric methods are highly accessible and largely intuitive. The trigonometric input-output (IO) equations for planar 4R linkages that have become the backbone of analysis and synthesis were first introduced by Ferdinand Freudenstein in the 1950s [6, 12]. The same trigonometric approach has been used for planar RRRP linkages as well as for those containing as many as two P-pairs [2].

The algebraic IO equation for a planar 4R linkage is an algebraic polynomial that relates the tangent half-angle parameter of the input joint angle to the tangent half-angle parameter of the output joint angle in terms of the link lengths [13, 14]. A polynomial is algebraic if the coefficients are rational numbers[2]. This IO equation can be derived algorithmically [15] without explicit reference to trigonometry using the Denavit-Hartenberg (DH) parametrisation of the linkage kinematic geometry [16], Study's kinematic mapping [17], and Gröbner bases [18, 19]. Algebraic IO equations for any closed RRRP and PRRP kinematic chain can be similarly derived from the kinematic geometry but, as it turns out, this is unnecessary. Recent work by Rotzoll et al. [15, 20] has yielded the remarkable result that the algebraic IO equations for planar four-bar linkages that contain one, two, three, or even four P-pairs are embedded in the general planar 4R algebraic IO equation. That is, one need only collect the planar 4R algebraic IO equation in terms of the variable input and output parameters.

Consider the planar 4R closed kinematic chain illustrated in Figure 5. The basis vector directions of the non-moving coordinate reference system are x_0-y_0. The coordinate system origin is located at the rotation centre of the input link ground-fixed R-pair, while the x_0-axis points towards the rotation centre of that of the output link. The general IO equation algorithm described in [15] cannot directly be used to derive the IO equations for RRRP or PRRP linkages, or their inversions, but it doesn't need to because the respective IO equations are naturally embedded in that of the planar 4R. The algebraic IO equation of an arbitrary planar 4R linkage illustrated in Figure 5 is represented as

[2] A rational number can be expressed exactly as the ratio of two integers. The number $3.333\cdots$ is rational because it can be expressed exactly by the ratio 1/3, whereas the number $\sqrt{2}$ is irrational because it cannot be expressed exactly by such a ratio.

$$Av_1^2v_4^2 + Bv_1^2 + Cv_4^2 - 8a_1a_3v_1v_4 + D = 0, \tag{1}$$

where

$$\begin{aligned}
A &= (a_1 - a_2 - a_3 + a_4)(a_1 + a_2 - a_3 + a_4) = A_1A_2;\\
B &= (a_1 - a_2 + a_3 + a_4)(a_1 + a_2 + a_3 + a_4) = B_1B_2;\\
C &= (a_1 - a_2 + a_3 - a_4)(a_1 + a_2 + a_3 - a_4) = C_1C_2;\\
D &= (a_1 + a_2 - a_3 - a_4)(a_1 - a_2 - a_3 - a_4) = D_1D_2;\\
v_1 &= \tan\left(\frac{\theta_1}{2}\right); \quad v_4 = \tan\left(\frac{\theta_4}{2}\right).
\end{aligned}$$

The joint angle parameters v_1 and v_4 represent the tangent half-angles of linkage input and output angles, θ_1 and θ_4. The eight bilinear factors of the coefficients A, B, C, and D in Equation (1) depend on the numerical values of the four a_i link lengths. In this formulation the input link, a_1, is always positive but the remaining three a_i directed distances are the unique eight permutations of positive and negative signs in each factor. Hence, the eight bilinear factors represent eight distinct planes. Note that these permutations in sign only applies to the arithmetic operations of addition and subtraction, they do not represent the sign of the numeric value of the directed length. Treating the four a_i as homogeneous coordinates with a_4 as the homogenising coordinate one can uniformly scale the numerical values of the four a_i by dividing by a_4, which is always an arbitrary nonzero number for any real 4R linkage, without affecting the functional relationship $v_4 = f(v_1)$. Treating the a_i as mutually orthogonal basis directions in the hyperplane $a_4 = 1$ the eight planes intersect in the only uniform polyhedral compound [21], called the stellated octahedron, which has order 48 octahedral symmetry: a regular double tetrahedron that intersects itself in a regular octahedron [22]. The location of a point in this space completely determines the mobility of the input and output links and hence it is termed the *design parameter space* of planar 4R linkages.

There has always existed an almost innate understanding that as the radius of a sphere tends towards infinity it can be considered as the plane at infinity. Projective geometry has, of course, shown that this is indeed the case mathematically [23]. The axes of a spherical 4R linkage intersect at the centre of the sphere, see the spherical 4R illustrated in Figure 6b, while those of a planar 4R are mutually parallel but intersect in a unique point on the line at infinity in the projective extension of the Euclidean plane of the 4R mechanism. Therefore, there arose the notion in the 1800's that planar 4R mechanisms are special cases of spherical 4R linkages on the surface of a sphere of infinite radius. This notion was proved to be true in [24] and more recently in [15] where the proof is relatively straightforward using the algebraic form of the IO equation.

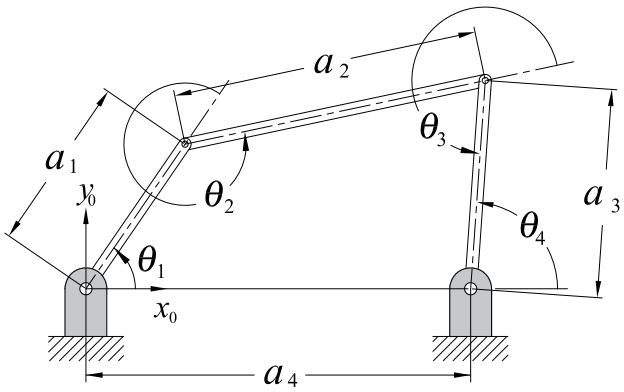

Fig. 5. Planar 4R closed kinematic chain.

The design parameters of a spherical 4R are four nonzero arc length angle parameters, which are the tangent half-angle parameters, α_i, of the arc length angles, τ_i, such that $\alpha_i = \tan(\tau_i/2)$. The algebraic IO equation of a spherical 4R contains eight bicubic factors in the α_i. These eight cubic factors are singular cubic surfaces [21] in the sense that they all contain only 12 and not the maximum number of 27 lines [25]. Each cubic surface contains three real finite lines which intersect in an equilateral triangle and different pairs of the eight cubic surfaces have a different line in common. Treating the four α_i as mutually orthogonal basis directions and projecting into the hyperplane $\alpha_4 = 1$ reveals the design parameter space of spherical 4R linkages. Each distinct point in this space is a unique spherical 4R and the mobility of the input and output links is completely determined by its location in this space. It turns out that the eight cubic surfaces in the spherical 4R design parameter space intersect the planar 4R design parameter space in the 12 edges of the double tetrahedra, see Figure 6a. The vertices of the tetrahedra are the vertices of the equilateral triangles on each cubic surface while the edges are the lines themselves.

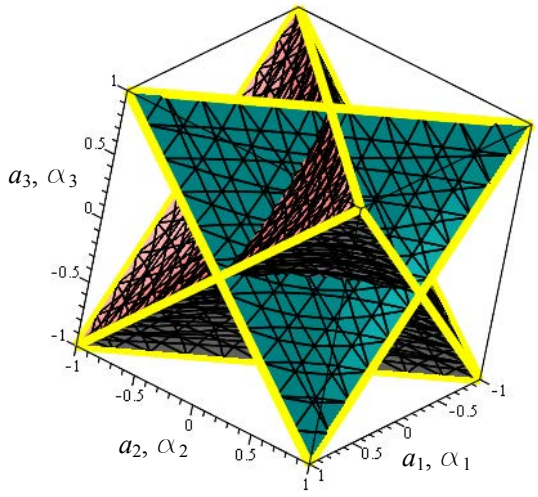

(a) Twelve lines common to the spherical and planar 4R design parameter spaces.

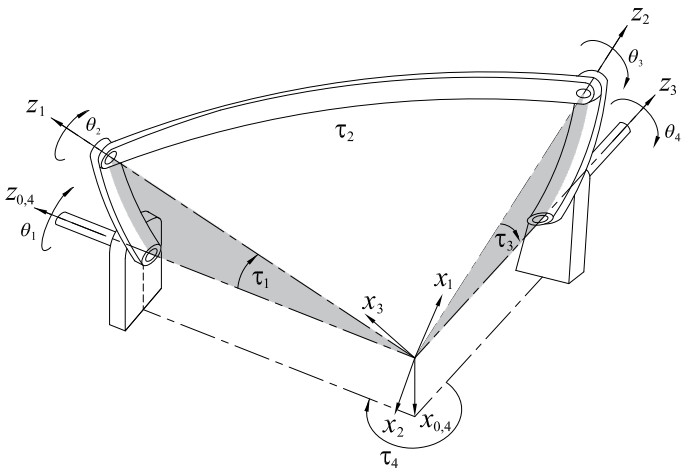

(b) A spherical 4R mechanism.

Fig. 6. Design parameter space intersections and a planar RRRP linkage.

In what follows attention is focused on the design parameter space of the planar RRRP mechanism since no information on this space exists in the literature. The algebraic IO equation for planar 4R linkages is collected in terms of the variable input link angle parameter, $v_1 = \tan(\theta_1/2)$, and the variable slider translation, a_3, see Figure 7a. The result is a 4^{th} order planar curve in v_1 and a_3 with algebraic properties very different from that of the planar 4R. These properties and their implications will be discussed. The algebraic IO equation of the RRRP linkage contains only four bilinear factors in the design constants a_1, a_2, and a_4. Treating these three a_i as mutually orthogonal basis directions reveals the structure of the four planes that the four bilinear factors imply. Moreover, the mobility conditions on the input joint range of angular displacement implied by the location of a point in this space will be derived.

To additionally make this paper a useful comprehensive reference for the mechanism design and analysis project in MAAE 3004, *Dynamics of Machinery*, a straightforward method for exact dimensional synthesis for planar RRRP function generator mechanisms will be discussed, and the coupler point curves for planar 4R and RRRP linkages will be derived. Next, in Subsection 3.1, the algebraic IO equation for planar RRRP mechanisms will be presented. However, before interpreting the planar RRRP algebraic IO equation in Section 6, some elementary concepts need to be discussed from an advanced standpoint starting in Section 5.

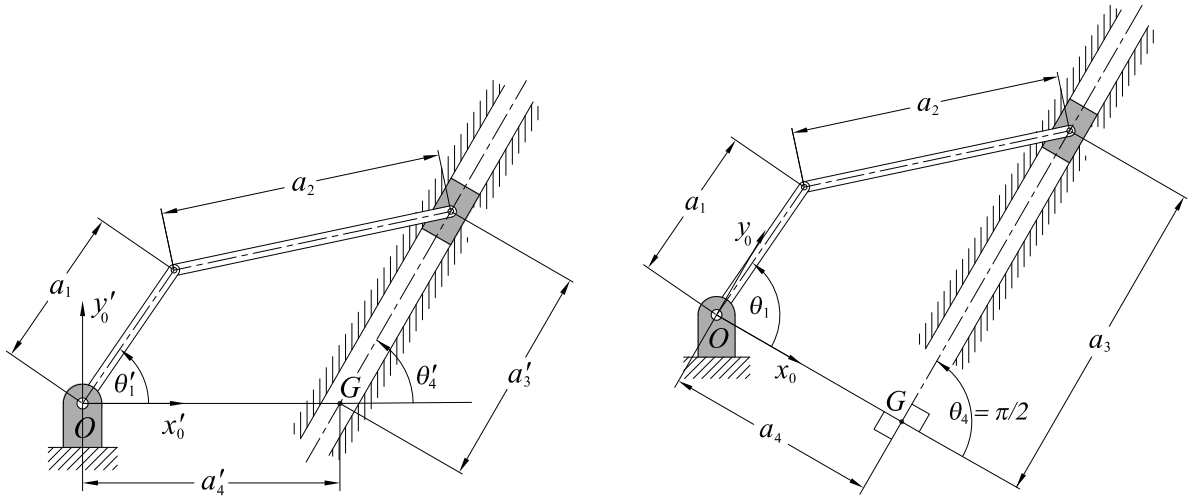

(a) General P-pair orientation.

(b) Orthogonal P-pair orientation.

Fig. 7. Planar RRRP linkage.

3.1. Planar RRRP Algebraic IO Equation

Consider the planar RRRP linkage illustrated in Figure 7a. The variables are the input joint angle θ_1' and the slider translation distance a_3' while the design parameters are the constant link lengths a_1, a_2, a_4', and the inclination angle of the P-pair, $v_4' = \tan(\theta_4'/2)$. Re-collecting Equation (1) in terms of $v_1' = \tan(\theta_1'/2)$ and a_3' yields

$$\begin{gathered}(v'^2_4+1)v'^2_1a'^2_3+(v'^2_4+1)a'^2_3+2(v'_4-1)(v'_4+1)(a_1-a'_4)a'_3-8a_1a'_3v'_4v'_1- \\ 2(v'_4-1)(v'_4+1)(a_1+a_4)v'^2_1a'_3+(a_1+a_2+a'_4)(a_1-a_2+a'_4)(v'4^2+1)v'^2_1+ \\ (a_1+a_2-a'_4)(a_1-a_2-a'_4)(v'^2_4+1)=0.\end{gathered} \tag{2}$$

Without loss in generality, the general design constant slider angle θ_4', illustrated in Figure 7a, can always be set to $\pi/2$ with a suitable transformation of the x_0'-y_0' coordinate system, such that the distance a_4' along the x_0'-axis is transformed to the different distance a_4 along the new x_0-axis which is orthogonal to the longitudinal axis of symmetry (the centre-line) of the slider, as illustrated in Figure 7b. In other words, by rotating x_0'-y_0' about it's origin to x_0-y_0 so that $\theta_4 = \pi/2$. This will change the length of a_4' to a_4 and the location of point G on the P-pair longitudinal centre-line thereby changing the zero for the slider translation a_3. Regardless, any RRRP linkage can be so represented [26, 27]. Making the substitution

$$\theta_4 \;=\; \frac{\pi}{2} \quad \Rightarrow \quad v_4^{'} \;=\; \tan\left(\frac{\theta_4}{2}\right) \;=\; 1$$

in Equation (2) makes several terms vanish revealing a more compact and elegant, but still completely general, RRRP algebraic IO equation:

$$v_1^2a_3^2+Av_1^2+a_3^2-4a_1v_1a_3+B \;=\; 0, \tag{3}$$

where

$$\begin{aligned} A &= A_1A_2 = (a_1+a_2+a_4)(a_1-a_2+a_4), \\ B &= B_1B_2 = (a_1+a_2-a_4)(a_1-a_2-a_4), \\ v_1 &= \tan\left(\frac{\theta_1}{2}\right); \quad v_4 = \tan\left(\frac{\theta_4}{2}\right) = \tan\left(\frac{\pi/2}{2}\right) = 1. \end{aligned}$$

4. FUNCTION GENERATOR SYNTHESIS

In this section we will solve the exact kinematic synthesis problem for a planar RRRP function generating mechanism. Mechanism synthesis involves determining the link lengths required to generate a particular type of desired motion. Most automated manufacturing and assembly mechanical systems require four-bar mechanisms where the output link moves as a particular function of the input link motion to position a tool to execute a desired task. Since the general planar RRRP algebraic IO equation contains only three design parameters: the three unknown link lengths a_1, a_2, and a_4, assuming the offset directed distance a_4 is perpendicular to the slider direction of reciprocating translation with $v_4 = 1$. If the desired task can be modelled with three precise slider locations that are functions of the input link angle θ_1, or angle parameter $v_1 = \tan(\theta_1/2)$, then we can generate three synthesis equations with $a_{3_i} = f(\theta_{1_i})$, where i is not the complex number $\sqrt{-1}$ but is instead a counting index whose value is 1, 2, or 3 determined by each of the three IO pairs (each pair of input angle and slider location *precision values*). Then, it is a simple matter to solve the three IO equations for the three unknown link lengths a_1, a_2, and a_4. Since the three IO equations are quadratic in the link lengths, there will in general be two solutions. Let's now examine the meaning of these two possible solutions with several examples.

Consider a beer bottle capping system. Full bottles of beer move along a conveyor belt at a constant rate with specific constant distances between the bottles. The device that places the cap on the bottle must move at the same rate as, and parallel to the conveyor, place and crimp a cap on the bottle, then return to a kinematically neutral location to start the process again. This continuous process can be modelled as the bottling operation for a single bottle, but as an infinitely repeating single discrete step: the bottle enters a control volume, moves at a constant rate along a rigidly defined path, maintained by a funneling chute, to a location where the capping tool held by the output link of an RRRP mechanism places and crimps the cap; the next bottle enters the control volume as the RRRP linkage returns to crimp a cap it.

Example 4.1: Negative Link Lengths Before computing possible link lengths the junior engineer in charge of determining the function governing the motions makes the design decision to mount the P-pair sliding direction to be parallel to the conveyor direction and that the shaft of RRRP actuator motor is perpendicular to the conveyor and slider travel directions, and we assign the x_0-axis to be the common normal between the motor shaft axis and the P-pair longitudinal centre line. Suppose that the function correlating the slider location to the shaft angle is

$$a_3 \quad = \quad -\frac{9}{4}\sin(\theta_1) - 3. \tag{4}$$

Suppose further that the precision input angles and output values of a_3 that exactly satisfy the function specified by Equation (4) are empirically determined by the junior engineer, who measures the IO pairs with a very precise laser theodolite that is set up on one side of the conveyor, to be those listed in Table 2 where the angles are specified in degrees and the lengths in centimetres. Notice that the function requires that θ_1 and a_3 increase in opposite directions: as θ_1 increases a_3 decreases. Populating Equation (3) with the three

i^{th} pair	Input angle (deg) θ_{1_i}	Slider location a_{3_i}
$i = 1$	5°	-3.196100421 cm
$i = 2$	40°	-4.446272122 cm
$i = 3$	85°	-5.241438071 cm

Table 2. Precision I0 pairs for uniform input angle spacing.

IO pairs yields the following three equations:

$$\begin{aligned} 10.23453064 + 0.5581790323a_1 + 0.1906277937e^{-2}(a_1 - a_2 + a_4)(a_1 + a_2 + a_4) + (a_1 - a_2 - a_4)(a_1 + a_2 - a_4) &= 0; \\ 22.38826533 + 6.473242823a_1 + 0.1324743315(a_1 - a_2 + a_4)(a_1 + a_2 + a_4) + (a_1 - a_2 - a_4)(a_1 + a_2 - a_4) &= 0; \\ 50.54045520 + 19.21157241a_1 + 0.8396628208(a_1 - a_2 + a_4)(a_1 + a_2 + a_4) + (a_1 - a_2 - a_4)(a_1 + a_2 - a_4) &= 0. \end{aligned}$$

Solving the three equations simultaneously for the three unknown link lengths a_1, a_2, and a_4 gives the two solutions listed in Table 3

Solution	a_1	a_2	a_4
1	-1.952184536 cm	3.321470078 cm	-0.5751750055 cm
2	-1.952184536 cm	-3.321470078 cm	-0.5751750055 cm

Table 3. The two solutions to the exact synthesis problem.

The junior engineer is puzzled: what does a *negative length* mean? Euclidean geometry very explicitly states that distances are always greater than or equal to zero, but never less than zero [28]. The explanation lies in the fact that the link lengths are really directed distances. Consider a unit position vector locating the point $(x,y) = (1,1)$. Multiplying the vector by the scalar -1 simply rotates the vector direction by $\pi = 180^\circ$ making it locate the point $(x,y) = (-1,-1)$. Both vectors are oriented at 45° relative to the positive x-axis and their magnitudes are both $\sqrt{2}$, but they point in opposite directions.

The directed distance -1.952184536 cm represents the input link. In the second precision configuration of the mechanism a_1 is oriented at 40° relative to the positive x_0-axis indicated in Figure 7b, but points in the opposite direction to the centre line of a_1, this is graphically illustrated in Figure 8. Since a_4 always points along the x_0-axis, a negative value for this distance simply places the slider centre line along the negative x_0-axis.

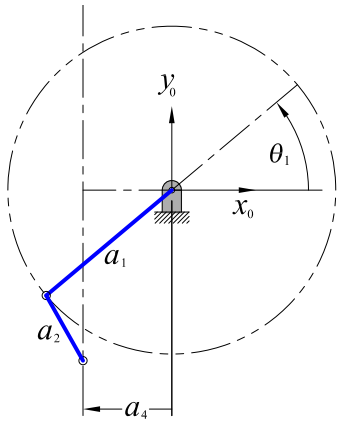

Fig. 8. Negative link length meaning for a_1 and a_4.

The sign of the coupler directed distance, a_2, is of no consequence in the shape coefficients of the RRRP algebraic IO equation. Only the coefficients A and B in Equation (3) contain the coupler length a_2. Expanding these two coefficients leads to

$$A = A_1A_2 = (a_1 + a_2 + a_4)(a_1 - a_2 + a_4) = a_1^2 + 2a_1a_4 - a_2^2 + a_4^2; \quad (5)$$

$$B = B_1B_2 = (a_1 + a_2 - a_4)(a_1 - a_2 - a_4) = a_1^2 - 2a_1a_4 - a_2^2 + a_4^2. \quad (6)$$

The shape of the algebraic IO equation of every planar RRRP function generating mechanism is affected by the number $-a_2^2$, which is always a negative number regardless of the sign of the numerical value of a_2.

However, as we shall see in Section 8, the complete mobility classification of the input link requires both positive and negative values of the coupler directed length $\pm a_2$. Since the coupler correlates the rotation of the input link to the translation (linear, or curvilinear) of the slider then directed distance $+a_2$ points from the distal R-pair centre of the input link to the R-pair connecting the coupler to the slider. The directed distance $-a_2$ simply points in the opposite direction: from the R-pair centre connecting the coupler to the slider to the distal R-pair centre of the input link. Therefore, relative to the non-moving coordinate system x_0-y_0, the direction of the length a_2 has no effect on the generated function, but it's sign affects the input link mobility classification.

4.1. Uniform and Chebyshev Distribution of Precision Configurations

For many applications exact synthesis is sufficient. In fact, before computers that could perform the numerical optimisation of large IO sets existed, three precision configuration synthesis was essentially all that was available. You will note that in the preceding exact synthesis problem that the specified input angles were uniformly distributed over the desired input angle range between 5°-85°. In the 1840s P.L. Chebyshev reasoned that the structural error function of the generated output of the linkage subtracted from the specified function output could be analysed to locate inflection points on the associated curve where the tangent is horizontal [29]. At these locations the error of the output is insensitive to changes in input, so these should be the values for the IO precision configurations. For a planar RRRP linkage the three precision configurations are located according to the following equation using the Chebyshev distribution function:

$$\theta_{1_i} = a + h\cos\left(\frac{(2i-1)\pi}{6}\right), \quad i \in \{1,2,3\}, \tag{7}$$

where

$$a = \frac{1}{2}(\theta_{1_{\text{initial}}} + \theta_{1_{\text{end}}}) \tag{8}$$

and

$$h = \frac{1}{2}(\theta_{1_{\text{end}}} - \theta_{1_{\text{initial}}}) \tag{9}$$

so that a_3 satisfies the function at the three values of θ_{1_i}. Again, the letter i is not the imaginary number $\sqrt{-1}$, rather it is a counting index whose value is 1, 2, or 3.

Example 4.2 We will consider the exact synthesis problem with Chebyshev spacing for approximating the function in Equation (4). Let us compute the Chebyshev distribution of the IO pairs using Equation (7) in an effort reduce the structural error to its minimum value for three IO precision configurations. Note that the angular ranges a and h must be specified in radians, and the value computed for θ_{1_i} will also be given in radians. Note further that these IO pairs will be ordered from large to small because of the way the ratio is specified.

The Chebyshev distribution for input angles and output slider locations is listed in Table 4. The three synthesis equations have the form:

$$\begin{aligned}
46.07293212 + 17.38696712a_1 + 0.6951810353(a_1 - a_2 + a_4)(a_1 + a_2 + a_4) + (a_1 - a_2 - a_4)(a_1 + a_2 - a_4) &= 0;\\
24.69346590 + 7.606601721a_1 + 0.1715728754(a_1 - a_2 + a_4)(a_1 + a_2 + a_4) + (a_1 - a_2 - a_4)(a_1 + a_2 - a_4) &= 0;\\
11.68643221 + 1.234450898a_1 + 0.8216741368e^{-2}(a_1 - a_2 + a_4)(a_1 + a_2 + a_4) + (a_1 - a_2 - a_4)(a_1 + a_2 - a_4) &= 0.
\end{aligned}$$

i^{th} pair	Input angle θ_{1_i} (rad)	Slider location a_{3_i}
$i=1$	$(1/4)\pi+(1/9)\pi\sqrt{3}$	-5.213326005 cm
$i=2$	$(1/4)\pi$	-4.590990258 cm
$i=3$	$(1/4)\pi-(1/9)\pi\sqrt{3}$	-3.404583734 cm

Table 4. Precision IO pairs for Chebyshev spacing.

These three synthesis equations are solved simultaneously for the three unknown link lengths and are listed in Table 5. The three link lengths are somewhat different from those for the uniform distribution listed in Table 3. If a structural error analysis were performed on the both sets of link lengths one would find that the area between specified and generated functions, the structural error, would be smaller for the Chebyshev spacing.

Solution	a_1	a_2	a_4
1	-1.908252574 cm	3.341820771 cm	-0.5372675934 cm
2	-1.908252574 cm	-3.341820771 cm	-0.5372675934 cm

Table 5. The two solutions to the exact synthesis problem with Chebyshev IO spacing.

4.2. Importance of Location and Orientation of Measurement Reference Coordinate Systems

In the previous two examples a junior engineer placed the measurement system reference coordinate system so that the motion of the bottles on the conveyor belt was in a particular direction. Suppose the laser theodolite was positioned and calibrated so that the motion of the conveyor was in the -y direction of the measurement coordinate system. What if the junior engineer was set up on the opposite side of the conveyor when the measurements were made? The conveyor would appear to be moving in the opposite direction: bottles would move parallel to the +y axis of the measurement coordinate system.

Example 4.3 For the engineer on the other side of the conveyor the function in Equation (4) is multiplied by -1:

$$a_3 = \frac{9}{4}\sin(\theta_1)+3. \tag{10}$$

Meanwhile, the precision IO pairs are now measured to be those listed in Table 6. In this case, a_3 increases as θ_1 increases.

i^{th} pair	Input angle θ_{1_i} (deg)	Slider location a_{3_i}
$i=1$	5°	3.196100421 cm
$i=2$	40°	4.446272122 cm
$i=3$	85°	5.241438071 cm

Table 6. Precision I0 pairs for uniform distribution.

Populating Equation (3) with these three new IO pairs yields the following three equations:

$$\begin{aligned}
10.23453064-0.5581790323a_1+0.1906277937e^{-2}(a_1-a_2+a_4)(a_1+a_2+a_4)+(a_1-a_2-a_4)(a_1+a_2-a_4) &= 0;\\
22.38826533-6.473242823a_1+0.1324743315(a_1-a_2+a_4)(a_1+a_2+a_4)+(a_1-a_2-a_4)(a_1+a_2-a_4) &= 0;\\
50.54045520-19.21157241a_1+0.8396628208(a_1-a_2+a_4)(a_1+a_2+a_4)+(a_1-a_2-a_4)(a_1+a_2-a_4) &= 0.
\end{aligned}$$

This set of three synthesis equations is only different from the first set in that the coefficient for a_1 is now multiplied by -1, but otherwise they are the same. Solving the three equations simultaneously for the three unknown link lengths a_1, a_2, and a_4 gives the two solutions listed in Table 7.

Solution	a_1	a_2	a_4
1	1.952184536 cm	3.321470078 cm	0.5751750055 cm
2	1.952184536 cm	-3.321470078 cm	0.5751750055 cm

Table 7. The two solutions for the exact synthesis problem for generating Equation (10).

In this case the positive value for a_1 of 1.952184536 cm in the second precision configuration of the mechanism a_1 is oriented at 40° relative to the positive x_0-axis indicated in Figure 7b and points in the same direction to the centre line of a_1, this is graphically illustrated in Figure 9. Since a_4 always points along the x_0-axis, a positive value for this distance simply places the slider centre line along the positive x_0-axis.

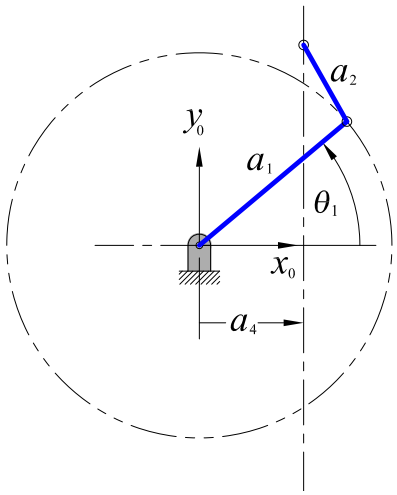

Fig. 9. Conventional link lengths for a_1 and a_4.

The exact function generation synthesis problem will lead to a linkage that exactly generates the desired function between input and output parameters, but only at the three specified precision configurations. For all other reachable intermediate configurations the generated function value will be different from the specified value that satisfies the desired function. This error is known as the *structural error* [9]. If more than three precision configurations are specified the synthesis problem becomes over constrained, but using error optimisation techniques, such as least-squares optimisation, approximate solutions minimising the structural error may be obtained, see [30] for example. The larger the cardinality of the IO pair set, the more the error is minimised. This has led to the notion of infinite IO data sets obtained using integral vector calculus to obtain an error minimised over the entire IO range [31].

4.3. Summary of Directed Lengths in an RRRP Linkage

In the preceding examples of the results of the kinematic synthesis of planar RRRP function generators we have seen that negative directed link lengths need to be included when generating certain functions defined in certain reference coordinate systems. The input link and coupler can have directed lengths that are greater than or less than zero, but never identically equal to zero. The slider offset distance can be any number along

the x_0-axis: negative, zero, or positive:

$$a_1 \begin{cases} > & 0 \\ \neq & 0 \\ < & 0 \end{cases} ; \quad a_2 \begin{cases} > & 0 \\ \neq & 0 \\ < & 0 \end{cases} ; \quad a_4 \begin{cases} > & 0 \\ = & 0 \\ < & 0 \end{cases} .$$

4.4. Branch and Order Defects

Two problems that frequently arise in choosing precision pairs and the input angle range when designing a linkage for function generation and/or motion generation are the *branch defect* and *order defect* problems. The branch defect refers to the situation where a synthesised linkage that meets all mathematical prescribed requirements at each of the precision input angles, but cannot move continuously between all of them without needing to be disassembled from one assembly mode, and reassembled into the other. The order defect is the situation where the linkage can reach all precision poses in the same assembly configuration, but not in the desired order.

As an example of the branch defect, suppose the goal is to generate the following function

$$a_3 = 6\sin(\theta_1) - 1 \tag{11}$$

with an RRRP mechanism over the input angle range of 0°-90°. We choose a uniform distribution of accuracy points over the desired input angle range as

$$v_{1_i} = 0,\ \tan\left(\frac{\pi/4}{2}\right),\ \tan\left(\frac{\pi/2}{2}\right).$$

The values of the output angle parameter, a_3, for each of the specified input angle parameters v_1 are the same as for the previous example

$$\begin{aligned} a_{3_i} &= 6\sin\left(2\tan^{-1}(v_{1_i})\right) - 1 \\ &= -1,\ 3.242640688,\ 5. \end{aligned}$$

We obtain three equations by substituting the IO pairs of each v_{1_i}, a_{3_i} into Equation (3). Solving the three equations for a_1, a_2, and a_4 in Maple yields two distinct solutions where

$$\begin{aligned} &a_1 = 1.500000000, \quad a_2 = 4.609772229, \quad a_4 = -3.000000000, \text{ and} \\ &a_1 = 1.500000000, \quad a_2 = -4.609772229, \quad a_4 = -3.000000000. \end{aligned}$$

We select the first solution.

We can draw the linkage using the selected synthesised link lengths revealing the three poses illustrated in Figure 10a. However, we need to compare a plot of the desired function, where the input angle has been converted to $v_1 = \tan(\theta_1/2)$, to the generated IO curve both in the v_1-a_3 plane. The desired function, over a suitably large range for v_1, and the IO curve generated by the selected synthesised linkage is illustrated in Figure 10b. Note that we can see the structural error; that is the area between the curve of the function and the IO curve in the desired input angle parameter range, i.e. the difference between the specified IO values and the generated IO values over the continuous specified IO range. We observe the first prescribed value for v_1 and corresponding function value for a_3, the blue diamond with coordinates $(0,-1)$ in Figure 10b, lies exactly on the lower assembly mode, or branch. The following two input angle parameter and corresponding specified values for a_3 lie exactly in the upper assembly mode of the selected synthesised linkage. The mechanism cannot generate the function continuously over the desired input angle range without being taken apart and reassembled. This is precisely the branch defect problem. The designer must rethink the precision pose range to attempt to resolve the branch defect.

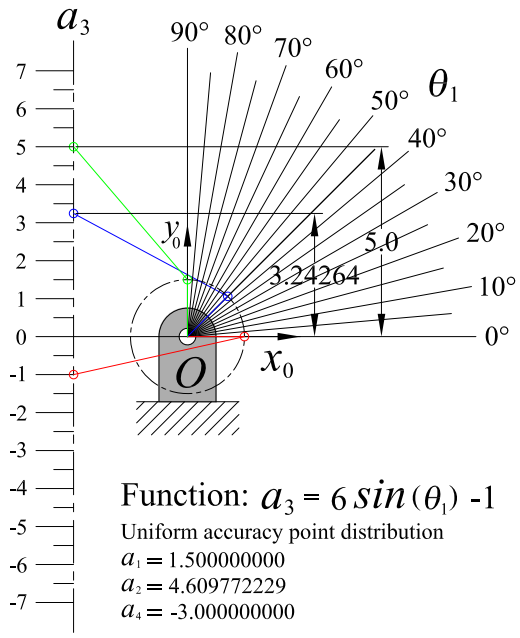

(a) Precision poses for $a_3 = 6\sin(\theta_1) - 1$.

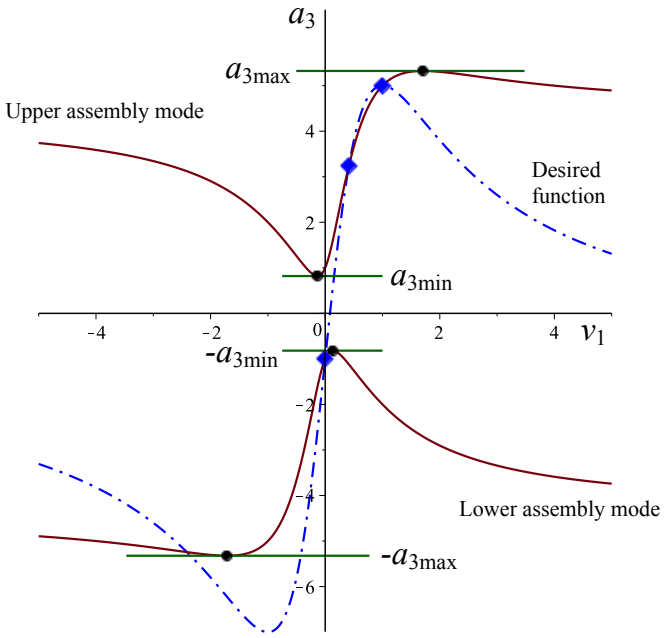

(b) Function and generated IO curve.

Fig. 10. Illustration of branch defect.

5. MULTIPLE POINTS AND ALGEBRAIC CURVES

An *algebraic curve* can be thought of as the path generated by the motion of a point. The curve is algebraic if the path the point traces can be mathematically represented by a polynomial equation in two variables where the coefficients are rational numbers. Planar curves of at least degree three can have multiple distinct branches and locations where the curve intersects itself. Similar statements apply to the algebraic IO curve: since they are degree four they can have multiple closed branches and self-intersect.

5.1. Assembly Modes and Working Modes

If the IO curve has two distinct branches then in order for the linkage to cover points in both branches it must be taken apart and reassembled in a different way. These two distinct linkage configurations, one for each branch of the curve, are called *assembly modes*, and an example of an IO curve with two distinct branches is illustrated in Figure 11a.

Working modes are subtly different. Consider the rocker-slider illustrated in Figure 11b. When the input angle reaches minimum or maximum values the mechanism instantaneously stops moving as the coupler becomes horizontal. Clearly, care must be taken in designing an actuation system for such linkages as the angular velocity of the motor drive shaft must decelerate, stop, and accelerate in the opposite sense in order to start the linkage moving again. In these configurations the mechanism is said to be *locked* because the coupler force line of action is perpendicular to the slider travel direction. The vertical component of force the coupler can transfer from the input link is zero, and even an infinite amount of torque supplied by the actuator at the base of the input link cannot make the slider move. A torsional spring in the R-pair connecting the coupler to the slider, or some other form of force capacitance, must be designed into the joint to make the slider move again, thereby breaking the lock.

Assuming the locking problem has been resolved, then moving away from these minimum or maximum input configurations the coupler can, in the absence of any compelling forces, arbitrarily continue to move

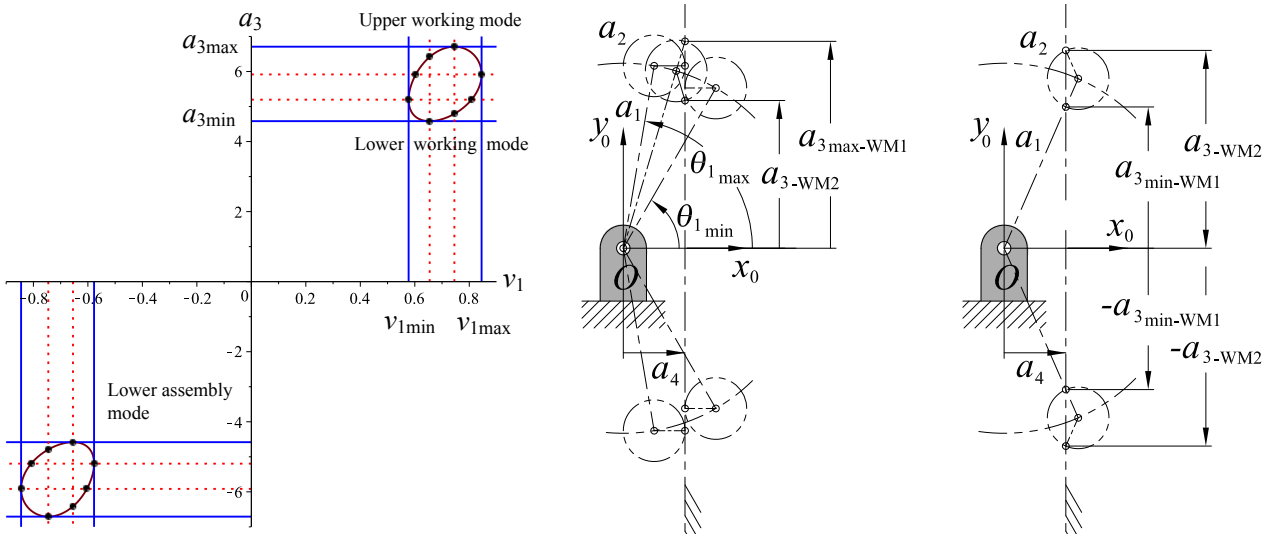

(a) Rocker: $a_1 = 6$, $a_2 = 1$, $a_4 = 2$.

(b) The two assembly and working modes.

Fig. 11. Assembly and working modes for an RRRP.

with a_3 either increasing, or decreasing. In Figure 11a the two assembly modes each have two working modes. The two working modes in each assembly mode are separated by the minimum and maximum input angle parameters which occur at the two vertical tangent points on each IO curve branch and represent $v_{1_{\min}}$ and $v_{1_{\max}}$ in the v_1-a_3 plane. At all other points on the IO curve a vertical line intersects it in an upper value for a_3 and a lower value. These are the working modes, and the branching points between each mode occur at $v_{1_{\min}}$ and $v_{1_{\max}}$.

In one working mode the slider can reach it's maximum value, labelled $a_{3_{\text{max}-\text{WM1}}}$ in Figure 11b, when the input link and coupler, a_1 and a_2, align. Whereas in the other working mode a_3 can't reach it's maximum value, the corresponding position is labelled and $a_{3_{\text{WM2}}}$ in Figure 11b. Note that in general in the plot of the algebraic IO curve of the linkage the slider position $a_{3_{\text{WM2}}}$ is always vertically opposed to $a_{3_{\text{max}-\text{WM1}}}$. This phenomenon can be explained by conceptually removing the R-pair connection between the coupler and slider to create a three link open kinematic chain. Now, at every input angle reachable by the closed RRRP linkage in a particular assembly mode the distal end of the coupler, that would normally be pin-connected to the slider, is free to move on a circle centred at the R-pair attachment to the input link. That circle, for all input angles between $\theta_{1_{\min}}$ and $\theta_{1_{\max}}$, or tangent half-angle parameters $v_{1_{\min}}$ and $v_{1_{\max}}$ in the plot of the IO curve, intersects the centre line of the slider in two points, represented by the vertically opposed points on the algebraic IO curve in the v_1-a_3 plane. Once the coupler has started to move either upward or downward in the slider it must continue on that path until the next input angle extreme is reached. Each of these possible slider directions are called working modes.

Assembly and working modes for specific linkages are easily identified by examining a plot of the algebraic IO curve in the v_1-a_3 plane. Assembly modes correspond to distinct branches of the IO curve. Working modes are similarly easily identified: if a vertical line parallel to the a_3-axis intersects a distinct branch of the IO curve in two points then there are two working modes in that assembly mode. Hence, the rocker-slider IO curve illustrated in Figure 11a has two assembly modes, and each one has two working modes.

All planar RRRP linkages can have multiple assembly and working modes and, it turns out, that certain input link angular displacement limits dictate the numbers. For example rocker-sliders that are non-folding (in a mechanism where the link lengths allow $v_1 = 0$ or π, while at the same time $a_3 = 0$, are said to

fold with the input link and coupler both laying on the x_0-axis) have two assembly modes each possessing two working modes, meaning that there are maximum and minimum input joint angles where the coupler becomes horizontal in the x_0-y_0 plane. Folding rocker-sliders have two assembly modes, each possessing two working modes, which intersect in a common point at the origin, called a *double point*. Two special subsets of rocker-slider are the so called π- and 0-rocker-sliders. All non-folding π-rocker-sliders rock in the range -$\theta_{1_{\min}}$ to $\theta_{1_{\min}}$ crossing the negative x_0-axis through π. Whereas input links that are 0-rockers rock in the range -$\theta_{1_{\max}}$ to $\theta_{1_{\max}}$ crossing the positive x_0-axis through 0. All non folding π- and 0-rocker-sliders each have but one assembly mode that has two working modes. Finally, all non-folding crank-sliders have two distinct assembly modes each having only one working mode and therefore no limits on the crank rotation angle. This discussion is summarised in Table 8, and will be elaborated on in greater depth in Section 6.1 where the same results will be tabulated again for a convenient reference.

Input link	Assembly modes	Working modes
Crank	2	1 in each assembly mode
Rocker	2	2 in each assembly mode
π-rocker	1	2
0-rocker	1	2

Table 8. Assembly and working modes.

5.2. Double Points

Each point of each distinct branch of an algebraic curve possesses at least one distinct tangent. What happens if the curve does not possess distinct branches or if the curve self-intersects? If a curve intersects itself then there must be more than one tangent to the curve at the self-intersection location. How can a point of the curve that possesses two, or more, tangents be classified? In the study of the kinematic geometry of mechanisms [27], and of algebraic differential geometry in general [10, 11], these special locations have important meanings for linkage velocities, accelerations, and jerks. These locations are usually called *multiple points* because there are multiple tangents at that point. They are also called *singular points* because the point is uniquely defined at that location, and hence *singular*. However, work with planar four-bar linkages requires only knowledge of *double points*, locations where a curve intersects itself a single time. A comprehensive account of multiple points can be found in [32] for the interested reader.

There are three species of double point that arise when the tangents to the curve at the double point are either a pair of distinct real lines, a pair of complex conjugate lines, or a pair of real but coincident lines. Methods to analytically identify the presence of double points of an algebraic curve and to determine the class of the double point are discussed next. The type of double point can be used to classify the mobility capability of input link.

To determine the type of double point (regular, isolated, or stationary), if they exist, the numerical value of the *discriminant* [11], a tool from algebraic differential geometry can be used. Planar rational algebraic curves are described by rational algebraic polynomials in two variables where the coefficients are rational numbers. A rational number can always be represented exactly as the ratio of two integers, as opposed to irrational numbers, such as π and $\sqrt{2}$, which cannot. For a rational algebraic equation $f(x,y)$ of degree $n \geq 3$ the double points, if they exist, are the common zeros, i.e. the solutions for (x,y), of the following

three equations:

$$\left.\begin{array}{rcl} f(x,y) & = & 0; \\ \dfrac{\partial f(x,y)}{\partial x} & = & 0; \\ \dfrac{\partial f(x,y)}{\partial y} & = & 0. \end{array}\right\} \tag{12}$$

If a solution exists then the planar algebraic curve self-intersects at the (x,y) coordinates corresponding to the solution(s) of Equations (12).

If the curve intersects itself a single time the corresponding multiple point is called a double point. The curve must possess two tangents at the double point and one unique tangent at every other point. The two tangents can be one of three kinds: two real distinct tangents; two real coincident tangents; or two complex conjugate tangents. If this sounds familiar that is because the discriminant of a quadratic equation determines whether the quadratic has two real distinct solutions, a single solution, or two complex conjugate solutions. Consider the general quadratic equation in a single variable

$$ax^2+bx+c \;=\; 0. \tag{13}$$

If $a \neq 0$ then the roots of Equation (13) are given by the well known quadratic formula

$$x \;=\; \frac{-b \pm \sqrt{b^2-4ac}}{2a}. \tag{14}$$

The discriminant for the quadratic equation in one variable is given by the value of the radicand, the number under the radical sign:

$$\Delta \;=\; b^2-4ac \begin{cases} > & 0 & \Rightarrow & \text{two real distinct roots,} \\ = & 0 & \Rightarrow & \text{one real root,} \\ < & 0 & \Rightarrow & \text{two complex conjugate roots.} \end{cases} \tag{15}$$

Because the equation only contains a single variable the discriminant is said to be of *the first fundamental form* [11].

The discriminant used to identify the type of double (multiple) point for planar algebraic curves in two variables is said to be of *the second fundamental form*, and is given by:

$$\Delta \;=\; \left(\frac{\partial^2 f(x,y)}{\partial x \partial y}\right)^2 - \frac{\partial^2 f(x,y)}{\partial x^2}\frac{\partial^2 f(x,y)}{\partial y^2} \begin{cases} > & 0 & \Rightarrow & \text{two real distinct tangents implies} \\ & & & \text{a } \textit{regular} \text{ double point (crunode);} \\ = & 0 & \Rightarrow & \text{two real coincident tangents implies} \\ & & & \text{a } \textit{stationary} \text{ double point (cusp);} \\ < & 0 & \Rightarrow & \text{two complex conjugate tangents implies} \\ & & & \text{an } \textit{isolated} \text{ double point (acnode).} \end{cases} \tag{16}$$

If a double point exists then it's species is revealed by evaluating Equation (16) at the (x,y) coordinates of the double point.

To illustrate the different nature of the three types of double point consider the following cubic equation

$$y^2 \;=\; (x-a)(x-b)(x-c) \tag{17}$$

where the constant coefficients have rational positive magnitudes such that $a < b < c$. This curve, illustrated in Figure 12a, is symmetric with respect to the x-axis since every value of x gives equal and opposite values of y. The curve intersects the x-axis at the three points $x = a$, $x = b$, and $x = c$. When $x < a$ the value of y^2 is negative, and y is imaginary. When $a < x < b$ then y^2 is positive, and there are two real, equal and opposite values for y. For values of $b < x < c$ the value for y^2 is again negative, and finally positive again for all values $x > c$. The curve therefore consists of a closed oval between a and b and an open branch beginning at c and extending infinitely in two directions beyond it. The curve illustrated in Figure 12a has $a = 2$, $b = 4$, and $c = 5$. These values will now be manipulated to yield examples of the three types of double point.

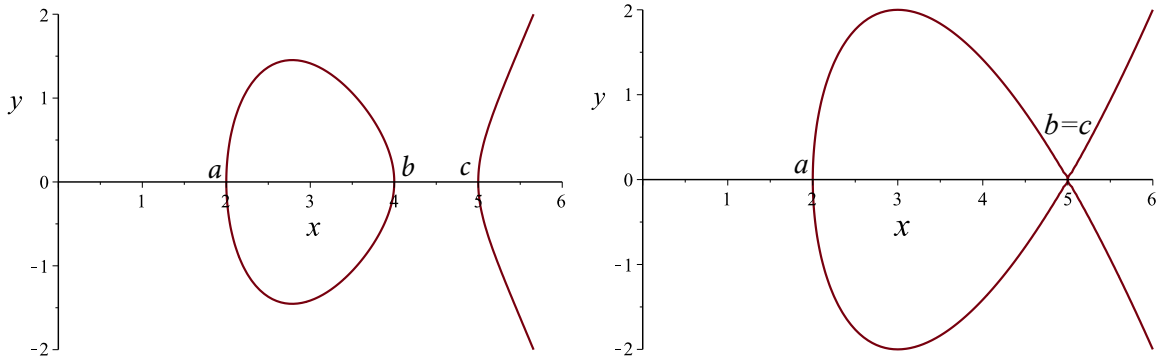

(a) Cubic with two real branches and no double points.

(b) A *regular double point*, or crunode.

Fig. 12. Species of double points: *regular*.

5.3. Regular Double Point (Crunode)

Expanding Equation (17) and collecting the terms in descending powers of x and y leads to a polynomial equation, $f(x,y) = 0$:

$$f(x,y) := \; x^3 - (a+b+c)x^2 + (ab+ac+bc)x - y^2 - abc \quad = \quad 0. \tag{18}$$

Let b vary in magnitude between the range $a \leq b \leq c$. As b increases in value the oval circuit increases in size maintaining it's location at a but growing towards c until $b = c$ and the curve crosses itself. In this example $a = 2$ and $b = c = 5$. Inspecting the curve illustrated in Figure 12b we see that at the double point, or node, the two branches of the curve meet, and each branch has it's own real, distinct tangent. Such a point is called a *regular double point*, or a *crunode*. There is only one common zero of Equation (18) and it's partial derivatives with respect to x and y: $(x,y) = (5,0)$. The discriminant of Equation (18) given by Equation (16) is

$$\Delta \quad = \quad 12x - 48. \tag{19}$$

Evaluating Equation (19) at the double point $(x,y) = (5,0)$ leads to

$$\Delta \quad = \quad 12 \; > \; 0,$$

which is a positive non-zero number, as it must be, since the multiple point is a regular double point, or crunode.

5.4. Isolated Double Point (Acnode, or Hermit Point)

As b moves in the opposite direction towards a, the original oval circuit in Figure 12a now shrinks in size until $b = a$, giving for $a = b = 2$ and $c = 5$

$$x^3 - 9x^2 + 24x - y^2 - 20 \quad = \quad 0. \tag{20}$$

as illustrated in Figure 13a. The cubic now possesses an *isolated double point* at $x = a = b = 2$. Isolated double points, also known as *acnodes* or *hermit points*, satisfy the equation of the cubic but do not appear to lie on the curve. The tangents to the curve at an isolated double point are a pair of complex conjugate lines. No real line through the isolated double point intersects the curve in more than two real points, confirming the necessary condition that a general real line cuts a cubic in three points. The reader should confirm that the common solution to Equation (20) and it's partial derivatives with respect to x and y is $(x, y) = (2, 0)$, and that the discriminant of Equation (20) evaluated at the double point is

$$\Delta \quad = \quad -12 \; < \; 0.$$

The result is a number less than zero, as it must be, since this is an isolated double point, or acnode.

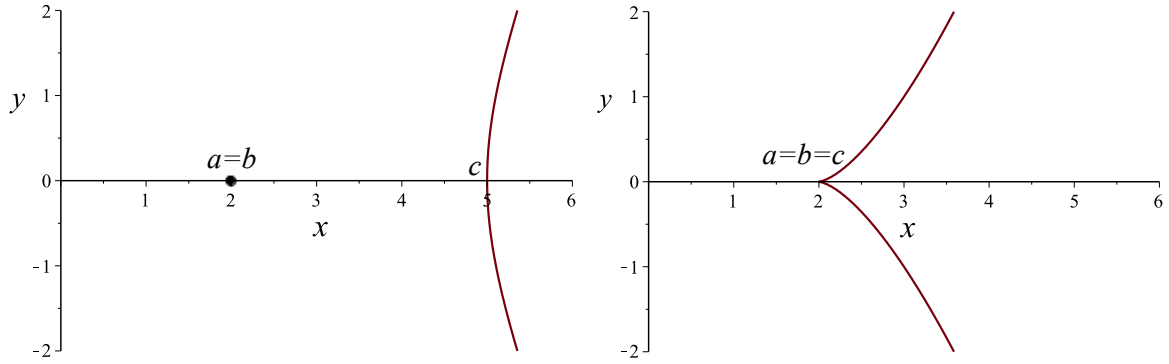

(a) An *isolated double point*, or acnode, or hermit point.

(b) A *stationary double point*, or spinode , or cusp.

Fig. 13. Species of double points: *isolated* and *stationary*.

5.5. Stationary Double Point (Spinode, or Cusp)

The third species of double point occurs if the equation of the tangent to the curve at a point becomes a perfect square. In this case the tangents at the self-intersection point, called a *stationary double point* are two real, but coincident lines. In the case of the cubic in Equation (17), if we allow both coefficients b and c to approach a then the two distinct branches of the curve merge into a single branch when $a = b = c$ and Equation (17) becomes

$$y^2 \quad = (x - a)^3. \tag{21}$$

When expanded and collected in terms of descending powers of x and y then Equation (21) can be expressed as the polynomial equation for $a = b = c = 2$

$$x^3 - 6x^2 + 12x - y^2 - 8 \quad = \quad 0. \tag{22}$$

This situation is illustrated in Figure 13b. The stationary double point where $x = a = b = c$ is also called a *cusp* or a *spinode*. They are called stationary double points because if the curve is generated by the motion

of a point then at a cusp the motion of the point in one direction comes to a stop and changes direction making the velocity of the point instantaneously zero at the stationary double point coordinates. The tangent at the cusp meets the curve in three coincident points at $(a,0)$ in Figure 13b. The reader should confirm that the common solution to Equation (22) and it's partial derivatives with respect to x and y is $(x,y) = (2,0)$, and that the discriminant of Equation (22) evaluated at the double point is

$$\Delta \quad = \quad 0.$$

The differential geometry implied by the discriminant demands that it's value, evaluated at the stationary double point $(x,y) = (2,0)$, is identically equal to zero.

6. INTERPRETING THE PLANAR RRRP ALGEBRAIC IO EQUATION

We are now in a position to interpret the planar RRRP algebraic IO equation. Analysing Equation (3) using the theory of planar algebraic curves [26, 33] one can easily prove that the general algebraic IO equation for planar RRRP linkages has the following three characteristics which are independent of the three constant design parameter lengths a_1, a_2, a_4, and constant angle parameter v_4 [20]. These three properties are true for every planar RRRP mechanism since they are independent of the three link length parameters and constant output angle parameter v_4.

1. Equation (3) is of degree $n = 4$ in variables v_1 and a_3 and is therefore a quartic curve in the plane spanned by v_1 and a_3. The shape characteristics of individual IO curves are determined by the link lengths a_1, a_2, and a_4.

2. The homogeneous form of this quartic curve, Equation (23), contains two double points each located at the intersections with the line at infinity of the v_1- and a_3-axes in the v_1-a_3 plane.

3. The quartic IO curve can have either genus $g = 1$ or $g = 0$. Therefore the maximum number of assembly modes of the associated linkage becomes $m = g + 1$ [14, 34], which is 2 for IO curves of genus 1. It will be shown that IO equations for folding RRRP mechanisms possess genus 0, while all other non-folding planar RRRP mechanisms have quartic IO curves that are genus 1.

These three characteristics are now proved to be true for all non-degenerate planar RRRP linkages. The first item is obvious by inspection. Only the constant term and terms of degree $n = 2$ are multiplied by coefficients containing constant link length parameters, while the term of degree $n = 4$ can only vanish if either variable v_1 or a_3 instantaneously become zero. For a planar RRRP mechanism to have mobility neither a_1 nor a_2 can be zero, so only coefficients A and B have the ability to vanish. If either, or both, vanish the degree of the IO equation is not reduced, hence the algebraic IO equation is always of degree $n = 4$.

The proof of the second item requires that Equation (3) be homogenised because the double points are located at infinity. This involves using an arbitrary homogenising coordinate, which will be called w, such that the two variables v_1 and a_3 are redefined to be the ratios $v_1 = v_1/w$ and $a_3 = a_3/w$ in Equation (3). When the result is multiplied by w^4, so that the variables are no longer ratios, one obtains

$$k_h := \; v_1^2 a_3^2 + A v_1^2 w^2 + a_3^2 w^2 - 4 a_1 v_1 a_3 w^2 + B w^4 \quad = \quad 0. \tag{23}$$

Now, every term in Equation (23) is homogeneously of degree $n = 4$ in the homogeneous variables v_1, a_3, and w. The presence of the homogeneous coordinate w conceptually extends the Euclidean plane to a bounding line at infinity that encloses the entire plane. The plane of the linkage is now infinite in extent yet bounded by an infinitely distant line. The line at infinity in the projective extension of the Euclidean plane of the RRRP linkage can be accessed mathematically when the homogenising coordinate is $w = 0$. Any

point on the line at infinity of the coordinate plane v_1 and a_3 extended by the homogenising coordinate w is expressed by ratio-type coordinates as $(v_1 : a_3 : w) = (v_1 : a_3 : 0)$. It is vitally important to remember that the origin of the projective extension of the IO parameter plane v_1, a_3 is expressed by $(0 : 0 : 1)$. The point corresponding to the set of ratios $(0 : 0 : 0)$ is undefined in the projective extension of the Euclidean plane and, therefore, does not exist.

We can think of projective geometry as Euclidean geometry with some axioms "left out", or changed. For instance there are no parallel lines, and no way to measure angles, or the distance between points. Parallel lines in the Euclidean plane maintain the same distance and extend infinitely, without bound, in two directions and never intersect. While we live in a 3D Euclidean space where parallel lines do exist and never intersect, the geometry of our vision contradicts this fact. Consider standing on a set of parallel train tracks. The centre lines of each rail are parallel lines in the plane where they exist, see Figure 14b, and certainly never intersect. If they did gradually become closer and closer, until they finally intersected, any train with wheels on constant length axles travelling on these tracks would surely derail!

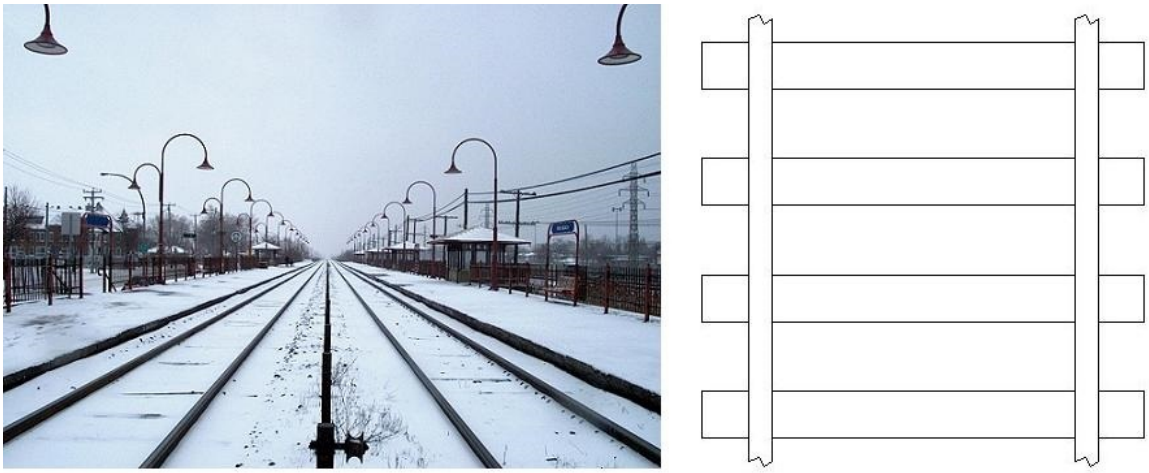

(a) (b)

Fig. 14. (a) What we see. (b) What is really there.

But consider what we actually see in the image of the train tracks in Figure 14a: the tracks appear to become closer to each other until they intersect at a point on the horizon. In fact, the power lines, fence lines, and lamp lines also appear to converge to and intersect in the very same point. In the geometry of our vision, which is the projective extension of the Euclidean space, the horizon line corresponds to the line at infinity $w = 0$, and is labelled L_∞. Consider Figure 15: in that figure points A and B lie on line r while points C and D lie on line s. The human eye in Figure 15 is located at the vantage point, while the conceptual plane of vision is pierced by lines r and s at points A and C, respectively. In the plane of vision the projected points B' and D' appear to be closer together than the actual points. Moreover, the projections of lines r and s appear to intersect in a point on a line orthogonal to their directions. This line is, conceptually, the line at infinity L_∞. We can actually analyse the geometry implied by different points at infinity by simply setting $w = 0$.

As discussed in Section 5 planar curves of degree $n \geq 3$ can self-intersect. The double points of Equation (23), that is the locations where the curve intersects itself, if they exist, are determined by solving Equation (23) together with its three partial derivatives with respect to the three variables v_1, a_3, and w.

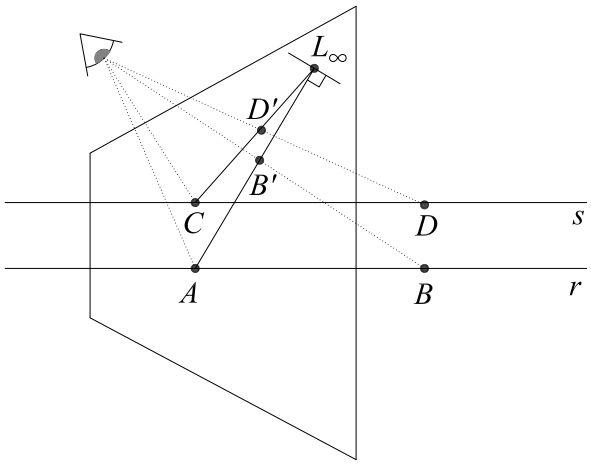

Fig. 15. The parallel lines of a pair of train tracks appear to converge to a point on a third line, the *horizon*, or the *line at infinity*, L_∞.

These three partial derivative equations are three homogeneous equations of degree three:

$$\left.\begin{array}{rcrcl} \dfrac{\partial k_h}{\partial v_1} & = & 2v_1a_3^2 + 2Av_1w^2 - 4a_1a_3w^2 & = & 0; \\ \dfrac{\partial k_h}{\partial a_3} & = & 2v_1^2a_3 + 2a_3w^2 - 4a_1v_1w^2 & = & 0; \\ \dfrac{\partial k_h}{\partial w} & = & 2Av_1^2w + 2a_3^2w - 8a_1v_1a_3w + 4Bw^3 & = & 0. \end{array}\right\} \tag{24}$$

Equation (23) and Equations (24) possess only two common solutions, excluding the legitimate algebraic, but undefined, solution of $(v_1 : a_3 : w) = (0 : 0 : 0)$, which are independent of the link lengths a_1, a_2, a_4, and the slider inclination angle v_4:

$$(v_1 : a_3 : w) \;=\; (1 : 0 : 0)\,;\;\; (0 : 1 : 0)\,. \tag{25}$$

The first double point, $(v_1 : a_3 : w) = (1 : 0 : 0)$, is located where every line parallel to the direction of the v_1-axis intersects the line at infinity in both the positive and negative directions parallel to v_1. The second, $(v_1 : a_3 : w) = (0 : 1 : 0)$, is located where every line parallel to the direction of the a_3-axis intersects the line at infinity in both the positive and negative directions parallel to a_3. These two double points, both located at infinity because $w = 0$ for each point, are common to all algebraic IO curves for every planar RRRP four-bar mechanism because they are independent of link lengths. Any individual planar RRRP IO curve can possess at most one additional double point whose existence depends on sums and differences of link lengths a_1, a_2, and a_4.

The proof of the first part of the third claim relies on the fact the algebraic IO equation for every RRRP linkage contains the same two double points. The *genus g* of an algebraic curve is defined as the difference between the maximum number of double points, $DP_{\max}$, for a curve of it's order and the actual number of double points, DP_{act}, the curve possesses [27]. The genus is conveniently expressed by the following equation

$$g \;=\; DP_{\max} - DP_{\text{act}}. \tag{26}$$

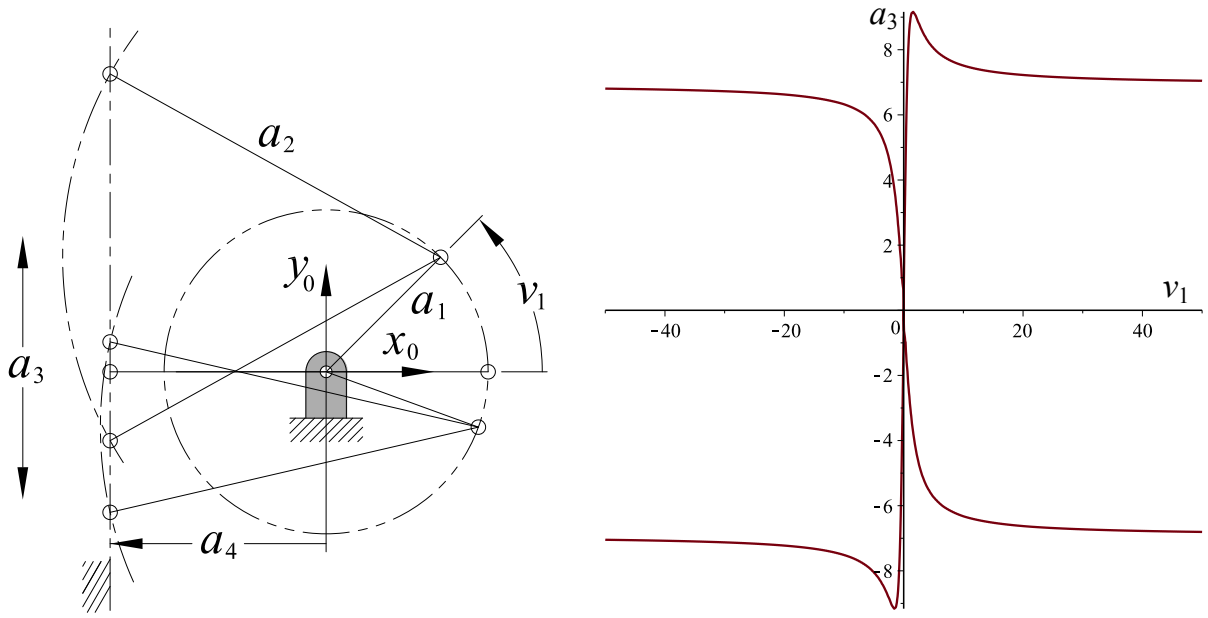

(a) A folding RRRP crank-slider.

(b) IO curve of folding RRRP crank-slider.

Fig. 16. A folding RRRP transition crank with $a_1 = 3$, $a_2 = 7$, and $a_4 = -4$.

The genus of an algebraic curve is therefore an integer greater than or equal to zero: $g \geq 0$.

It is well known [32] that the maximum number of double points, $DP_{\max}$, a curve of order n can have is

$$DP_{\max} \quad = \quad \frac{1}{2}(n-1)(n-2). \tag{27}$$

Hence, a curve of order $n = 4$ can have a maximum of three double points. The algebraic IO curve for every planar RRRP linkage possesses at least two as proved by the existence of only a pair common solutions to Equations (23) and (24), therefore it can never be deficient by more than one. In other words, the genus of the planar RRRP linkage algebraic IO curve is always at most

$$g \quad = \quad 3-2 \quad = \quad 1. \tag{28}$$

The second part of the third claim is proved by the answer to the question: are there any values of a_1, a_2, and a_4 that lead to an IO curve with a third real finite double point and genus $g = 0$? It turns out that there are several ways this can occur. Foldable crank-sliders require that both $v_1 = 0$, $a_3 = 0$, and that coefficient $B = 0$. Since there are no real values of the link lengths that lead to both $B_1 = 0$ and $B_2 = 0$ simultaneously, then either $a_2 = a_1 + a_4$ or $a_2 = a_1 - a_4$. These are the exact conditions required for an RRRP linkage that can fold with links a_1, a_2, and of course a_4, all aligned on the x_0-axis. Such linkages are called *transition linkages* since they have only one assembly mode, but two distinct ranges of motion. The input link is a crank, but the output link is restricted to two ranges: $a_3 \geq 0$ or $a_3 \leq 0$. In the folded configuration $a_3 = 0$ implying that the mechanism can transition between either range of motion. See the end of Section 8 for the link length requirements for foldable 0- and π-rockers.

A folding crank-slider RRRP mechanism is illustrated in Figure 16a where $a_1 = 3$, $a_2 = 7$, and $a_4 = -4$. It is very important to note that $a_4 < 0$, called the *offset distance* of the centre line of the P-pair from the origin of the $x_0 - y_0$ coordinate system, is a real number that is less than zero. The directed length a_4 can be positive, negative, and even zero. However, the values of the directed lengths a_1 and a_2 can only be greater

than or less than zero, but never zero. If either, or both, $a_1 = 0$ and $a_2 = 0$ the resulting linkage is a rigid structure that has no mobility. A folding RRRP mechanism has link lengths that allow it to fold when $v_1 = 0$ and $a_3 = 0$ making a_1 and a_2 align with a_4 on the x_0-axis. From the folded configuration where $a_3 = 0$ the coupler can transition into either motion range. It's IO curve has the finite double point at the IO curve origin $(v_1, a_3) = (0,0)$, as illustrated in Figure 16b. The folding configuration occurs at the double point on the origin where both $v_1 = 0$ and $a_3 = 0$. The double point can be approached from any path along the IO curve and may be exited along any one of four paths as well, nicely illustrating the transition behaviour. As can be seen in the mechanism's IO curve in Figure 16b, for any specified value of v_1 there are two possible values for a_3 and for any desired value for a_3 there are two possible values for v_1 with the exception of the double point. The folding behaviour suggests that predicting and controlling the direction the slider moves in as the input angle rotates through 360° is not possible without additional springs, stops, or other passive mechanical components.

All RRRP linkages that are not foldable possess IO curves that are genus 1 and therefore the linkages possess a maximum of two distinct assembly modes.

6.1. Identifying the Type of Double Point

The reason for considering all this seemingly outlandish mathematics from the world of algebraic geometry [35] is that it leads to very elegant and easy to manipulate algebraic tools that are completely free from the chains of trigonometric analysis [20]! The type of double points of a particular algebraic IO equation, in part, implies every possible limit, if they exist, on the rotation of the input link a_1 and motion limits of the output link a_3. This information, obtained at an almost trivial computational expense, is a powerful and completely new design and analysis tool for four-bar mechanisms! Here we limit ourselves to planar RRRP linkages, but these tools apply to every possible four-bar linkage that generates motion in the plane, on the surface of a sphere, and in 3D space!

In general, double points can have real or complex (imaginary) tangents depending on the values of the three constant link lengths a_1, a_2, and a_4, which in turn helps determine the limits of the mobility of the linkage. Here a subtly different form of the discriminant is used compared to Equation (16) in Section 5.2 because homogenous coordinates are used here to identify double points at infinity. The discriminant of Equation (23), evaluated at a double point, reveals whether that double point has a pair of real or complex conjugate tangents [10] in turn yielding information about the topology of the mechanism [14]. To keep track of the coordinates used in Equation (29) let $(x_1 : x_2 : x_3) = (v_1 : a_3 : w)$. The discriminant and the meaning of its value are [10, 11]

$$\Delta = \left(\frac{\partial^2 k_h}{\partial x_i \partial w}\right)^2 - \frac{\partial^2 k_h}{\partial x_i^2}\frac{\partial^2 k_h}{\partial w^2} \begin{cases} > 0 \;\Rightarrow\; \text{regular double point (crunode)}, \\ = 0 \;\Rightarrow\; \text{stationary double point (cusp)}, \\ < 0 \;\Rightarrow\; \text{isolated double point (acnode)}. \end{cases} \tag{29}$$

The discriminant of the homogeneous IO equation of a planar RRRP linkage, Equation (23), evaluated at the point at infinity $(v_1 : a_3 : w) = (1 : 0 : 0)$ on the v_1-axis is obtained by setting $i = 2$ in Equation (29), i.e. ∂a_3, while the discriminant evaluated at the other point at infinity on the a_3-axis is obtained by setting $i = 1$

in the discriminant equation, i.e. ∂v_1, giving

$$\Delta_{v_{1_{a_4\geq 0}}} = \left(\frac{\partial^2 k_h}{\partial a_3 \partial w}\right)^2 - \frac{\partial^2 k_h}{\partial a_3^2}\frac{\partial^2 k_h}{\partial w^2} = -4A_1A_2 = -4(a_1+a_2+a_4)(a_1-a_2+a_4), \quad (30)$$

$$\Delta_{v_{1_{a_4<0}}} = \left(\frac{\partial^2 k_h}{\partial a_3 \partial w}\right)^2 - \frac{\partial^2 k_h}{\partial a_3^2}\frac{\partial^2 k_h}{\partial w^2} = -4B_1B_2 = -4(a_1+a_2-a_4)(a_1-a_2-a_4), \quad (31)$$

$$\Delta_{a_3} = \left(\frac{\partial^2 k_h}{\partial v_1 \partial w}\right)^2 - \frac{\partial^2 k_h}{\partial v_1^2}\frac{\partial^2 k_h}{\partial w^2} = -4. \quad (32)$$

The value of Equation (32) is always negative regardless of the link lengths and the double point at the intersection of the line at infinity $w = 0$ and the direction of translation of the P-pair slider is always an isolated double point. The fact that this double point is always an acnode is reassuring since it means that the slider of the P-pair always possesses finite translation limits. This is because the acnode is an isolated double point at infinity on every a_3-axis. Because it is an isolated point means that while the linear travel of the slider of the associated P-pair might be very large, it is never infinite. The algebraic IO curves for RRRP linkages where the input link is a crank, 0-rocker, π-rocker, and rocker are illustrated in Figure 17. With some imagination, the four distinct curves in the v_1-a_3 coordinate plane illustrate the double points along the coordinate axes at infinity: the one on the a_3-axis is clearly always an isolated double point that does not appear to be on the curve even though its coordinates satisfy the algebraic equation of the IO curve.

The discriminant for the double point $(v_1 : a_3 : w) = (1 : 0 : 0)$ at the intersection of the line at infinity $w = 0$ and the R-pair axis in Equation (30) will be positive, negative, or identically zero depending on the numerical values of the a_i. Certainly, the classification of the mobility of the input and output links is determined by these values. However, this is still ongoing research and the fine details are not quite ready to be used as design tools in MAAE 3004. We will instead consider design and analysis tools that are derived from the kinematic geometry of the mechanism and the derivatives of the planar RRRP algebraic IO equation in Section 7.

The plots of the IO curves in Figure 17 reveal general information regarding the topology of the associated linkages. Figure 17a reveals that the crank-slider has two distinct assembly modes and that the input link is a crank in each. Looking at each distinct branch of the IO curve we can see that v_1 commences at $v_1 = \tan -\pi/2 = -\infty$, passes through $v_1 = 0$, and proceeds to $v_1 = \tan \pi/2 = \infty$, confirming the ability of the link to traverse both π and 0, thereby indicating that it is indeed a crank. Even though the double point at infinity on the v_1-axis for this linkage is regular because $\Delta_{v_{1_{a_4\geq 0}}} > 0$ meaning that there are no limits on the input link angle, the linkage can't branch between assembly modes when $\theta_1 = \pm\pi$. The linkage must be physically disassembled to change assembly modes. Moreover, there are no perpendicular tangents to either branch of the IO curve that are vertical (parallel to the a_3-axis meaning that each assembly mode has but one working mode.

Figure 17b reveals the linkage is a π-rocker with one assembly mode and two working modes that can traverse $v_1 = \pm\infty$, but not $v_1 = 0$. The input link rocks between $\pm\theta_{1_{\min}}$. Since the double point at infinity on the v_1-axis for this linkage is an acnode (isolated) because $\Delta_{v_{1_{a_4\leq 0}}} < 0$, and hence there is a finite limit on input link rotation. Moreover, in the configuration where the input joint angle is $\theta_{1_{\min}}$, the coupler aligns with the x_0-axis, which is called an *input singularity*. In this configuration, in the absence of external compelling forces, the linkage can arbitrarily switch between working modes thereby exhibiting unpredictable slider displacement, see the left side of Figure 18. All RRRP linkages whose input link is a rocker exhibit this type of singularity, which is discussed further in Section 7.

Figure 17c reveals the linkage is a 0-rocker with one assembly mode and two working modes that can traverse $v_1 = 0$, but not $v_1 = \pm\infty \Rightarrow \theta_1 = \pm\pi$. The two working modes are not immediately obvious looking

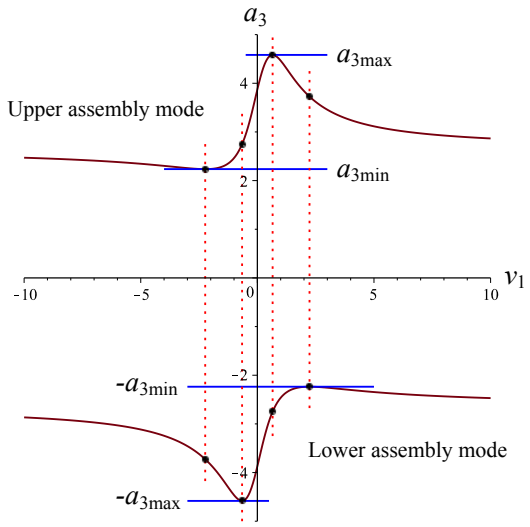

(a) Crank: $a_1 = 1$, $a_2 = 4$, $a_4 = 2$. Note that v_1 can reach infinity, corresponding to π radians, where it reaches the regular double point on the v_1-axis from two directions and returns to pass through $v_1 = 0$. **Crank-sliders have two assembly modes with one working mode in each**.

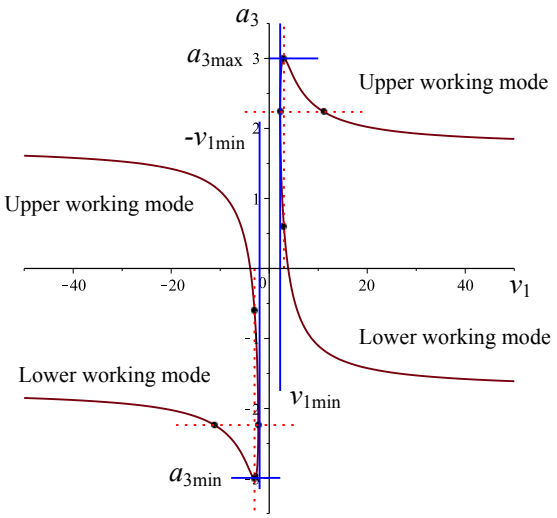

(b) π-rocker: $a_1 = 3$, $a_2 = 2$, $a_4 = -4$. Note that v_1 can reach infinity, corresponding to π radians where it passes through an isolated double point, from two directions, but cannot cross $v_1 = 0$. **π-rocker-sliders have one assembly mode with two working modes**.

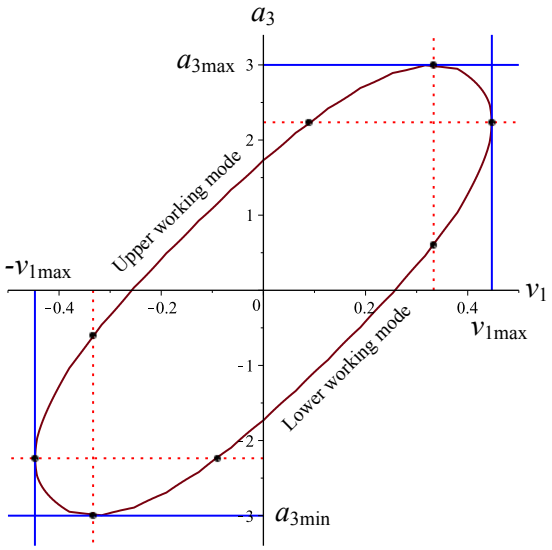

(c) 0-rocker: $a_1 = 3$, $a_2 = 2$, $a_4 = 4$. **0-rocker-sliders have one assembly mode with two working modes**.

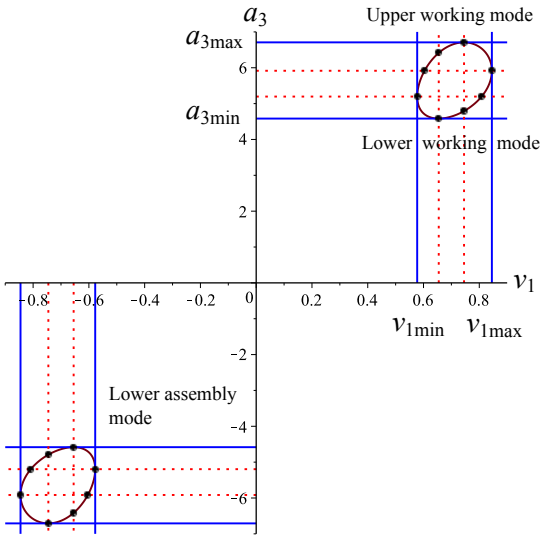

(d) Rocker: $a_1 = 6$, $a_2 = 1$, $a_4 = 2$. **Rocker-sliders have two assembly modes with two working modes in each**.

Fig. 17. IO curves in the v_1-a_3 coordinate plane.

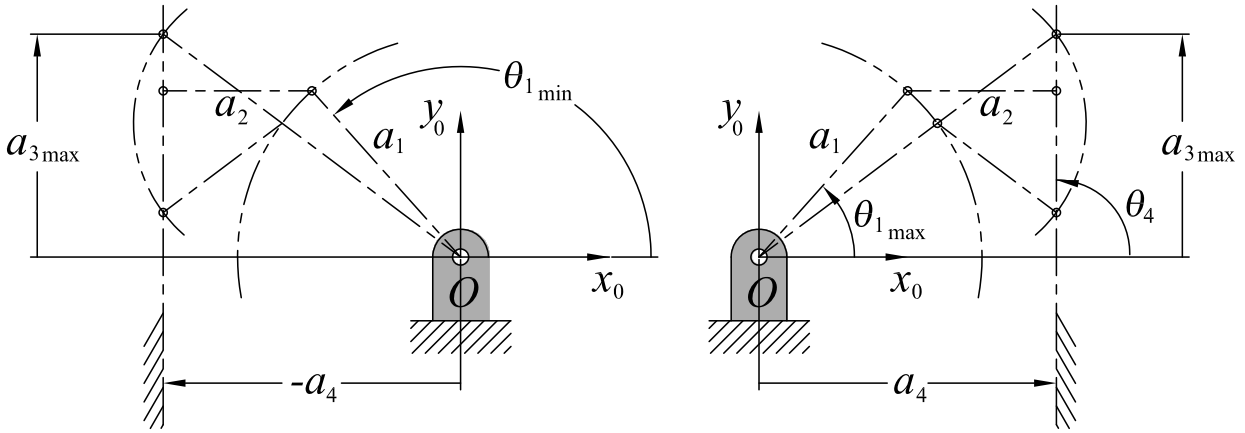

Fig. 18. A π-rocker and a 0-rocker each with one assembly mode but two working modes.

at the IO curve. It is a continuous curve suggesting that only one working mode exists. The two working modes manifest themselves as two distinct ranges of motion. Consider the 0-rocker schematically illustrated in the right side of Figure 18. This linkage has the link lengths $a_1 = 3$, $a_2 = 2$, and $a_4 = 4$. From the unique configuration required by the maximum possible input angle, $\theta_{1_{\max}}$, where the coupler is horizontal, as the input link changes it's sense of rotation from counter-clockwise to clockwise, the output slider can either move upward to $a_{3_{\max}}$ where the input link a_1 and coupler a_2 align, or instead move downward to the lower position indicated in Figure 18. The only way a designer can ensure that the slider moves in the desired working mode, either upward or downward from the horizontal when the input is at $\pm\theta_{1_{\max}}$ is by the addition of stops, springs, or other passive elements to ensure the desired motion of the slider. The branch points between working modes are observable in Figure 17c where the IO curve tangents are vertical, which occurs at $\pm v_{1_{\max}}$.

Finally, Figure 17d reveals a rocker with two working modes in each of two assembly modes that can traverse neither $v_1 = \pm\infty$ nor $v_1 = 0$. The link lengths are $a_1 = 6$, $a_2 = 1$, and $a_4 = 2$. As will be discussed in Section 7, there exist both maximum and minimum input angles for this linkage, and it rocks within a relatively small range restricted by the closed interval between 0 and π. Clearly, the linkage must be disassembled to move from the positive min/max input angles to the lower negative min/max values. The maximum value for the input angle can be obtained using the trigonometric relation

$$\theta_{1_{\max}} \;=\; \cos^{-1}\left(\frac{a_4 - a_2}{a_1}\right) \;=\; \pm 80.40593177^\circ,$$

while the minimum input angle can be similarly computed as

$$\theta_{1_{\min}} \;=\; \cos^{-1}\left(\frac{a_4 + a_2}{a_1}\right) \;=\; \pm 60^\circ.$$

However, we will see that we can rid ourselves of the chains of trigonometry with the differential approach outlined in Section 7 to obtain the extreme values for a_3 and those of v_1, if they exist, with a simple function evaluation. Compare the results here to the comprehensive results expressed in Equation (61) in Subsection 7.3.4 obtained using differential calculus.

The results of the discussion on assembly and working modes are summarised in Table 9.

Input link	Assembly modes	Working modes
Crank	2	1 in each assembly mode
Rocker	2	2 in each assembly mode
π-rocker	1	2
0-rocker	1	2

Table 9. Assembly and working modes.

7. COMPUTING EXTREMA USING DIFFERENTIAL CALCULUS: SINGULARITY ANALYSIS

The slider translation limits always exist since the double point at infinity on the a_3-axis in the v_1-a_3 plane is always an isolated point. However, the existence of $v_{1_{\text{min/max}}}$ depends on link length conditions. The values for $a_{3_{\text{min/max}}}$ and $v_{1_{\text{min/max}}}$, if these exist, can be easily determined using differential calculus, which reveals a completely trigonometry-free classification scheme for the input and output link mobility of planar RRRP linkages.

In addition, $a_{3_{\text{min/max}}}$ and $v_{1_{\text{min/max}}}$ are directly linked to determining mechanical and mathematical singularities: singular configurations of the linkage. The study of singular configurations is not trivial and fills numerous articles, books, and also lead to many discussions among kinematicians. They all agree though that if a mechanism approaches a singular configuration, the mechanism becomes uncontrollable because the DOF of the mechanism instantaneously changes, and thus, must be addressed! A mechanical singularity, if it exists, is defined to be a configuration of a mechanism where the subsequent behaviour of the mechanism as it exits the singularity, if it can, is not predictable, or the forces or torques required to leave the singularity become either infinite or nondeterministic.

When the underlying engineering equations of a mechanism or machine are evaluated at the singular configuration (if any exists), then those equations exhibit mathematical singularity. Singularities can be obtained by examining the tangent space of the IO-equation $F(v_1, a_3) = 0$. Since F is, in general, an n-dimensional implicit function of the input and the output variables, the tangent space can be evaluated by taking the derivative of the IO equation with respect to time and is defined as [36]:

$$\mathbf{J}_{\mathrm{O}}\dot{a}_3 + \mathbf{J}_{\mathrm{I}}\dot{v}_1 \;=\; 0, \tag{33}$$

where

$$\mathbf{J}_{\mathrm{O}} \;=\; \frac{\partial F}{\partial a_3}, \text{ and } \mathbf{J}_{\mathrm{I}} \;=\; \frac{\partial F}{\partial v_1}. \tag{34}$$

The determinants of the input Jacobian $\mathbf{J}_{\mathrm{I}}$ and the output Jacobian $\mathbf{J}_{\mathrm{O}}$ can be used to classify the linkage's singular configurations. There are three different singularity groups.

1. If $\det(\mathbf{J}_{\mathrm{I}}) = 0$ the linkage is in an **input singularity**, also referred to an inverse-kinematics singularity. For a serial robot arm this occurs at the workspace boundary where the arm is completely stretched out. In the example of the RRRP, it can be used to determine $a_{3_{\text{min/max}}}$. In this position the linkages loses one, or more, degrees of freedom and is said to be *locked*.

2. If $\det(\mathbf{J}_{\mathrm{O}}) = 0$ the linkage is in an **output singularity**, also referred to direct-kinematics singularity. This configuration occurs when the input link is at a dead-point where the rotation of the input link must change direction. Thus, in the example of the RRRP, it can be used to determine $v_{1_{\text{min/max}}}$. In this configuration the linkage gains a degree of freedom.

3. If both $\det(\mathbf{J}_{\mathrm{I}}) = 0$ and $\det(\mathbf{J}_{\mathrm{O}}) = 0$ the linkage is in a **combined singularity**. This typically requires special link lengths.

7.1. Computing $v_{1_{\text{crit}}}$ to Determine $a_{3_{\text{min/max}}}$: Input Singularity

To determine $a_{3_{\text{min/max}}}$ we must first determine the critical values of v_1 which will be labelled as $v_{1_{\text{crit}}}$. Solving the RRRP algebraic IO equation for a_3 yields two solutions, which are the two working modes within each assembly mode:

$$a_3 = \frac{(2a_1v_1) \pm \sqrt{-\left((a_1-a_2+a_4)v_1^2-a_1-a_2+a_4\right)\left((a_1+a_2+a_4)v_1^2-a_1+a_2+a_4\right)}}{v_1^2+1},$$

which can be represented more compactly as

$$a_3 = \frac{(2a_1v_1) \pm \sqrt{-\left(A_2v_1^2-B_1\right)\left(A_1v_1^2-B_2\right)}}{v_1^2+1}. \tag{35}$$

Now our algebraic IO equation is expressed as $a_3 = f(v_1)$. The minimum and maximum values for a_3 are obtained by computing the critical values $v_{1_{\text{crit}}}$ of Equation (35). These critical values, if they exist, cause the derivative of a_3 with respect to v_1 to vanish:

$$\frac{\partial a_3}{\partial v_1} = 0. \tag{36}$$

The symbolic form of this derivative results in a very large and cumbersome expression which can be easily computed using a computer algebra software, such as Maple, but it is not of any utility to display it here. Rather, the values of v_1 that cause Equation (36) to be true are what is important. They are generally called the *critical values* of the function in Equation (35). The critical value equations of $v_{1_{\text{crit}}}$ for Equation (36) were computed using Maple, but could be obtained by hand with skill, determination, and patience; they are:

$$v_{1_{\text{crit}_1}} = \pm\frac{\sqrt{(a_1+a_2+a_4)(a_1+a_2-a_4)}}{a_1+a_2+a_4} = \pm\frac{\sqrt{A_1B_1}}{A_1}; \tag{37}$$

$$v_{1_{\text{crit}_2}} = \pm\frac{\sqrt{(a_1-a_2+a_4)(a_1-a_2-a_4)}}{a_1-a_2+a_4} = \pm\frac{\sqrt{A_2B_2}}{A_2}. \tag{38}$$

Equation (35) for any particular assemblable and movable RRRP mechanism will evaluate to extreme values of a_3 at $v_{1_{\text{crit}}}$ as $a_{3_{\text{min/max}}} = f(v_{1_{\text{crit}}})$. Because the double point at infinity on the a_3-axis in the v_1-a_3 plane is isolated (an acnode) then at least one of the critical values of v_1 from Equations (37) or (38) must always exist (in other words, be real numbers): $v_{1_{\text{crit}_1}}$ and $v_{1_{\text{crit}_2}}$ cannot simultaneously be complex (imaginary numbers where the radicand is less than zero). Consider the radicands in each equation. Depending on the signed link lengths $\pm a_1$, $\pm a_2$, and $\pm a_4$, it can be shown that the radicands of $\sqrt{A_1B_1}$ and $\sqrt{A_2B_2}$ cannot simultaneously be complex.

Consider for a moment only positive link lengths. Clearly, the factor A_1 must be greater than zero. Moreover, if $B_1 < 0$ then $a_4 > a_1 + a_2$ resulting in a linkage that can't be assembled, see Figure 19. In fact, $B_1 > 0$ represents the *validity condition* for positive link lengths stating that for an assemblable and moveable planar RRRP linkage it must be that

$$a_4 < a_1 + a_2. \tag{39}$$

However, in the general case the link lengths are directed line segments: their values can be positive or negative. The slider offset distance a_4 can additionally be identically zero. The conclusion is that all four linear factors of the IO curve, A_1, A_2, B_1, and B_2, must be used to determine and classify the mobility of the mechanism.

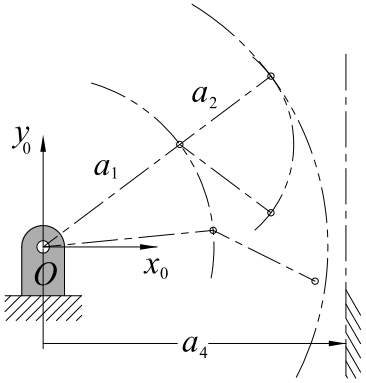

Fig. 19. An unassemblable RRRP because $a_4 > a_1 + a_2$.

7.2. Computing $a_{3_{\text{crit}}}$ to Determine $v_{1_{\text{min/max}}}$: Output Singularity

The classification scheme for the angular displacement limits of the input link a_1 depends on the critical values of a_3, abstractly labelled as $a_{3_{\text{crit}}}$. We shall see that these angular limits for the input angle parameter $v_{1_{\text{min/max}}}$, if they exist, depend only on the numerical values of the four linear factors A_1, A_2, B_1, and B_2 which can be either positive, zero, or negative. If the algebraic IO curve possesses no vertical tangents then input link joint angle limits do not exist. To identify the critical values of a_3 we must first solve the RRRP algebraic IO equation for v_1, rearranging the algebraic IO equation as the function $v_1 = f(a_3)$. There are two solutions, which represent the two possible assembly modes of the mechanism:

$$v_1 = \frac{(2a_1a_3) \pm \sqrt{-(a_1^2+a_2^2-a_3^2-a_4^2+2a_1a_2)(a_1^2+a_2^2-a_3^2-a_4^2-2a_1a_2)}}{a_1^2+2a_1a_4-a_2^2+a_3^2+a_4^2}. \tag{40}$$

We now equate the partial derivative of v_1 with respect to a_3 to zero:

$$\frac{\partial v_1}{\partial a_3} = 0. \tag{41}$$

The critical value equations are:

$$a_{3_{\text{crit}_1}} = \pm\sqrt{(a_1+a_2+a_4)(a_1-a_2-a_4)} = \pm\sqrt{A_1B_2}; \tag{42}$$

$$a_{3_{\text{crit}_2}} = \pm\sqrt{(a_1-a_2+a_4)(a_1+a_2-a_4)} = \pm\sqrt{A_2B_1}. \tag{43}$$

If the critical values of a_3 exist then the angular displacement limits of the input link are computed as $v_{1_{\text{min/max}}} = f(a_{3_{\text{crit}}})$. It is to be seen that the existence of $a_{3_{\text{crit}}}$ requires either, or both, of Equations (42) and (43) to be real valued.

7.3. Examples

We will now compute the extrema for the a_1 input link angles and the a_3 slider translation for the four IO curves illustrated in Figure 17. This novel solution technique reveals the extrema of both working modes in each assembly mode, something which, the best knowledge of the authors, is not to be found in the existing literature with the exception of [36]. In that paper the author use the derivatives of the trigonometric form of the input-output correlation, they do not to explicitly identify the assembly and working mode solutions, rather only the forward kinematics solutions.

7.3.1. Crank

The extrema for the crank IO curve illustrated in Figure 17a will now be computed: the link lengths are $a_1 = 1$, $a_2 = 4$, and $a_4 = 2$. Observe that the curve possesses no vertical tangents, hence there this crank has two assembly modes, but only one working mode in each. To obtain the critical values of v_1 we obtain the function $a_3 = f(v_1)$:

$$a_3 = \frac{2v_1 + \pm\sqrt{7v_1^4 + 26v_1^2 + 15}}{v_1^2 + 1}. \tag{44}$$

Next, the partial derivative $\partial a_3/\partial v_1$ is computed, equated to zero, and solved for $v_{1_{\text{crit}}}$ yielding solutions for each assembly mode (note, linkages of this type have two assembly modes but onle one working mode in each):

$$v_{1_{\text{crit}_1}} = -2.236067977,\ 0.6546536709; \tag{45}$$

$$v_{1_{\text{crit}_2}} = 2.236067977,\ -0.6546536709. \tag{46}$$

The corresponding four limiting values of a_3 are obtained by back substituting the values of $v_{1_{\text{crit}}}$ into Equation (44). In this case, the computed values of $a_{3_{\text{min}}}$ and $a_{3_{\text{max}}}$ in each assembly mode has an associated value for a_3 in the opposite assembly mode. This unexpected algebraic behaviour is explicitly revealed by $v_{1_{\text{crit}}}$. The limiting values are listed in Table 10, and illustrated in Figure 20. Note that in the figure the two assembly modes are abbreviated as "AM1" and "AM2", while the associated values for a_3 in the opposite assembly modes are abbreviated as "alt".

Upper assembly mode		Lower assembly mode
$a_{3_{\text{min}}}$	2.236067978	-2.236067978
$a_{3_{\text{alt}}}$	-3.726779963	3.726779963
$a_{3_{\text{max}}}$	4.582575695	-4.582575695
$a_{3_{\text{alt}}}$	-2.749545416	2.749545416

Table 10. Slider translation limits.

Since the input link in this mechanism is designed to be a crank, then clearly there will be no input joint angle parameter limits $v_{1_{\text{min/max}}}$. Still, in the interest of rigour we will now attempt to identify $a_{3_{\text{crit}}}$ by solving the crank IO equation for v_1 leading to

$$v_1 = \frac{2a_3 \pm \sqrt{-a_3^4 + 26a_3^2 - 105}}{a_3^2 - 7}. \tag{47}$$

Next, compute the partial derivative $\partial v_1/\partial a_3 = 0$ and solve for $a_{3_{\text{crit}}}$. The solutions evaluate to

$$a_{3_{\text{crit}}} = \begin{cases} \pm 5.916079783\, i, \\ \pm 1.732050808\, i. \end{cases} \tag{48}$$

We conclude that there are no input joint angle limits. Moreover, in general we can conclude that if there are no real values for $a_{3_{\text{crit}}}$ then the input link will always be a crank. In this case the linear coefficient factors A_2 and B_2 are both less than zero:

$$A_2 = a_1 - a_2 - a_4 = 1 - 4 - 2 = -5 < 0;$$
$$B_2 = a_1 - a_2 + a_4 = 1 - 4 + 2 = -1 < 0.$$

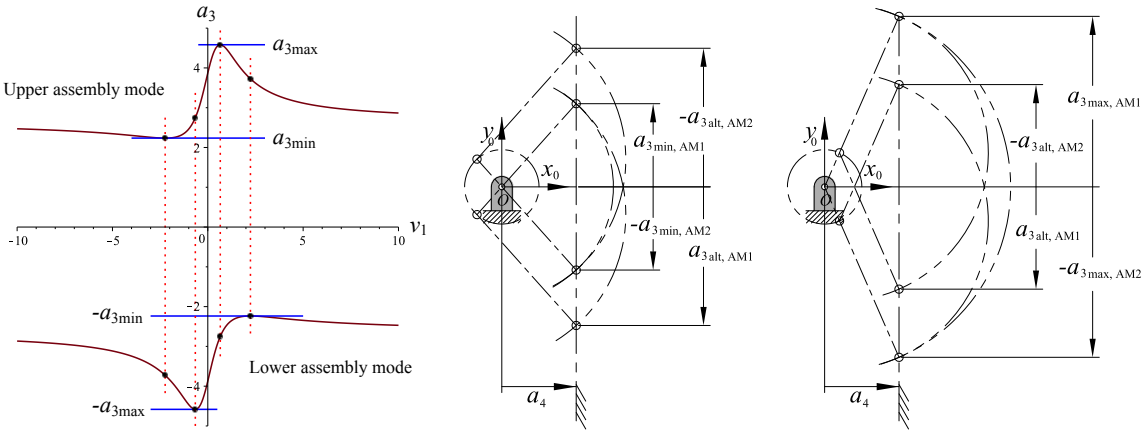

(a) IO curve and critical points for input crank.

(b) Slider translation limits for input crank.

Fig. 20. Crank-slider with $a_1 = 1$, $a_2 = 4$, and $a_4 = 2$: **two assembly modes with one working mode in each**.

Hence, both conditions in Equations (42) and (43) evaluate to complex (imaginary) numbers:

$$a_{3_{\text{crit}_1}} = \pm\sqrt{A_1 B_2} = \pm\sqrt{(7)(-5)} = \sqrt{-35} = \pm 5.916079783\, i;$$

$$a_{3_{\text{crit}_2}} = \pm\sqrt{A_2 B_1} = \pm\sqrt{(-1)(3)} = \pm\sqrt{-3} = \pm 1.732050808\, i.$$

7.3.2. π-rocker

We can create a π-rocker with the link lengths $a_1 = 3$, $a_2 = 2$, and $a_4 = -4$. The algebraic IO equation for this mechanism, illustrated in Figure 21, is expressed in the form $a_3 = f(v_1)$ as:

$$a_3 = \frac{6v_1 \pm \sqrt{3v_1^4 - 6v_1^2 - 45}}{v_1^2 + 1}. \tag{49}$$

The partial derivative $\partial a_3/\partial v_1$ is computed, equated to zero, and solved for $v_{1_{\text{crit}}}$ yielding solutions for each working mode:

$$v_{1_{\text{crit}_1}} = \pm 3; \tag{50}$$

$$v_{1_{\text{crit}_2}} = \pm 1.290994449\, i. \tag{51}$$

We find that $v_{1_{\text{crit}_1}}$ is real-valued while $v_{1_{\text{crit}_2}}$ is complex because the linear factor $A_2 < 0$. Back substituting the values for $v_{1_{\text{crit}}}$ into Equation (49) reveals the slider translation limits in both working modes (note, this type of linkage has only one assembly mode) listed in Table 11. These values require a bit of explanation. The absolute slider displacement limits are indeed $a_{3_{\text{min/max}}}$ are indeed ± 3. However, the other values of $\pm 3/5$ are not the min/max values in the opposite working mode, rather they are the alternate values of a_3 that result from the critical values for v_1.

The π-rocker-slider IO curve and the linkage that generates it are illustrated in Figures 21 and 22. By design, this linkage is a π-rocker-slider and hence the input link rocks between $\pm\theta_{1_{\text{min}}}$, there are no values for $\pm\theta_{1_{\text{max}}}$. So, there will be at most two of four values for $a_{3_{\text{crit}}}$ obtained by solving the IO equation for $v_1 = f(a_3)$

$$v_1 = \frac{6a_3 \pm \sqrt{-a_3^4 - 6a_3^2 + 135}}{a_3^2 - 3}. \tag{52}$$

Upper working mode	Lower working mode
$a_{3_{\max/\min}}$	3	-3
$a_{3_{\text{alt}}}$	3/5	-3/5

Table 11. Slider translation limits for input π-rocker.

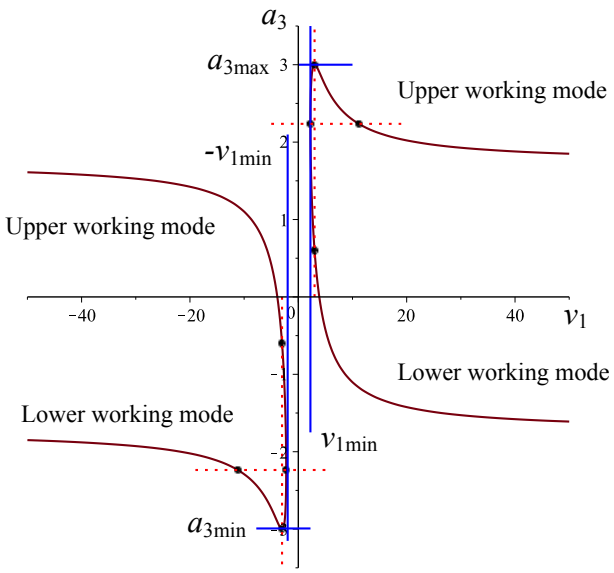

Fig. 21. IO curve and critical points for input π-rocker.

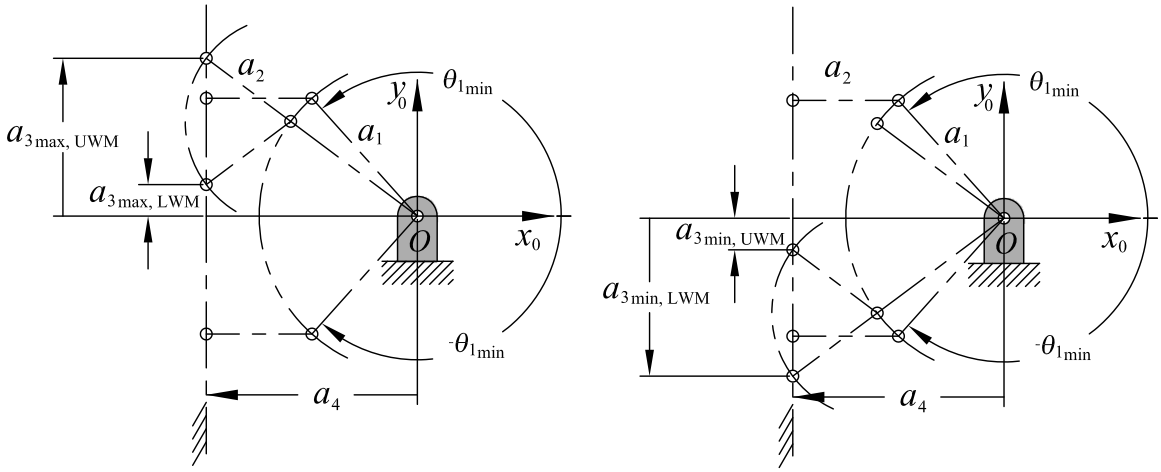

Fig. 22. π-rocker-slider with $a_1 = 3$, $a_2 = 2$, and $a_4 = -4$: **one assembly mode with two working modes**.

The partial derivative $\partial v_1/\partial a_3 = 0$ must now be solved, revealing

$$a_{3_{\text{crit}_{1,\,2}}} \quad = \quad \pm 2.236067977, \;\; \pm 5.196152424\, i.$$

The reason that $a_{3_{\text{crit}_2}}$ is a complex number is because the link lengths cause the linear factor A_2 to be less

than zero:

$$A_2 \;=\; a_1 - a_2 + a_4 \;=\; 3-2-4 \;=\; -3 \;<\; 0,$$

so that

$$a_{3_{\text{crit}_2}} \;=\; \pm\sqrt{A_2 B_1} \;=\; \pm\sqrt{(-3)(9)} \;=\; \pm\sqrt{-27} \;=\; \pm 5.196152424\, i.$$

The real values for the input link minimum angle parameter $\pm v_{1_{\text{min}}}$ as well as $\pm v_{1_{\text{alt}}}$ (and therefore input angle limits angle $\pm\theta_{\text{min}}$ as well as $\pm\theta_{\text{alt}}$) are revealed by substituting the two real values for $a_{3_{\text{crit}}}$ into Equation (52):

$$\begin{aligned} v_{1_{\text{min}}} &= \pm 2.236067978; \\ v_{1_{\text{alt}}} &= \pm 11.18033990; \\ \theta_{1_{\text{min}}} &= \pm 131.8103149^\circ; \\ \theta_{1_{\text{alt}}} &= \pm 169.7778205^\circ. \end{aligned}$$

The second solution for $\theta_{1_{\text{alt}}} = \pm 169.7778205^\circ$ exists, but does not correspond to an input angle extreme, see Figure 21.

7.3.3. 0-rocker

We will create a 0-rocker that is just the previous π-rocker mirrored in the y_0-axis, therefore it has link lengths $a_1 = 3$, $a_2 = 2$, and $a_4 = 4$. The 0-rocker-slider IO curve and the linkage that generates it are illustrated in Figure 23. The algebraic IO equation for this mechanism is expressed in the form $a_3 = f(v_1)$ as:

$$a_3 \;=\; \frac{6v_1 \pm \sqrt{-45v_1^4 - 6v_1^2 + 3}}{v_1^2 + 1}. \tag{53}$$

The partial derivative $\partial a_3/\partial v_1$ is computed, equated to zero, and solved for $v_{1_{\text{crit}}}$ yielding solutions for each working mode:

$$v_{1_{\text{crit}_1}} \;=\; \pm\frac{1}{3}; \tag{54}$$

$$v_{1_{\text{crit}_2}} \;=\; \pm 0.774596669\, i. \tag{55}$$

As for the π-rocker, we find that $v_{1_{\text{crit}_1}}$ is real-valued while $v_{1_{\text{crit}_2}}$ is complex, but in this case, because the linear factor $B_2 < 0$. Back substituting these values for $v_{1_{\text{crit}}}$ into Equation (53) reveals the slider translation limits in both working modes (note, this type of linkage has only one assembly mode) listed in Table 12. These values require a bit of explanation. The absolute slider displacement limits are indeed $a_{3_{\text{min/max}}}$ are indeed ± 3. However, the other values of $\pm 3/5$ are not the min/max values in the opposite working mode, rather they are the alternate values of a_3 that result from the critical values for v_1.

By design, this linkage is a 0-rocker-slider and hence the input link rocks between $\pm\theta_{1_{\text{max}}}$, there are no values for $\pm\theta_{1_{\text{min}}}$. So, there will be at most two of four values for $a_{3_{\text{crit}}}$ obtained by solving the IO equation for $v_1 = f(a_3)$

$$v_1 \;=\; \frac{6a_3 \pm \sqrt{-a_3^4 - 6a_3^2 + 135}}{a_3^2 + 45}. \tag{56}$$

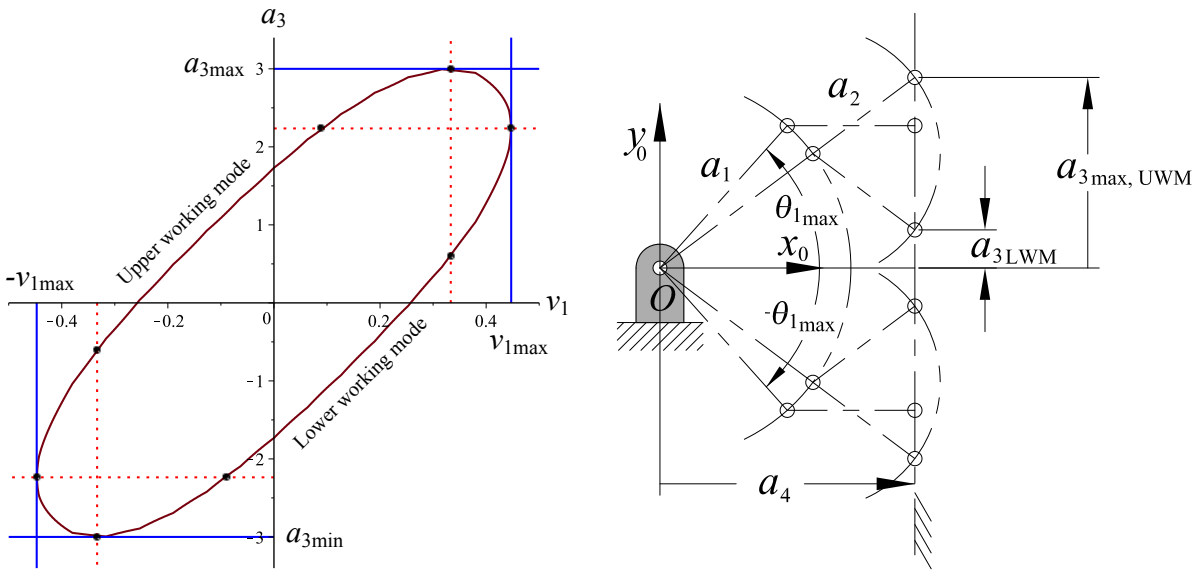

(a) IO curve and critical points for input 0-rocker.

(b) Slider translation limits for input 0-rocker.

Fig. 23. 0-rocker-slider with $a_1 = 3$, $a_2 = 2$, and $a_4 = 4$: **one assembly mode with two working modes**.

Upper working mode	Lower working mode	
$a_{3_{max/min}}$	3	3
$a_{3_{alt}}$	3/5	-3/5

Table 12. Slider translation limits for input 0-rocker.

The partial derivative $\partial v_1/\partial a_3 = 0$ must now be solved, revealing

$$a_{3_{crit_{1,2}}} = \mp 5.196152424\, i, \ \pm 2.236067977.$$

The reason that $a_{3_{crit_1}}$ is a complex number is because the link lengths cause the linear factor B_2 to be less than zero:

$$B_2 = a_1 - a_2 - a_4 = 3 - 2 - 4 = -3 < 0,$$

so that

$$a_{3_{crit_1}} = \pm\sqrt{A_1 B_2} = \pm\sqrt{(9)(-3)} = \pm\sqrt{-27} = \pm 5.196152424\, i.$$

The real values for the input link minimum angle parameter $\pm v_{1_{max}}$ as well as $\pm v_{1_{alt}}$ (and therefore input angle limits angle $\pm\theta_{max}$) are revealed by substituting the two real values for $a_{3_{crit}}$ into Equation (56):

$$\begin{aligned} v_{1_{max}} &= \pm 0.4472135954; \\ v_{1_{alt}} &= \pm 0.08944271904; \\ \theta_{1_{max}} &= \pm 48.18968509^\circ; \\ \theta_{1_{alt}} &= \pm 10.22217938^\circ. \end{aligned}$$

The second solution for $\theta_{1_{alt}} = \pm 10.22217938^\circ$ exists, but does not correspond to an input angle extreme, see Figure 23a.

7.3.4. Rocker

Finally, we will create a rocker that has link lengths $a_1 = 6$, $a_2 = 1$, and $a_4 = 2$. The rocker-slider IO curve and the linkage that generates it are illustrated in Figures 24a and 24b. The algebraic IO equation for this mechanism is expressed in the form $a_3 = f(v_1)$ as:

$$a_3 = \frac{12v_1 \pm \sqrt{-63v_1^4 + 66v_1^2 - 15}}{v_1^2 + 1}. \tag{57}$$

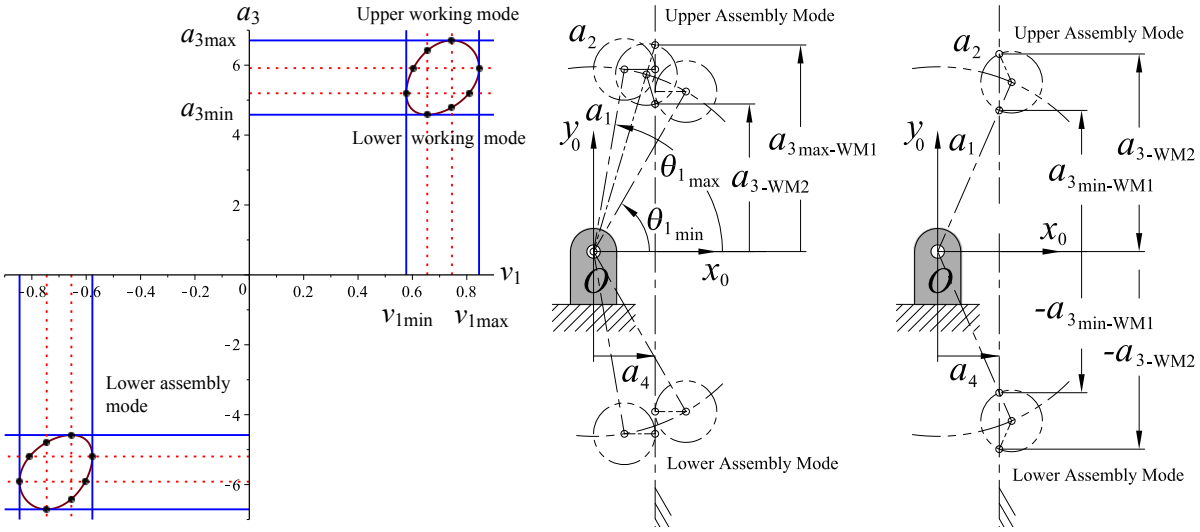

(a) IO curve and critical points for input rocker.

(b) Slider translation limits for input rocker.

Fig. 24. Rocker-slider with $a_1 = 6$, $a_2 = 1$, and $a_4 = 2$: **two assembly modes with two working modes in each**.

The partial derivative $\partial a_3/\partial v_1$ is computed, equated to zero, and solved for $v_{1_{crit}}$ yielding solutions for each working mode:

$$v_{1_{crit_1}} = \pm 0.7453559923; \tag{58}$$

$$v_{1_{crit_2}} = \pm 0.6546536709. \tag{59}$$

As opposed to the π- and 0-rockers, we find that $v_{1_{crit_1}}$ and $v_{1_{crit_2}}$ are both real-valued. Back substituting these values for $v_{1_{crit}}$ into Equation (57) reveals the slider translation limits in both assembly and working modes listed in Table 13.

By design, this linkage is a rocker-slider and hence the input link rocks between $\pm\theta_{1_{max}}$ and $\pm\theta_{1_{min}}$. So, there must be four values for $a_{3_{crit}}$ obtained by solving the IO equation for $v_1 = f(a_3)$

$$v_1 = \frac{12a_3 \pm \sqrt{-a_3^4 + 66a_3^2 - 945}}{a_3^2 + 63}. \tag{60}$$

The partial derivative $\partial v_1/\partial a_3 = 0$ must now be solved, revealing

$$a_{3_{crit_{1,2}}} = \pm 5.916079783,\ \pm 5.196152424.$$

Upper assembly mode	Upper working mode	Lower working mode
$a_{3_{\text{max/min}}}$	6.708203948	4.582575697
$a_{3_{\text{alt}}}$	4.791574227	6.415605970
Lower assembly mode	Upper working mode	Lower working mode
$a_{3_{\text{max/min}}}$	-6.708203948	-4.582575697
$a_{3_{\text{alt}}}$	-4.791574227	-6.415605970

Table 13. Slider translation limits for input rocker.

The real values for the input link limiting angle parameters $\pm v_{1_{\text{min/max}}}$ (and therefore input angle limits angle $\pm\theta_{\text{min/max}}$) are revealed by substituting the values for $a_{3_{\text{crit}}}$ into Equation (60):

$$\left.\begin{array}{llll} v_{1_{\text{max}}} = \pm 0.84515425, & v_{1_{\text{max-alt}}} = \pm 0.6036816104; \\ \theta_{1_{\text{max}}} = \pm 80.40593176^\circ, & \theta_{1_{\text{max-alt}}} = \pm 62.23721622^\circ; \\ v_{1_{\text{min}}} = \pm 0.5773502683, & v_{1_{\text{min-alt}}} = \pm 0.8082903782; \\ \theta_{1_{\text{min}}} = \pm 60^\circ, & \theta_{1_{\text{min-alt}}} = \pm 77.89655121^\circ. \end{array}\right\} \tag{61}$$

The second solutions for $\theta_{1_{\text{max-alt}}} = \pm 62.23721622^\circ$ and $\theta_{1_{\text{min-alt}}} = \pm 77.89655121^\circ$ both exist, but do not correspond input angle extremes, see Figure 24a.

The observations based on the results of the preceding four examples are listed in Table 14. However, in that table negative values for directed link lengths a_1 and a_4 have been considered. This general input link mobility classification will be discussed in Section 8.

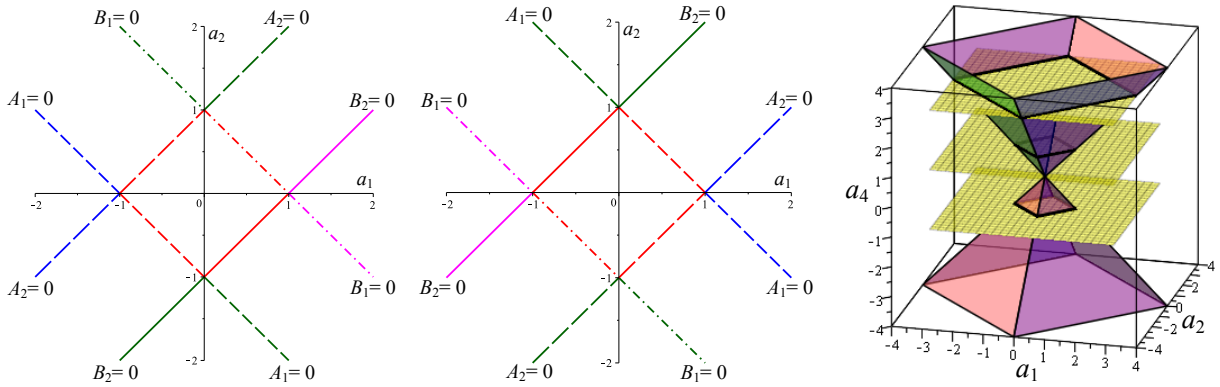

(a) Projected into the plane $a_4 = 1$. (b) Projected into the plane $a_4 = -1$. (c) Pyramid-plane intersections.

Fig. 25. RRRP design parameter space.

8. PLANAR RRRP DESIGN PARAMETER SPACE

In the context of the parametrisation used to obtain Equation (3) the four bilinear coefficient factors A_1, A_2, B_1, and B_2 each contain one of the four possible permutations of addition to, and subtraction from, a_1 of the remaining link lengths a_2 and a_4. These bilinear factors can be thought of as four distinct planes in a space spanned by three mutually orthogonal basis direction vectors for each one of the link lengths a_1, a_2, and a_4, which we call the *design parameter space*. Each distinct point in the space represents the three

	Input link	$v_{1_{\text{crit}_1}} = \pm\frac{\sqrt{A_1B_1}}{A_1}$	$v_{1_{\text{crit}_2}} = \pm\frac{\sqrt{A_2B_2}}{A_2}$	$a_{3_{\text{crit}_1}} = \pm\sqrt{A_1B_2}$	$a_{3_{\text{crit}_2}} = \pm\sqrt{A_2B_1}$	Angle limit
1.	Crank	$\mathbb{R}$	$\mathbb{R}$	$\mathbb{C}$	$\mathbb{C}$	None
2.	NA	$\mathbb{C}$	$\mathbb{R}$	$\mathbb{C}$	$\mathbb{C}$	NA
3.	NA	$\mathbb{R}$	$\mathbb{C}$	$\mathbb{C}$	$\mathbb{C}$	NA
4.	NA	$\mathbb{C}$	$\mathbb{C}$	$\mathbb{C}$	$\mathbb{C}$	NA
5.	Rocker	$\mathbb{R}$	$\mathbb{R}$	$\mathbb{R}$	$\mathbb{R}$	$\pm\theta_{1_{\text{min/max}}}$
6.	NA	$\mathbb{C}$	$\mathbb{R}$	$\mathbb{R}$	$\mathbb{R}$	NA
7.	NA	$\mathbb{R}$	$\mathbb{C}$	$\mathbb{R}$	$\mathbb{R}$	NA
8.	NA	$\mathbb{C}$	$\mathbb{C}$	$\mathbb{R}$	$\mathbb{R}$	NA
9.	NA	$\mathbb{R}$	$\mathbb{C}$	$\mathbb{R}$	$\mathbb{R}$	NA
10.	NA	$\mathbb{R}$	$\mathbb{C}$	$\mathbb{C}$	$\mathbb{C}$	NA
11.	NA	$\mathbb{C}$	$\mathbb{R}$	$\mathbb{R}$	$\mathbb{R}$	NA
12.	NA	$\mathbb{C}$	$\mathbb{R}$	$\mathbb{C}$	$\mathbb{C}$	NA
13.	π-rocker	$\mathbb{R}$	$\mathbb{C}$	$\mathbb{R}$	$\mathbb{C}$	$\pm\theta_{1_{\text{min}}}$
14.	0-rocker	$\mathbb{R}$	$\mathbb{C}$	$\mathbb{C}$	$\mathbb{R}$	$\pm\theta_{1_{\text{max}}}$
15.	0-rocker	$\mathbb{C}$	$\mathbb{R}$	$\mathbb{R}$	$\mathbb{C}$	$\pm\theta_{1_{\text{max}}}$
16.	π-rocker	$\mathbb{C}$	$\mathbb{R}$	$\mathbb{C}$	$\mathbb{R}$	$\pm\theta_{1_{\text{min}}}$

Table 14. Complete input link mobility classification: $\mathbb{R}$ = real number; $\mathbb{C}$ = complex number; NA = not assemblable.

directed link lengths of a distinct planar RRRP linkage. These four planes each contain a triangular face of a regular square pyramid whose axis is perpendicular to the plane $a_4 = 0$, illustrated in Figure 25c. The four planes bound four distinct regions in planes parallel to $a_4 = 0$, where each bounded region contains points representing linkages with different input link mobility characteristics. The input link length a_1 and coupler length a_2 can have positive or negative values, whereas the slider offset a_4 can additionally be zero.

The function generated by any planar RRRP linkage depends only the numerical value of these three design-constant link lengths. We will consider intersections of a_1 and a_2 with planes where a_4 is greater than, less than, and identically equal to zero. Different non-zero values for a_4 simply scale the amplitude of a desired slider position as a function of the input angle parameter: $a_3 = a_4 f(v_1)$. Figure 25c shows intersections of the design parameter pyramid with the three planes $a_4 = \pm 1$ and $a_4 = 3$, illustrating the scaling effect for different values of a_4. Figure 25a illustrates the intersection of the regular square pyramid with the plane $a_4 = 1$ while Figure 25b illustrates the intersection of the regular square pyramid with the plane $a_4 = -1$.

In each intersection of a_1 and a_2 with planes where $a_4 > 0$ the four parameter planes of the algebraic IO equation, Equation (3) intersect each plane $a_4 < 0$ in the four plane traces illustrated in Figure 25a. These traces have the equations $A_1 = 0$, $A_2 = 0$, $B_1 = 0$, and $B_2 = 0$. Linkages consisting of points on these plane traces represent either folding linkages or non-movable structures. Points in the regions separated by the plane traces represent linkages with very specific displacement capabilities, while points on the interior of the square that has vertices $(a_1, a_2) = (\pm 1, 0),\ (0, \pm 1)$ represent non-assemblable linkages. We will now determine which linkage types occupy the eight distinct trace-bound regions on the exterior of the unit

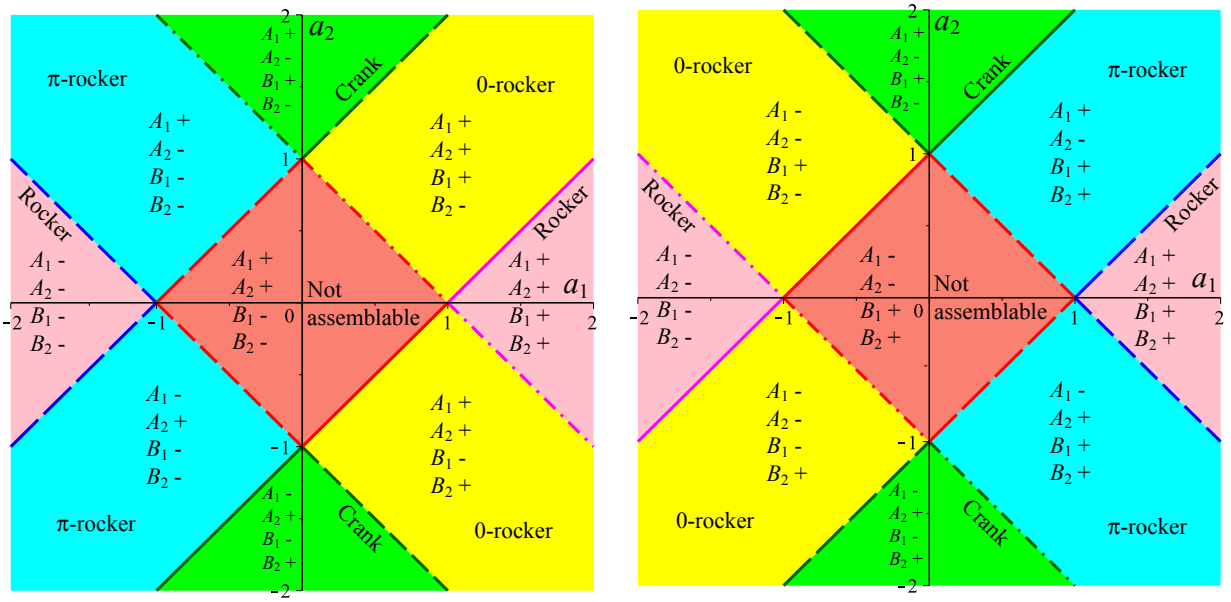

(a) Linkage type regions in the plane $a_4 = 1$.

(b) Linkage type regions in the plane $a_4 = -1$.

Fig. 26. Feasible linkage type regions within the design parameter space in the planes $a_4 = \pm 1$.

squares illustrated in Figure 26.

8.1. Design Parameter Subspaces for RRRP Linkages

Distinct points in the intersection of the design parameter pyramid with the planes $a_4 = \pm 1$, see Figure 26, represent distinct RRRP linkages with different input link mobility. The traces of the plane faces of the design parameter pyramid in the two families of planes where $a_4 > 0$ and $a_4 < 0$, as well as the plane $a_4 = 0$, beg several curious questions.

1. What is the significance of the points of intersection of the four plane traces, i.e. the vertices $(a_1, a_2) = (\pm 1, 0),\ (0, \pm 1)$ of the square, or any location on the a_1- and a_2-axes?

2. What is the significance of the location of a point within the nine distinct regions bounded by the four traces?

3. What is the significance of points laying on the plane traces themselves?

Question 1. The answer to the first question is relatively straightforward. Four different pairs of plane traces intersect in four different points on the a_1- and a_2-axes at the four different coordinates $(\pm 1, 0)$ and $(0, \pm 1)$. Each point requires either a_1 or a_2 to have zero length. The resulting linkage has no mobility because it consists of two R-pairs having the same axis, and the third connected to the slider. Such a linkage is a rigid structure with zero mobility, if it can be assembled at all. The same holds true for any point located on either of the a_1- or a_2-axes.

Question 2. To answer the second question we now consider all distinct permutations of complex and real values for the critical numbers, first discussed in Section 7 where four permutations were demonstrated. However, there are 16 possible permutations of the four critical numbers with two potential outcomes, real or complex. The permutations are listed in Table 14, which gives us the classification scheme for the existence of input angle limits. This differential algebraic classification is completely general, free from trigonometric

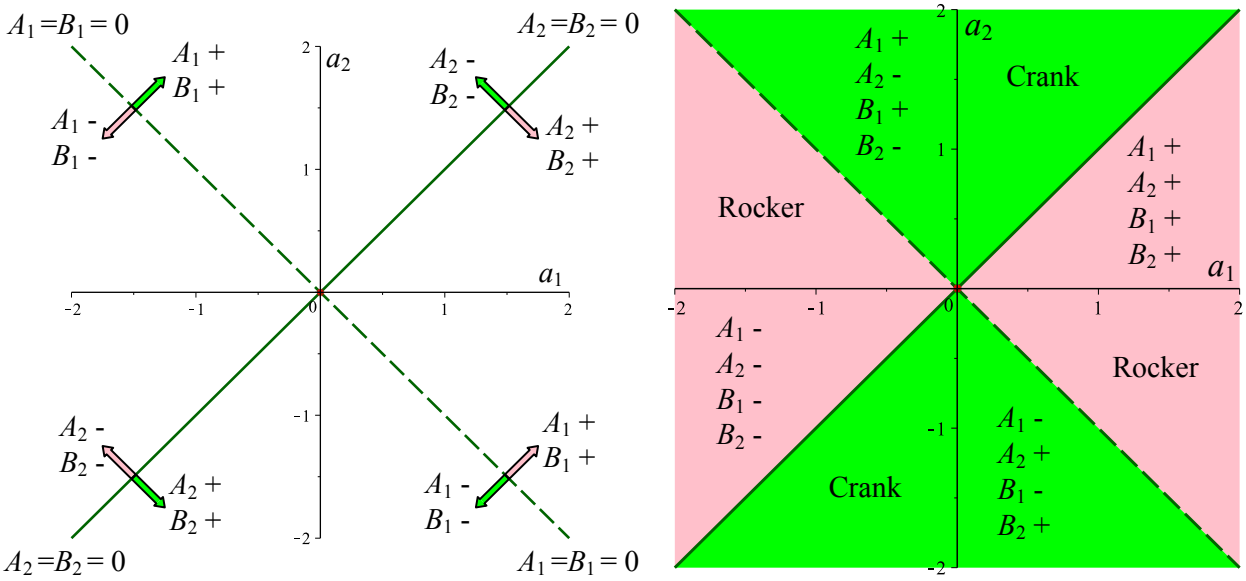

(a) Design parameter pyramid traces in $a_4 = 0$.

(b) Linkage type regions in the plane $a_4 = 0$.

Fig. 27. RRRP design parameter space in the plane $a_4 = 0$.

relations, and accounts for all possibilities of positive and negative directed link lengths. Moreover, once the critical values have been computed, it is remarkably straight forward to classify the mobility of the input link using the observations described in [1, 20, 37, 38].

However, the design parameter pyramid plane traces in the planes $a_4 > 0$, $a_4 < 0$, and $a_4 = 0$ yield a simple geometric classification for the mobility of the input link which is also general, and completely free from trigonometry. Consider the planes $a_4 > 0$, one of which is illustrated in Figures 25a and 26a. We can immediately observe that the input link mobility is symmetric with respect to the a_1-axis, indicating that the sign of the numerical value of a_2 is irrelevant for the shape coefficients of the IO equation, only it's absolute value plays a role. That is, the sign of the length of the coupler is not required to determine the algebraic IO equation. However, examining Figure 26, the signs of a_1, a_2, and a_4 are all required for determining mobility limits of the input link.

We will now consider individual and groups of rows in Table 14 in light of observations in [1, 20, 37, 38], as well as the geometric boundaries in the pyramid intersections in various a_4 planes.

Case 1: Non-foldable Cranks. It is clear that for an input link to be a non-foldable crank then there the critical values for a_3 must be complex indicating that there are no limiting values for the input angle parameter v_1, or by extension input angle θ_1. For this to occur, then the numbers $a_{3_{\text{crit}_1}} = \sqrt{A_1B_2} = \mathbb{C}$ and $a_{3_{\text{crit}_2}} = \sqrt{A_2B_1} = \mathbb{C}$, in turn meaning that the two products A_1B_2 and A_2B_1 must both be less than zero. This can only happen in one of two ways which result in the input link being a crank: either $(A_1,A_2,B_1,B_2) = (-,+,-,+)$, or $(A_1,A_2,B_1,B_2) = (+,-,+,-)$. The only two other possibilities of $(A_1,A_2,B_1,B_2) = (+,+,-,-)$ and $(A_1,A_2,B_1,B_2) = (-,-,+,+)$ mean that the lengths of the links and offset distance are such that the linkage cannot be assembled. These four cases are illustrated in Figures 26 and 27. In the case of Figure 27, which represents the intersection of the planar RRRP design parameter space with the plane $a_4 = 0$, the four pyramid face plane traces converge to the same two lines. Moreover, the four vertices of the square, representing linkages that are non-movable structures along the square edges and simply non-assemblable for all points on the interior in Figure 26, converge to the same point: the origin in Figure 27b.

There are two corresponding sets of inequalities regarding the link length for the input link to be a non-folding crank. The first one, see Figures 26a, 26b and 27b, is

$$\left.\begin{array}{rcrcrcl} A_1 &=& a_1+a_2+a_4 &>& 0 &\Rightarrow& A_1 \;+ \\ A_2 &=& a_1-a_2+a_4 &<& 0 &\Rightarrow& A_2 \;- \\ B_1 &=& a_1+a_2-a_4 &>& 0 &\Rightarrow& B_1 \;+ \\ B_2 &=& a_1-a_2-a_4 &<& 0 &\Rightarrow& B_2 \;- \end{array}\right\} \tag{62}$$

In order to guarantee that all four inequalities in Equations (62) lead to three distinct alternate expressions for the Grashof conditions on the link lengths, only one of which needs be satisfied to guarantee the input link is a crank

$$\begin{array}{lllll} a_4 > 0 & \text{and} & a_4 < a_2 & \text{and} & a_2 > a_4 \pm a_1, \quad \text{or} \\ a_4 = 0 & \text{and} & a_2 > 0 & \text{and} & a_2 > \pm a_1, \quad \text{or} \\ a_4 < 0 & \text{and} & -a_4 < a_2 & \text{and} & \pm a_1 < a_2 + a_4. \end{array} \tag{63}$$

The second set of inequalities that must be satisfied for the input link to be a crank is

$$\left.\begin{array}{rcrcrcl} A_1 &=& a_1+a_2+a_4 &<& 0 &\Rightarrow& A_1 \;- \\ A_2 &=& a_1-a_2+a_4 &>& 0 &\Rightarrow& A_2 \;+ \\ B_1 &=& a_1+a_2-a_4 &<& 0 &\Rightarrow& B_1 \;- \\ B_2 &=& a_1-a_2-a_4 &>& 0 &\Rightarrow& B_2 \;+ \end{array}\right\} \tag{64}$$

In order to guarantee that all four inequalities in Equations (64) are satisfied leads to three different link length conditions, only one of which needs be satisfied to guarantee the input link is a crank

$$\begin{array}{lllll} a_4 > 0 & \text{and} & a_2 < -a_4 & \text{and} & a_2 + a_4 < \pm a_1, \quad \text{or} \\ a_4 = 0 & \text{and} & a_2 < 0 & \text{and} & a_2 < \pm a_1, \quad \text{or} \\ a_4 < 0 & \text{and} & a_2 < a_4 & \text{and} & a_2 - a_4 < \pm a_1. \end{array} \tag{65}$$

Case 2: Non-foldable Rockers. In order for the input link to be a non-foldable rocker then all four critical values, $v_{1_{\text{crit}_{1,2}}}$ and $a_{3_{\text{crit}_{1,2}}}$, must exist as real numbers. . The input link of these linkages is restricted rock in the angular range between 0 and π. There are two corresponding link length conditions for the input link to be a non-folding rocker. The first one is, see Figures 26a and 26b:

$$\left.\begin{array}{rcrcrcl} A_1 &=& a_1+a_2+a_4 &>& 0 &\Rightarrow& A_1 \;+ \\ A_2 &=& a_1-a_2+a_4 &>& 0 &\Rightarrow& A_2 \;+ \\ B_1 &=& a_1+a_2-a_4 &>& 0 &\Rightarrow& B_1 \;+ \\ B_2 &=& a_1-a_2-a_4 &>& 0 &\Rightarrow& B_2 \;+ \end{array}\right\} \tag{66}$$

In order to guarantee that all four inequalities in Equations (66) are satisfied leads to the following three groups of link length conditions, where only one condition needs to be satisfied to indicate the linkage being

considered is indeed a rocker-slider. The first group is, see Figure 26b

$$a_4 < 0 \text{ and } \begin{cases} 1. & a_2 < 0 & \text{and} & a_4 < a_2 & \text{and} & -a_2 - a_4 < a_1, & \text{or} \\ 2. & a_2 > 0 & \text{and} & a_2 < -a_4 & \text{and} & a_2 - a_4 < a_1, & \text{or} \\ 3. & a_2 < a_4 & \text{and} & -a_2 - a_4 < a_1, & \text{or} & & \\ 4. & a_2 = a_4 & \text{and} & -2a_4 < a_1, & \text{or} & & \\ 5. & a_2 = -a_4 & \text{and} & -2a_4 < a_1, & \text{or} & & \\ 6. & -a_4 < a_2 & \text{and} & a_2 - a_4 < a_1. & & & \end{cases} \tag{67}$$

The second group is, see Figure 27

$$a_4 = 0 \text{ and } \begin{cases} 1. & a_2 < 0 & \text{and} & -a_2 < a_1, & \text{or} \\ 2. & a_2 > 0 & \text{and} & a_2 < a_1. & \end{cases} \tag{68}$$

The third group that satisfies the inequalities in Equations (66) is

$$a_4 > 0 \text{ and } \begin{cases} 1. & a_2 < 0 & \text{and} & -a_4 < a_2 & \text{and} & a_4 - a_2 < a_1, & \text{or} \\ 2. & a_2 > 0 & \text{and} & a_2 < a_4 & \text{and} & a_2 + a_4 < a_1, & \text{or} \\ 3. & a_2 < -a_4 & \text{and} & a_4 - a_2 < a_1, & \text{or} & & \\ 4. & a_2 = -a_4 & \text{and} & 2a_4 < a_1, & \text{or} & & \\ 5. & a_2 = a_4 & \text{and} & 2a_4 < a_1, & \text{or} & & \\ 6. & a_4 < a_2 & \text{and} & a_2 + a_4 < a_1. & & & \end{cases} \tag{69}$$

The second set of conditions for an input link crank are as follows, see Figures 26 and 27

$$\left.\begin{array}{rclcrcl} A_1 & = & a_1 + a_2 + a_4 & < & 0 & \Rightarrow & A_1 \; - \\ A_2 & = & a_1 - a_2 + a_4 & < & 0 & \Rightarrow & A_2 \; - \\ B_1 & = & a_1 + a_2 - a_4 & < & 0 & \Rightarrow & B_1 \; - \\ B_2 & = & a_1 - a_2 - a_4 & < & 0 & \Rightarrow & B_2 \; - \end{array}\right\} \tag{70}$$

In order to guarantee that all four inequalities in Equations (70) are satisfied leads to the following three groups of link length conditions, where only one condition needs to be satisfied to indicate the linkage being considered is indeed a rocker-slider. The first group is, see Figure 26b

$$a_4 < 0 \text{ and } \begin{cases} 1. & a_2 < 0 & \text{and} & a_4 < a_2 & \text{and} & a_1 < a_2 + a_4, & \text{or} \\ 2. & a_2 > 0 & \text{and} & a_2 < -a_4 & \text{and} & a_1 < a_4 - a_4, & \text{or} \\ 3. & a_2 < a_4 & \text{and} & a_1 < a_2 + a_4, & \text{or} & & \\ 4. & a_2 = a_4 & \text{and} & a_1 < 2a_4, & \text{or} & & \\ 5. & a_2 = -a_4 & \text{and} & a_1 < 2a_4, & \text{or} & & \\ 6. & -a_4 < a_2 & \text{and} & a_1 < a_4 - a_2. & & & \end{cases} \tag{71}$$

The second group is, see Figure 27

$$a_4 = 0 \text{ and } \begin{cases} 1. & a_2 < 0 & \text{and} & a_1 < a_2, & \text{or} \\ 2. & a_2 > 0 & \text{and} & a_1 < -a_2. & \end{cases} \tag{72}$$

The third group that satisfies the inequalities in Equations (70) is

$$a_4 > 0 \text{ and } \begin{cases} 1. & a_2 < 0 & \text{and} & -a_4 < a_2 & \text{and} & a_1 < a_2 - a_4, & \text{or} \\ 2. & a_2 > 0 & \text{and} & a_2 < a_4 & \text{and} & a_1 < -a_2 - a_4, & \text{or} \\ 3. & a_2 < -a_4 & \text{and} & a_1 < a_2 - a_4, & \text{or} & & \\ 4. & a_2 = -a_4 & \text{and} & a_1 < -2a_4, & \text{or} & & \\ 5. & a_2 = a_4 & \text{and} & a_1 < a_- a_4, & \text{or} & & \\ 6. & a_4 < a_2 & \text{and} & a_1 < -a_2 - a_4. & & & \end{cases} \tag{73}$$

Case 3: Non-foldable 0-Rockers. Examining Figures 26a and 26b, it is to be seen that there are four distinct permutations of signs for the bi-linear factors of the coefficients in the IO equation, Equation (3), that restrict the range of motion of the input link to rock through 0, the positive x_0-axis, between the limits of $\pm\theta_{1_{\max}}$. We will now consider them one at a time.

0-Rocker Condition 1: In order for the input link to be a non-foldable 0-rocker then, according to Rows 14 and 15 in Table 14, either the critical values $v_{1_{\text{crit}_1}}$ and $a_{3_{\text{crit}_2}}$ must exist as real numbers, or $v_{1_{\text{crit}_2}}$ and $a_{3_{\text{crit}_1}}$ must exist as real numbers. The corresponding link length conditions for the input link to be a non-folding 0-rocker are therefore either

$$\left.\begin{array}{rclcrcl} A_1 &=& a_1+a_2+a_4 &>& 0 &\Rightarrow& A_1 \;+ \\ A_2 &=& a_1-a_2+a_4 &>& 0 &\Rightarrow& A_2 \;+ \\ B_1 &=& a_1+a_2-a_4 &>& 0 &\Rightarrow& B_1 \;+ \\ B_2 &=& a_1-a_2-a_4 &<& 0 &\Rightarrow& B_2 \;- \end{array}\right\} \tag{74}$$

To simultaneously satisfy all four inequalities in Equation (74) then one of the following conditions on the link lengths must be true

$$a_4 > 0 \text{ and } \begin{cases} a_2 < a_4 & \text{and} & a_2 > 0 & \text{and} & a_1 < a_2 + a_4 & \text{and} & a_1 > a_4 - a_2, & \text{or} \\ a_2 = a_4 & \text{and} & a_1 < 0 & \text{and} & a_1 < 2a_4, & \text{or} & & \\ a_4 < a_2 & \text{and} & a_1 < a_2 + a_4 & \text{and} & a_1 > a_4 - a_2. & & & \end{cases} \tag{75}$$

0-Rocker Condition 2: In order for the input link to be a non-foldable 0-rocker then, according to Rows 14 and 15 in Table 14, either the critical values $v_{1_{\text{crit}_1}}$ and $a_{3_{\text{crit}_2}}$ must exist as real numbers, or $v_{1_{\text{crit}_2}}$ and $a_{3_{\text{crit}_1}}$ must exist as real numbers. The corresponding link length conditions for the input link to be a non-folding 0-rocker are therefore either

$$\left.\begin{array}{rclcrcl} A_1 &=& a_1+a_2+a_4 &>& 0 &\Rightarrow& A_1 \;+ \\ A_2 &=& a_1-a_2+a_4 &>& 0 &\Rightarrow& A_2 \;+ \\ B_1 &=& a_1+a_2-a_4 &<& 0 &\Rightarrow& B_1 \;- \\ B_2 &=& a_1-a_2-a_4 &>& 0 &\Rightarrow& B_2 \;+ \end{array}\right\} \tag{76}$$

To simultaneously satisfy all four inequalities in Equation (76) then one of the following conditions on the link lengths must be true

$$a_4 > 0 \text{ and } \begin{cases} a_2 < -a_4 & \text{and} & a_1 < a_4 - a_2 & \text{and} & a_1 > -a_2 - a_4, & \text{or} & \\ a_2 = -a_4 & \text{and} & a_1 > 0 & \text{and} & a_1 < 2a_4, & \text{or} & \\ -a_4 < a_2 & \text{and} & a_2 > 0 & \text{and} & a_1 < a_4 - a_2 & \text{and} & a_1 > a_2 + a_4. \end{cases} \tag{77}$$

0-Rocker Condition 3: In order for the input link to be a non-foldable 0-rocker then, according to Rows 14 and 15 in Table 14, either the critical values $v_{1_{\text{crit}_1}}$ and $a_{3_{\text{crit}_2}}$ must exist as real numbers, or $v_{1_{\text{crit}_2}}$ and $a_{3_{\text{crit}_1}}$ must exist as real numbers. The corresponding link length conditions for the input link to be a non-folding 0-rocker are therefore either

$$\left.\begin{array}{rcrcrcl} A_1 &=& a_1+a_2+a_4 &<& 0 &\Rightarrow& A_1 \;- \\ A_2 &=& a_1-a_2+a_4 &<& 0 &\Rightarrow& A_2 \;- \\ B_1 &=& a_1+a_2-a_4 &>& 0 &\Rightarrow& B_1 \;+ \\ B_2 &=& a_1-a_2-a_4 &<& 0 &\Rightarrow& B_2 \;- \end{array}\right\} \tag{78}$$

To simultaneously satisfy all four inequalities in Equation (78) then one of the following conditions on the link lengths must be true

$$a_4<0 \text{ and } \left\{\begin{array}{llllll} a_2<-a_4 & \text{and} & a_2>0 & \text{and} & a_1<a_2+a_4 & \text{and} \quad a_1>a_4-a_2, \quad \text{or} \\ a_2=-a_4 & \text{and} & a_1>0 & \text{and} & a_1>2a_4, & \text{or} \\ -a_4<a_2 & \text{and} & a_2>0 & \text{and} & a_1<-a_2-a_4 & \text{and} \quad a_1>a_4-a_2. \end{array}\right. \tag{79}$$

0-Rocker Condition 4: In order for the input link to be a non-foldable 0-rocker then, according to Rows 14 and 15 in Table 14, either the critical values $v_{1_{\text{crit}_1}}$ and $a_{3_{\text{crit}_2}}$ must exist as real numbers, or $v_{1_{\text{crit}_2}}$ and $a_{3_{\text{crit}_1}}$ must exist as real numbers. The corresponding link length conditions for the input link to be a non-folding 0-rocker are therefore either

$$\left.\begin{array}{rcrcrcl} A_1 &=& a_1+a_2+a_4 &<& 0 &\Rightarrow& A_1 \;- \\ A_2 &=& a_1-a_2+a_4 &<& 0 &\Rightarrow& A_2 \;- \\ B_1 &=& a_1+a_2-a_4 &<& 0 &\Rightarrow& B_1 \;- \\ B_2 &=& a_1-a_2-a_4 &>& 0 &\Rightarrow& B_2 \;+ \end{array}\right\} \tag{80}$$

To simultaneously satisfy all four inequalities in Equation (80) then one of the following conditions on the link lengths must be true

$$a_4<0 \text{ and } \left\{\begin{array}{llllll} a_2<a_4 & \text{and} & a_1<a_2-a_4 & \text{and} & a_1>a_2+a_4, & \text{or} \\ a_2=a_4 & \text{and} & a_1<0 & \text{and} & a_1>2a_4, & \text{or} \\ a_4<a_2 & \text{and} & a_2<0 & \text{and} & a_1<a_4-a_2 & \text{and} \quad a_1>a_2+a_4. \end{array}\right. \tag{81}$$

Case 4: Non-foldable π-Rockers. Examining Figures 26a and 26b, it is to be seen that there are four distinct permutations of signs for the bi-linear factors of the coefficients in the IO equation, Equation (3), that restrict the range of motion of the input link to rock through π, the negative x_0-axis, between the limits of $\pm\theta_{1_{\text{min}}}$. We will now consider them one at a time.

π-Rocker Condition 1: In order for the input link to be a non-foldable π-rocker then, according to Rows 13 and 16 in Table 14, either the critical values $v_{1_{\text{crit}_1}}$ and $a_{3_{\text{crit}_1}}$ must exist as real numbers, or $v_{1_{\text{crit}_2}}$ and $a_{3_{\text{crit}_2}}$ must exist as real numbers. The corresponding link length conditions for the input link to be a non-folding π-rocker are therefore either

$$\left.\begin{array}{rcrcrcl} A_1 &=& a_1+a_2+a_4 &>& 0 &\Rightarrow& A_1 \;+ \\ A_2 &=& a_1-a_2+a_4 &<& 0 &\Rightarrow& A_2 \;- \\ B_1 &=& a_1+a_2-a_4 &<& 0 &\Rightarrow& B_1 \;- \\ B_2 &=& a_1-a_2-a_4 &<& 0 &\Rightarrow& B_2 \;- \end{array}\right\} \tag{82}$$

To simultaneously satisfy all four inequalities in Equation (82) then one of the following conditions on the link lengths must be true

$$a_4 > 0 \text{ and } \begin{cases} a_2 < a_4 & \text{and} & a_2 > 0 & \text{and} & a_1 < a_2 - a_4 & \text{and} & a_1 > -a_2 - a_4, & \text{or} \\ a_2 = a_4 & \text{and} & a_1 < 0 & \text{and} & a_1 < -2a_4, & \text{or} & & \\ a_4 < a_2 & \text{and} & a_1 < a_4 - a_2 & \text{and} & a_1 > -a_2 - a_4. & & & \end{cases} \tag{83}$$

π-Rocker Condition 2: In order for the input link to be a non-foldable π-rocker then, according to Rows 13 and 16 in Table 14, either the critical values $v_{1_{\text{crit}_1}}$ and $a_{3_{\text{crit}_1}}$ must exist as real numbers, or $v_{1_{\text{crit}_2}}$ and $a_{3_{\text{crit}_2}}$ must exist as real numbers. The corresponding link length conditions for the input link to be a non-folding π-rocker are therefore either

$$\left.\begin{array}{rcrcrcl} A_1 &=& a_1 + a_2 + a_4 &<& 0 &\Rightarrow& A_1 \;- \\ A_2 &=& a_1 - a_2 + a_4 &>& 0 &\Rightarrow& A_2 \;+ \\ B_1 &=& a_1 + a_2 - a_4 &<& 0 &\Rightarrow& B_1 \;- \\ B_2 &=& a_1 - a_2 - a_4 &<& 0 &\Rightarrow& B_2 \;- \end{array}\right\} \tag{84}$$

To simultaneously satisfy all four inequalities in Equation (84) then one of the following conditions on the link lengths must be true

$$a_4 > 0 \text{ and } \begin{cases} a_2 < -a_4 & \text{and} & a_1 < a_2 + a_4 & \text{and} & a_1 > a_2 - a_4, & \text{or} \\ a_2 = -a_4 & \text{and} & a_1 < 0 & \text{and} & a_1 < -2a_4, & \text{or} \\ a_2 > -a_4 & \text{and} & a_2 < 0 & \text{and} & a_1 < -a_2 - a_4 & \text{and} \quad a_1 > a_2 - a_4. \end{cases} \tag{85}$$

π-Rocker Condition 3: In order for the input link to be a non-foldable π-rocker then, according to Rows 13 and 16 in Table 14, either the critical values $v_{1_{\text{crit}_1}}$ and $a_{3_{\text{crit}_1}}$ must exist as real numbers, or $v_{1_{\text{crit}_2}}$ and $a_{3_{\text{crit}_2}}$ must exist as real numbers. The corresponding link length conditions for the input link to be a non-folding π-rocker are therefore either

$$\left.\begin{array}{rcrcrcl} A_1 &=& a_1 + a_2 + a_4 &>& 0 &\Rightarrow& A_1 \;+ \\ A_2 &=& a_1 - a_2 + a_4 &<& 0 &\Rightarrow& A_2 \;- \\ B_1 &=& a_1 + a_2 - a_4 &>& 0 &\Rightarrow& B_1 \;+ \\ B_2 &=& a_1 - a_2 - a_4 &>& 0 &\Rightarrow& B_2 \;+ \end{array}\right\} \tag{86}$$

To simultaneously satisfy all four inequalities in Equation (86) then one of the following conditions on the link lengths must be true

$$a_4 < 0 \text{ and } \begin{cases} a_2 < -a_4 & \text{and} & a_2 > 0 & \text{and} & a_1 < a_2 - a_4, & \text{or} \\ a_2 = -a_4 & \text{and} & a_1 < 0 & \text{and} & a_1 > -2a_4, & \text{or} \\ a_2 > -a_4 & \text{and} & a_1 < a_2 - a_4 & \text{and} & a_1 > a_2 + a_4. & \end{cases} \tag{87}$$

π-Rocker Condition 4: In order for the input link to be a non-foldable π-rocker then, according to Rows 13 and 16 in Table 14, either the critical values $v_{1_{\text{crit}_1}}$ and $a_{3_{\text{crit}_1}}$ must exist as real numbers, or $v_{1_{\text{crit}_2}}$ and $a_{3_{\text{crit}_2}}$ must exist as real numbers. The corresponding link length conditions for the input link to be a non-folding

π-rocker are therefore either

$$\left.\begin{array}{rclcrcl} A_1 &=& a_1+a_2+a_4 &<& 0 &\Rightarrow& A_1 \;- \\ A_2 &=& a_1-a_2+a_4 &>& 0 &\Rightarrow& A_2 \;+ \\ B_1 &=& a_1+a_2-a_4 &>& 0 &\Rightarrow& B_1 \;+ \\ B_2 &=& a_1-a_2-a_4 &>& 0 &\Rightarrow& B_2 \;+ \end{array}\right\} \tag{88}$$

To simultaneously satisfy all four inequalities in Equation (88) then one of the following conditions on the link lengths must be true

$$a_4 < 0 \text{ and } \left\{\begin{array}{llllll} a_2 < a_4 & \text{and} & a_1 < -a_2-a_4 & \text{and} & a_1 > a_4-a_2, & \text{or} \\ a_2 = a_4 & \text{and} & a_1 < 0 & \text{and} & a_1 < -2a_4, & \text{or} \\ a_4 < a_2 & \text{and} & a_2 < 0 & \text{and} & a_1 < -a_2-a_4 & \text{and} \quad a_1 > a_2-a_4. \end{array}\right. \tag{89}$$

Question 3. The answer to the third question requires a reminder of what the third question is: what is the significance of points laying on the plane traces in Figures 26 and 27? In regions where the associated linkages can be assembled they can be foldable cranks, foldable 0-rockers, or foldable π-rockers. Recall that the definition of a folding RRRP linkage is that links a_1, a_2, and a_4 can align along the x_0-axis necessitating that $a_3 = 0$ while simultaneously $\theta_1 = 0$, or π, in turn meaning that the tangent half-angle input parameter $v_1 = 0$, or ∞. Hence, by their very definition, planar RRRP linkages whose input links are rockers can never fold, because they are restricted to rock in the range between $\theta_{1_{\min}}$-$\theta_{1_{\max}}$ where $\theta_{1_{\min}} > 0$ and $\theta_{1_{\max}} < \pi$ above the x_0-axis, or below the x_0-axis in the range between the maximum limits $-\theta_{1_{\min}} < 0$ and $-\theta_{1_{\max}} > \pi$. Folding linkages correspond to points laying on the boundary border-lines in Figures 26 and27. The three cases of folding RRRP linkages will now be considered one at a time.

Case 1: Folding Cranks. The plane traces in Figure 26 have equations $A_1 = 0$, $A_2 = 0$, $B_1 = 0$, and $B_2 = 0$. Points laying on segments that are symmetric with respect to the a_1-axis, the horizontal axis represent foldable cranks. As is readily seen in Figure 26, points laying on different segments of the same lines are foldable π-rockers and 0-rockers. The conditions for a point in any intersection with $a_4 =$ a non-zero constant are given by

$$\left.\begin{array}{rcccccl} A_1 &=& a_1+a_2+a_4 &=& 0 &\Rightarrow& a_1 = -a_2-a_4, \\ A_2 &=& a_1-a_2+a_4 &=& 0 &\Rightarrow& a_1 = a_2-a_4, \\ B_1 &=& a_1+a_2-a_4 &=& 0 &\Rightarrow& a_1 = a_4-a_2, \\ B_2 &=& a_1-a_2-a_4 &=& 0 &\Rightarrow& a_1 = a_2+a_4. \end{array}\right\} \tag{90}$$

Note that in Figure 26 cranks bridge both 0- and π-rockers on both the positive and negative a_2-axes. Along the plane trace $A_1 = 0$, the line segment whose points correspond to input link cranks requires $a_1 > 0$ and $a_2 < 0$. In this case, $a_1 > 0$ if, and only if, $a_2 > a_4$. Similar conditions for folding cranks exist along the three other plane traces.

Case 2: Folding 0-Rockers. The plane traces in Figure 26 show that foldable 0-rockers can only occur along the positive a_1-axis when $a_4 > 0$ and along the -a_1-axis when $a_4 < 0$. Referring to Figure 26, one can see that 0-rockers only occur along the plane traces $B_1 = B_2 = 0$ in Equations 90 for values of $a_1 \geq 1$ and $a_4 > 0$, and along $A_1 = A_2 = 0$ for values of $a_1 \leq -1$ and $a_4 < 0$. Along $B_2 = 0$ we see that both a_1 and a_2 are greater than zero as well as $a_4 > 0$. This folding 0-rocker condition requires that $a_2 = a_1 - a_4$. In order for $a_2 > 0$ then it must be that $a_1 > a_4$. A similar condition can be derived for points along $B_1 = 0$ as well as for folding 0-rockers in planes where $a_4 < 0$.

Case 3: Folding π-Rockers. The plane traces in Figure 26 show that foldable π-rockers can only occur along the $-a_1$-axis when $a_4 > 0$ and along the a_1-axis when $a_4 < 0$. Referring to Figure 26, one can see that π-rockers only occur along the plane traces $A_1 = A_2 = 0$ in Equations 90 for values of $a_1 \leq -1$ and $a_4 > 0$, as well as along traces $B_1 = B_2 = 0$ when $a_1 \geq 1$ and $a_4 < 0$. Along $A_1 = 0$ we see that $a_1 \geq 1$ and $a_2 < 0$ while $a_4 < 0$ as well. This folding π-rocker condition requires that $a_2 = -a_4 - a_1 <$. In order for $a_2 < 0$ then it must be that $a_4 < a_1$, that is -a_4 is a larger negative number than -a_1. Similar conditions apply to points along $A_2 = 0$, $B_1 = 0$, and $B_2 = 0$.

9. COUPLER POINT CURVES

One of the earliest recorded examples of mechanical system design for guiding a point along a curve belongs to Archimedes (ca. 287-212 BC). He was born in Syracuse in the ancient Greek colony of Sicily, but he studied mathematics at the Museum in Alexandria [3] between 250-240 BC under the direction of Conon of Samos. Conon was a mathematician who was a pupil of Euclid and became the custodian of the library of Alexandria after Euclid's death. Archimedes work is the first recorded systematic study of mechanism design and analysis, although undoubtedly these concepts were widely studied earlier everywhere there were humans who could formulate abstract thoughts. However, the very first patent [8] for a mechanism designed to move a point along a desired curve belongs to James Watt (1736-1819) awarded more than 2000 years after Archimedes death.

9.1. Planar 4R Coupler Point Curves

The coupler point curve for an arbitrary planar 4R mechanism is geometrically very rich. An arbitrary point on the coupler, which will be called Point *C*, is constrained by the fact that two of the coupler's points move on the fixed-centred circles described by the motions of the input and output links, see Figure 28. The curve traced by point *C* is, in general, a curve of degree 6, bearing the formidable name of *tri-circular sextic*, see [27] for a full explanation of what this name means. But briefly, because two of the coupler points move on circles it turns out that every planar 4R coupler curve possesses the same three pairs of complex conjugate multiple points at infinity which are common to every circle.

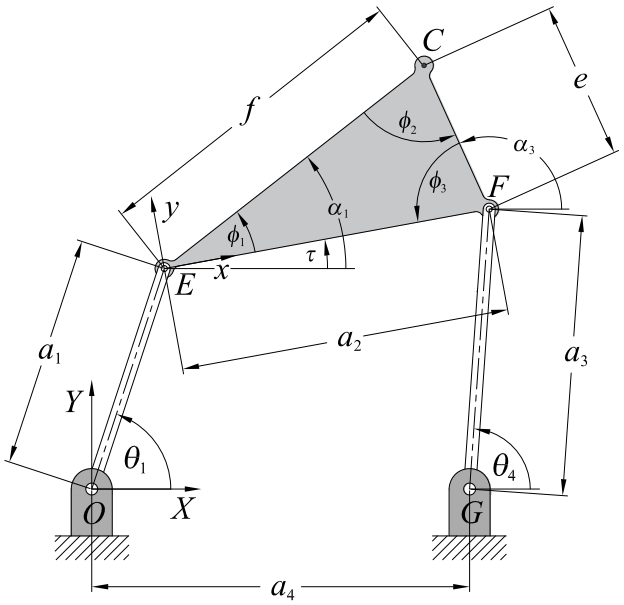

Fig. 28. Planar 4R coupler point geometric parameters.

The following derivation of the coupler point curve of a planar 4R mechanism was devised by Samuel Roberts [39] in 1876. The coordinates of points E and F in the $X-Y$ coordinate system whose origin is located at the centre of the ground-fixed R-pair on the left, see Figure 28, in terms of the location of the coupler point C with coordinates (X_C, Y_C) in the same coordinate system:

$$\mathbf{E} = \begin{bmatrix} X_C - f\cos\alpha_1 \\ Y_C - f\sin\alpha_1 \end{bmatrix}; \tag{91}$$

$$\mathbf{F} = \begin{bmatrix} X_C - e\cos\alpha_3 - a_4 \\ Y_C - e\sin\alpha_3 \end{bmatrix}. \tag{92}$$

Because points E and F move on fixed-centred circles it must be that $\mathbf{E}\cdot\mathbf{E} = a_1^2$ and $\mathbf{F}\cdot\mathbf{F} = a_3^2$, so we can write

$$X_C^2 - 2X_C f\cos(\alpha_1) + f^2 + Y_C^2 - 2Y_C f\sin(\alpha_1) - a_1^2 = 0, \tag{93}$$

and

$$X_C^2 - 2X_C e\cos(\alpha_3) - 2X_C a_4 + e^2 + 2e\cos(\alpha_3)a_4 + a_4^2 + Y_C^2 - 2Y_C e\sin(\alpha_3) - a_3^2 = 0. \tag{94}$$

It will be convenient to express α_3 in terms of α_1 and ϕ_2. For this we can use the triangle interior/exterior angle rule [28]. Consider the triangle illustrated in Figure 29a. Consider that

$$\phi_1 + \phi_2 + \phi_3 = \pi,$$

and

$$\phi_3 + \phi_4 = \pi.$$

Then we can say that

$$\phi_4 = \pi - \phi_3,$$

and

$$\phi_1 + \phi_2 = \pi - \phi_3.$$

Therefore

$$\phi_1 + \phi_2 = \phi_4. \tag{95}$$

The same rule holds for the triangle shown in Figure 29b, that is τ can be added to both sides of Equation (95) without changing it's validity:

$$\underbrace{(\phi_1 + \tau)}_{\alpha_1} + \phi_2 = \underbrace{(\phi_4 + \tau)}_{\alpha_3}.$$

Therefore

$$\alpha_1 + \phi_2 = \alpha_3. \tag{96}$$

Make this substitution in Equation (94) and use the identity

$$\cos(\alpha_1 + \phi_2) = \cos\alpha_1\cos\phi_2 - \sin\alpha_1\sin\phi_2 \tag{97}$$

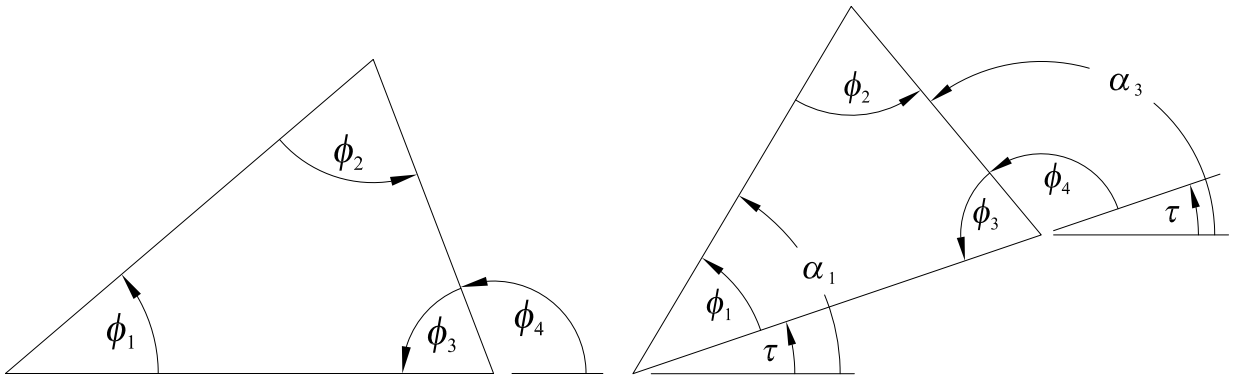

(a) Triangle angle rule.

(b) Triangle angle rule adapted for coupler.

Fig. 29. Triangle angle rules.

to separate the angles in the trigonometric arguments giving two equations in $\cos\alpha_1$ and $\sin\alpha_1$:

$$\begin{aligned} S_1\cos\alpha_1 + T_1\sin\alpha_1 &= U_1, \\ S_2\cos\alpha_1 + T_2\sin\alpha_1 &= U_2, \end{aligned}$$

where

$$\begin{array}{rclcrcl} S_1 &=& 2X_C f, & \| & S_2 &=& 2e\left((X_C - a_4)\cos\phi_2 + Y_C\sin\phi_2\right), \\ T_1 &=& 2Y_C f, & \| & T_2 &=& 2e\left(Y_C\cos\phi_2 - (X_C - a_4)\sin\phi_2\right), \\ U_1 &=& X_C^2 + Y_C^2 + f^2 - a_1^2. & \| & U_2 &=& X_C^2 + Y_C^2 + e^2 + a_4^2 - a_3^2. \end{array}$$

Arrange these two equations vector-matrix form as

$$\begin{bmatrix} S_1 & T_1 \\ S_2 & T_2 \end{bmatrix} \begin{bmatrix} \cos\alpha_1 \\ \sin\alpha_1 \end{bmatrix} = \begin{bmatrix} U_1 \\ U_2 \end{bmatrix}, \tag{98}$$

and solve Equations (98) for $\cos\alpha_1$ and $\sin\alpha_1$ using Cramer's rule:

$$\cos\alpha_1 = \frac{\begin{vmatrix} U_1 & T_1 \\ U_2 & T_2 \end{vmatrix}}{\begin{vmatrix} S_1 & T_1 \\ S_2 & T_2 \end{vmatrix}} = \frac{U_1T_2 - U_2T_1}{S_1T_2 - S_2T_1}, \text{ and} \tag{99}$$

$$\sin\alpha_1 = \frac{\begin{vmatrix} S_1 & U_1 \\ S_2 & U_2 \end{vmatrix}}{\begin{vmatrix} S_1 & T_1 \\ S_2 & T_2 \end{vmatrix}} = \frac{S_1U_2 - S_2U_1}{S_1T_2 - S_2T_1}. \tag{100}$$

Finally we enforce the identity $\cos^2\alpha_1 + \sin^2\alpha_1 = 1$ to obtain

$$(U_1T_2 - U_2T_1)^2 + (S_1U_2 - S_2U_1)^2 = (S_1T_2 - S_2T_1)^2,$$

or

$$(U_1T_2 - U_2T_1)^2 + (S_1U_2 - S_2U_1)^2 - (S_1T_2 - S_2T_1)^2 = 0. \tag{101}$$

The S_i and T_i coefficients in Equation (101) are linear functions in the coordinates of the coupler point X_C and Y_C, while the U_i are quadratic. The products U_iT_j and S_jU_i are of degree 3, and the squares of the differences are of order six. Hence, the coupler point curve of an arbitrary planar 4R mechanism represented by Equation (101) is of degree six, a *sextic*, agreeing with the well known theory of planar mechanisms [27].

9.2. Planar RRRP Coupler Point Curves

The planar RRRP mechanism can also be used to generate desired coupler point curves, though these curves have a much simpler geometry. These coupler point curves are generally quartics, that is they are of degree four. The quartic curve is generated because one coupler point, E in Figure 30, is constrained to move on a fixed centred circle while the other, Point F, moves on a line with fixed direction cosines. These curves only intersect the complex congugate circular points a single time, and are said to have a circularity of one.

We will now derive the general planar RRRP coupler point curve. The coupler geometry can be simply modelled in the same way as for the planar 4R, see Figure 30. The position vector of Point E in the $X-Y$

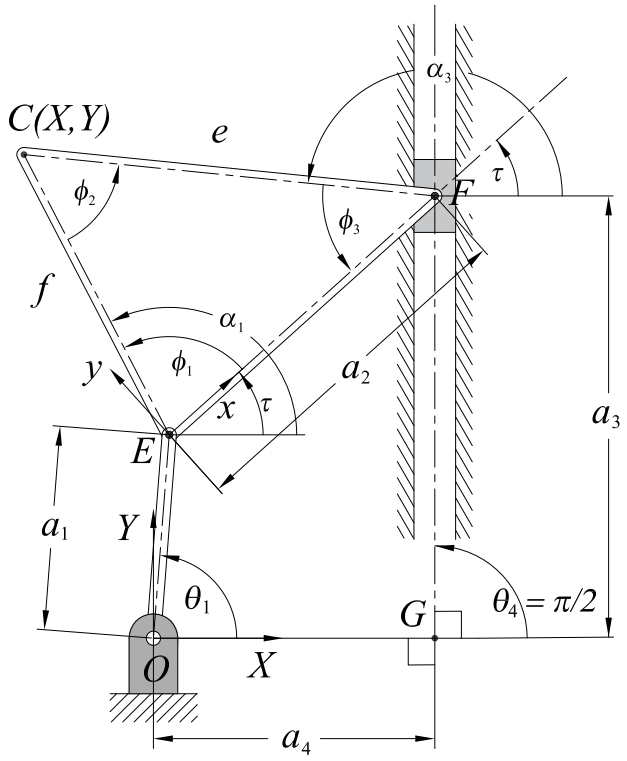

Fig. 30. Planar RRRP coupler point geometric parameters.

coordinate system can be expressed as a function of the coordinates of Point C and coupler triangle as for the 4R linkage:

$$\mathbf{E} = \begin{bmatrix} X_C - f\cos\alpha_1 \\ Y_C - f\sin\alpha_1 \end{bmatrix}. \tag{102}$$

Thanks to the rigid-body assumption, we can additionally state that

$$(X_C - f\cos\alpha_1)^2 + (Y_C - f\sin\alpha_1)^2 = a_1^2. \tag{103}$$

Another constraint is that

$$a_4 \quad = \quad X_C - e\cos\alpha_3. \tag{104}$$

Using the triangle interior/exterior angle rule again, Equation (96), we can re-write Equation (104) as

$$a_4 \quad = \quad X_C - e\cos(\alpha_1 + \phi_2). \tag{105}$$

Expand Equation (103) to obtain

$$X_C^2 - 2X_C f\cos\alpha_1 + f^2\cos^2\alpha_1 + Y_C - 2Y_C f\sin\alpha_1 + f^2\sin^2\alpha_1 - a_1^2 \quad = \quad 0. \tag{106}$$

We can simplify Equation (106) with the identity $\cos^2\alpha_1 + \sin^2\alpha_1 = 1$ as

$$X_C^2 + Y_C^2 - 2X_C f\cos\alpha_1 - 2Y_C f\sin\alpha_1 + f^2 - a_1^2 \quad = \quad 0. \tag{107}$$

Next, use the identity

$$\cos(\alpha_1 + \phi_2) \quad = \quad \cos\alpha_1\cos\phi_2 - \sin\alpha_1\sin\phi_2 \tag{108}$$

to simplify Equation (105), yielding

$$X_C + e(\sin\alpha_1\sin\phi_2 - \cos\alpha_1\cos\phi_2) - a_4 \quad = \quad 0. \tag{109}$$

We can now consider Equations (107) and (109) as two equations in $\cos\alpha_1$ and $\sin\alpha_1$:

$$\left.\begin{array}{rcl} P_1\cos\alpha_1 + Q_1\sin\alpha_1 & = & R_1, \\ P_2\cos\alpha_1 + Q_2\sin\alpha_1 & = & R_2, \end{array}\right\} \tag{110}$$

where

$$\begin{array}{rcl} P_1 & = & 2X_C f, \\ Q_1 & = & 2Y_C f, \\ R_1 & = & X_C^2 + Y_C^2 + f^2 - a_1^2. \end{array} \quad \left\| \quad \begin{array}{rcl} P_2 & = & e\cos\phi_2, \\ Q_2 & = & -e\sin\phi_2, \\ R_2 & = & X_C - a_4. \end{array}\right.$$

Arrange these equations vector-matrix form as

$$\begin{bmatrix} P_1 & Q_1 \\ P_2 & Q_2 \end{bmatrix} \begin{bmatrix} \cos\alpha_1 \\ \sin\alpha_1 \end{bmatrix} \quad = \quad \begin{bmatrix} R_1 \\ R_2 \end{bmatrix}, \tag{111}$$

and solve Equations (111) for $\cos\alpha_1$ and $\sin\alpha_1$ using Cramer's rule:

$$\cos\alpha_1 \quad = \quad \frac{\begin{vmatrix} R_1 & Q_1 \\ R_2 & Q_2 \end{vmatrix}}{\begin{vmatrix} P_1 & Q_1 \\ P_2 & Q_2 \end{vmatrix}} \quad = \quad \frac{R_1Q_2 - R_2Q_1}{P_1Q_2 - P_2Q_1}, \quad \text{and} \tag{112}$$

$$\sin\alpha_1 \quad = \quad \frac{\begin{vmatrix} P_1 & R_1 \\ P_2 & R_2 \end{vmatrix}}{\begin{vmatrix} P_1 & Q_1 \\ P_2 & Q_2 \end{vmatrix}} \quad = \quad \frac{P_1R_2 - P_2R_1}{P_1Q_2 - P_2Q_1}. \tag{113}$$

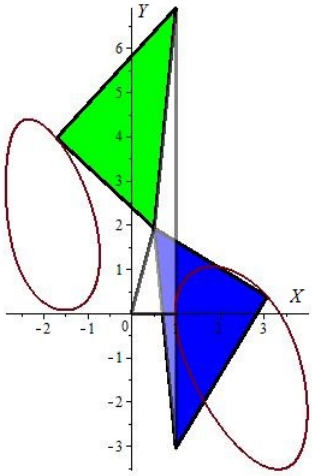

(a) Crank: $e = 4$, $f = 3$, $\phi_2 = \pi/2$, $a_1 = 2$, $a_4 = 1$.

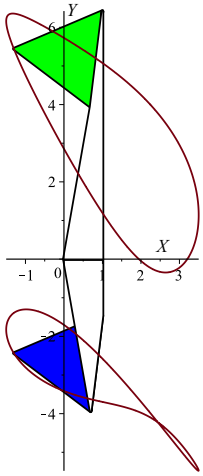

(b) Rocker: $e = 2.5$, $f = 2.5$, $\phi_2 = \pi/3$, $a_1 = 4$, $a_4 = 1$.

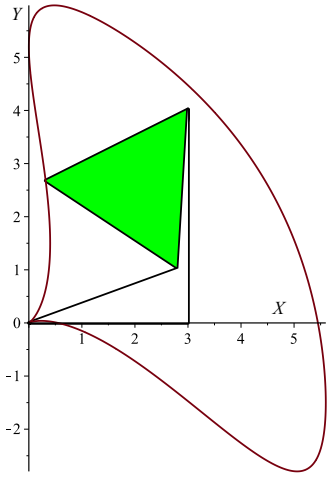

(c) 0-rocker: $e = 3$, $f = 3$, $\phi_2 = \pi/3$, $a_1 = 3$, $a_4 = 3$.

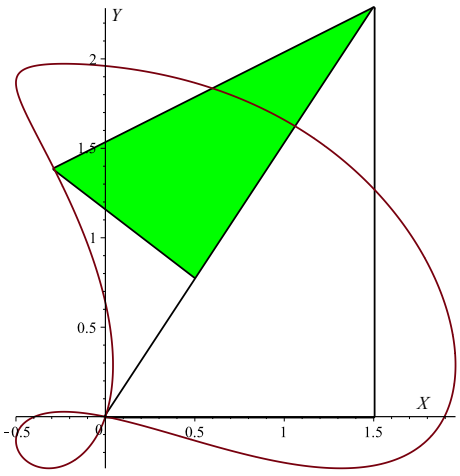

(d) 0-rocker: $e = 2$, $f = 1$, $\phi_2 = \pi/3$, $a_1 = 1$, $a_4 = 1.5$.

Fig. 31. Four different coupler point curves.

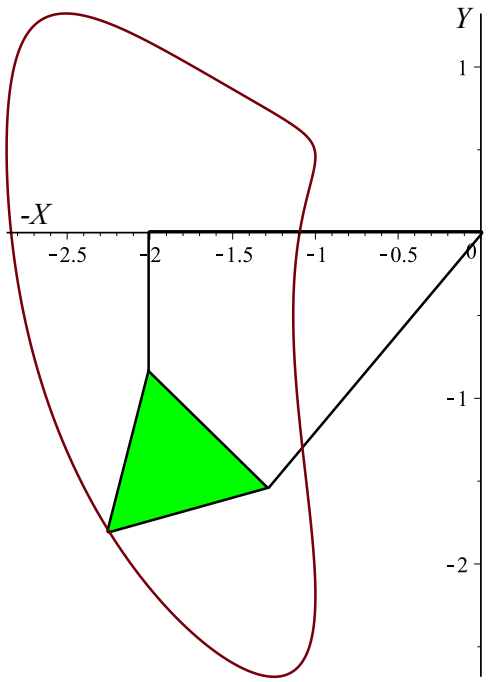

Fig. 32. π-rocker: $e = 2$, $f = 1$, $\phi_2 = \pi/3$, $a_1 = 2$, $a_4 = -2$.

Finally we enforce the identity $\cos^2\alpha_1 + \sin^2\alpha_1 = 1$ to obtain

$$(R_1Q_2 - R_2Q_1)^2 + (P_1R_2 - P_2R_1)^2 \quad = \quad (P_1Q_2 - P_2Q_1)^2,$$

or

$$(R_1Q_2 - R_2Q_1)^2 + (P_1R_2 - P_2R_1)^2 - (P_1Q_2 - P_2Q_1)^2 \quad = \quad 0. \tag{114}$$

The P_i and Q_i coefficients in Equation (114), together with the coefficient R_2, are linear in the coordinates of the coupler point X_C and Y_C, while R_1 is quadratic. The products R_1Q_2 and P_2R_1 are of order two, and the squares of the differences are of order four. Hence, the coupler point curve of an arbitrary planar RRRP mechanism represented by Equation (114) is of order four, a *quartic*, agreeing with the well known theory of planar mechanisms [27].

A quartic planar curve may contain as many as three multiple points, or self-intersections. It can be shown that every quartic coupler point curve for every planar RRRP linkage contains the complex conjugate imaginary circle points as a pair of isolated double points meaning that they can contain, at most, only one more double point. An RRRP linkage that generates an arbitrary planar quartic curve is specified by selecting values for the lengths a_1, a_4, e, and f, together with the angle ϕ_2. The quantities e, f, and ϕ_2 determine the coupler length a_2, and hence are sufficient to define the coupler point triangle.

Figure 31 illustrates four distinct types of coupler point curves for RRRP mechanisms whose input link is a crank, a rocker, and a 0-rocker. The coupler point curves were generated using the symbolic algebra software package Maple. The coupler triangle is either green or blue and the link lengths and coupler triangle were plotted using the *polygonplot* function.

The coupler curve for the crank illustrated in Figure 31a is a quartic curve that has two distinct branches. The linkage must be assembled in two different way to reach all points in both circuits of the coupler point curve. This crank coupler point curve contains no real double points. The rocker coupler point curve

illustrated in Figure 31b also possesses two distinct branches, but one of them has a regular double point. Figures 31c and 31d are 0-rocker coupler points curves possessing a stationary double point and a regular double point, respectively.

REFERENCES

1. Hayes, M.J.D., Rotzoll, M. and Husty, M.L. "Design Parameter Space of Planar Four-bar Linkages." Proceedings of the 15^{th} IFToMM World Congress, June 30-July 4, 2019.
2. Hartenberg, R. and Denavit, J. *Kinematic Synthesis of Linkages*. McGraw-Hill, Book Co., New York, N.Y., U.S.A., 1964.
3. Ceccarelli, M. *Distinguished Figures in Mechanism and Machine Science, Their Contributions and Legacies Part 1*. Springer, New York, U.S.A., 2007.
4. Reuleaux, F. *Theoretische kinematik: Grundzüge einer Theorie des Maschinenwesens*. Braunschweig, F. Vieweg und Sohn, 1875.
5. Reuleaux, F. *The Kinematics of Machinery: Outlines of a Theory of Machines,* Translated and Edited by A.B.W. Kennedy. MacMillan and Co., 1876.
6. Freudenstein, F. "Approximate Synthesis of Four-Bar Linkages." *Trans. ASME*, Vol. vol 77, pp. 853–861, 1955.
7. Burmester, L. *Lehrbuch der Kinematik*. Arthur Felix Verlag, Leipzig, Germany, 1888.
8. Watt, J. "Patent No. 1432, April 28, 1784.", 1784.
9. Uicker, J.J., Pennock, G.R. and Shigley, J.E. *Theory of Machines and Mechanisms,* 5^{th} edition. Oxford University Press, New York, N.Y., U.S.A., 2017.
10. Cipolla, R. and Giblin, P. *Visual Motion of Curves and Surfaces*. Cambridge University Press, Cambridge, U.K., 2000.
11. Kreyszig, E. *Differential Geometry*. Dover Publications, Inc., New York, N.Y., U.S.A., 1991.
12. Freudenstein, F. "An Analytical Approach to the Design of Fourlink Mechanisms." *Trans. ASME*, Vol. vol 77, pp. 483–492, 1954.
13. Hayes, M.J.D., Husty, M.L. and Pfurner, M. "Input-output Equation for Planar Four-bar Linkages." pp. 12–19. *16^{th} Advances in Robotic Kinematics*, eds. Lenarčič, J. and Parenti-Castelli, V., Springer, New York, 2018.
14. Husty, M.L. and Pfurner, M. "An Algebraic Version of the Input-Output Equation of Planar Four-Bar Mechanisms." pp. 746–757. *International Conference on Geometry and Graphics*, Milan, Italy, 2018.
15. Rotzoll, M., Hayes, M.J.D., Husty, M.L. and Pfurner, M. "A General Method for Determining Algebraic Input-output Equations for Planar and Spherical 4R Linkages." Accepted in the *17^{th} International Symposium: Advances in Robotic Kinematics*, Ljubljana, Slovenia, June 28-July 2, 2020.
16. Denavit, J. and Hartenberg, R.S. "A Kinematic Notation for Lower-pair Mechanisms Based on Matrices." *Trans ASME J. Appl. Mech.*, Vol. 23, p. 215–221, 1955.
17. Study, E. *Geometrie der Dynamen*. Teubner Verlag, Leipzig, Germany, 1903.
18. Adams, W. and Loustaunau, P. *An Introduction to Gröbner Bases*, Vol. 3. American Mathematical Society, Graduate Studies in Mathematics, 1994.
19. Cox, D., Little, J. and O'Shea, D. *Ideals, Varieties, and Algorithms: an Introduction to Computational Algebraic Geometry and Commutative Algebra,* second edition. Springer-Verlag, Berlin, Germany, 1997.
20. Rotzoll, M., Hayes, M.J.D. and Husty, M.L. "An Algebraic Input-Output Equation for Planar RRRP and PRRP Linkages." *Proceedings of the 10^{th} CCToMM Symposium on Mechanisms, Machines, and Mechatronics*, École de technologie supérieure, Montréal, QC, Canada, May 16-17, 2019.
21. Hayes, M.J.D., Rotzoll, M., Ingalls, C. and Pfurner, M. "Design Parameter Space of Spherical Four-bar Linkages." Accepted for Publication in the Proceedings of *EuCoMeS 2020, 8th European Conference on Mechanism Science*.
22. Coxeter, H.S.M. *Regular Polytopes, 3^{rd} Edition*. Dover Publications, Inc., New York, N.Y., U.S.A., 1973.
23. Coxeter, H.S.M. *Projective Geometry,* second edition. University of Toronto Press, Toronto, On., Canada, 1974.
24. McCarthy, J.M. "Planar and Spatial Rigid Motion as Special Cases of Spherical and 3-Spherical Motion." *Journal of Mechanisms, Transmissions, and Automation in Design*, Vol. 105, No. 3, pp. 569–575, 1983.
25. Segre, B. *The Non-singular Cubic Surfaces; a New Method of Investigation with Special Reference to Questions of Reality*. Oxford, The Clarendon Press, 1942.
26. Husty, M., Karger, A., Sachs, H. and Steinhilper, W. *Kinematik und Robotik*. Springer-Verlag, Berlin, Germany,

1997.
27. Hunt, K. *Kinematic Geometry of Mechanisms*. Clarendon Press, Oxford, England, 1978.
28. Euclid. *The Thirteen Books of the Elements,* second edition, translation by Sir T. L. Heath, vol's 1,2,3. Dover Publications, Inc., New York, N.Y., U.S.A., 1956.
29. Chebyshev, P.L. *Théorie des méchanismes connus sous le nom de parallélogrammes (1853) from "Oeuvres de P.L. Tchebychef"*. Markoff et Sonin, 1899.
30. Hayes, M.J.D., Parsa, K. and Angeles, J. "The Effect of Data-Set Cardinality on the Design and Structural Errors of Four-Bar Function-Generators." *Proceedings of the Tenth World Congress on the Theory of Machines and Mechanisms,* Oulu, Finland*, pages 437-442*, 1999.
31. Guigue, A. and Hayes, M.J.D. "Continuous Approximate Synthesis of Planar Function-generators Minimising the Design Error." *Mechanism and Machine Theory*, Vol. 101, pp. 158–167, DOI: 10.1016/j.mechmachtheory.2016.03.012, 2016.
32. Salmon, G. *A Treatise on the Higher Plane Curves,* third edition. Hodges, Foster, and Figgis, Dublin, Rep. of Ireland, 1879.
33. Primrose, E. *Plane Algebraic Curves*. MacMillan, 1955.
34. Harnack, A. "Über die Vielteiligkeit der ebenen algebraischen Kurven." In "Mathematische Annalen," pp. 189–198, 1876.
35. Abhyankar, S. *Algebraic Geometry for Scientists and Engineers*, Vol. 35. American Mathematical Society, Mathematical Surveys and Monographs, 1990.
36. Gosselin, C.M. and Angeles, J. "Singularity Analysis of Closed-loop Kinematic Chains." *IEEE Transactions on Robotics and Automation*, Vol. 6, No. 3, p. 281–290, 1990.
37. Murray, A.P. and Larochelle, P.M. "A Classification Scheme for Planar 4*R*, Spherical 4*R*, and Spatial *RCCR* Linkages to Facilitate Computer Animation." *Proceedings of 1998 ASME Design Engineering Technical Conferences (DETC'98)*, Atlanta, Georgia, U.S.A., September 13-16, 1998.
38. McCarthy, J.M. and Soh, G.S. *Geometric Design of Linkages, 2nd Edition* Interdiciplinaty Applied Mathematics. Springer, New York, N.Y., 2011.
39. Roberts, S. "On Three-bar Motion in Plane Space." *Proc. London Math. Soc.*, Vol. 7, pp. 286–318, 1876.